The $^{18}O(p,\alpha)^{15}N$ Reaction at E_p=40.93 MeV and Associated Spectrum Analysis Techniques

Johnson R. Campbell

Department of Physics
University of Manitoba
Winnipeg , Manitoba

A thesis submitted to the Department of Physics of the University of Manitoba in partial fulfillment of the requirements for the Degree of Master of Science .

THE $^{18}O(p\alpha)^{15}N$ REACTION AT Ep= 40.93 MeV AND ASSOCIATED SPECTRUM ANALYSIS TECHNIQUES

BY

JOHNSON ROSS CAMPBELL

A thesis submitted to the Faculty of Graduate Studies of the University of Manitoba in partial fulfillment of the requirements of the degree of

MASTER OF SCIENCE

Abstract

Angular distributions are presented for the $^{18}O(p,\alpha)^{15}N$ reaction , leading to several excited states of ^{15}N , at an incident proton energy of 40.93 MeV . The data was taken using a gas target using the high resolution facilities of the University of Manitoba Cyclotron . The extracted cross sections were compared with cluster form factor calculations using the finite range DWBA code DWUCK5 .

A peak fitting method , employing a peak model which explicitly accounts for the phenomena of "binning" in digital spectra is presented . Use is made of spline techniques to create a continuous , "area true " model from peaks taken from actual spectra . The fitting routine employs a Newton - Raphson iterative technique to solve the non-linear fitting equations , using the Poisson statistical distribution .

Acknowledgments

I would like to thank my advisor , Dr. W. Falk for his ideas and assistance concerning the investigations presented in this thesis .

I would also like to thank Dr. R. Abegg , Dr. O.A. Abouzeid , Dr. S. Datta , Dr. N. Davison , and Dr. S.P. Kwan for their assistance throughout the undertaking of this investigation .

Thanks also go to the computer and technical staff for their support .

Finally I would like to thank the Natural Sciences and Engineering Research Council for their financial support.

Table of Contents

Table of Contents (cont.)

Introduction

The subject matter of this thesis is divided into two major categories . One is the problem of fitting peaks in nuclear spectra containing narrow peak distributions , where the effect of "binning " of peaks is important . The other is the extraction and subsequent Distorted Wave Born Approximation (DWBA) analysis of several differential cross sections for states populated in the $^{18}O(p,\alpha)^{15}N$ reaction at E_p= 40.93 MeV .

The peak fitting method described in Chapter 2 utilizes a peak model which represents the measured peaks as histograms . These histograms are generated by integrating a continuous " underlying" peak function over a channel width and taking the value of this integration to be the value of the histogram over the channel width . Since the point on the continuous function at which the integration begins is arbitrary , an additional parameter , termed the "boundary shift" parameter , must be introduced to accurately characterize the peak .

Since a theoretical shape for the spectral peaks is often unavailable or inaccurate , a method of generating an approximation to this shape from an actual spectral histogram was developed . Use was made of an "area-true" spline polynomial interpolation to generate the underlying continuous function .

A computer code was written to solve the set of non-linear equations which must be solved to maximize the Poisson probability of the fit of the model to the data. The code utilized a Newton-Raphson technique in the solution of the equations .

In Chapter 3 DWBA calculations using the finite range DWUCK5 code are carried out and compared with the measured cross sections . The states excited by the $^{18}O(p,\alpha)^{15}N$ pickup reaction are compared with those of the $^{12}C(\alpha,p)^{15}N$ transfer reaction .

The study of a nuclear pickup or transfer reaction in the context that the reaction occurs in a single , "direct" step , should make a statement concerning the nature of the structure of the nucleus and the reaction mechanism itself . In the conventional form of the DWBA analysis the nucleons are assumed to be picked up out of spherical shell model levels characterized by definate nodal and angular momentum properties ((N,L) respectively) . The particle - hole nature of the nucleus may be investigated in this context . For instance, a state which is excited by the $^{18}O(p,\alpha)^{15}N$ reaction , but not by the $^{12}C(\alpha,p)^{15}N$ reaction , probably has a configuration containing a hole in the ^{12}C core of the residual ^{15}N state . In the DWBA calculations , the transferred cluster of three nucleons is represented as a single triton bound to a nuclear potential well , while the incoming

proton and alpha potential are represented by the Optical Model .

Chapter One

Experimental Considerations

The experiment was performed using the high resolution beam line of the University of Manitoba sector focused cyclotron , at an incident proton energy of 40.93 MeV using the associated 56 cm. scattering chamber . Figure 1-1 shows a floor plan of the laboratory .

The design [1] of the high resolution apparatus is such that the energy resolution , ΔE , of the beam on target is given by $\Delta E/E=5X10^{-4}$,FWHM , where E is the incident energy. The expected beam energy resolution for this experiment is therefore approximately 20keV FWHM . The beam intensity , measured in the Faraday cup , was typically 10 nA to 20 nA .

1-1 Target System , Detectors , and Electronics

The experimental set up of the target system was typical of gas cell experiments [2] (see fig. 1-2). For this particular set of experiments , a gas target system designed by Dr. R. Abegg was used . The target was built so as to take up as little volume as possible in the tubes carrying the gas to the cell. The target material consisted of 99% (manufacturer's estimate) ^{18}O gas purchased from the Monsanto Research Corporation . Incorporated into the cell was a National Semiconductor LX3702A pressure transducer .

The pressure transducer yielded straight calibration lines in the 0-15 PSI range with typical RMS deviations

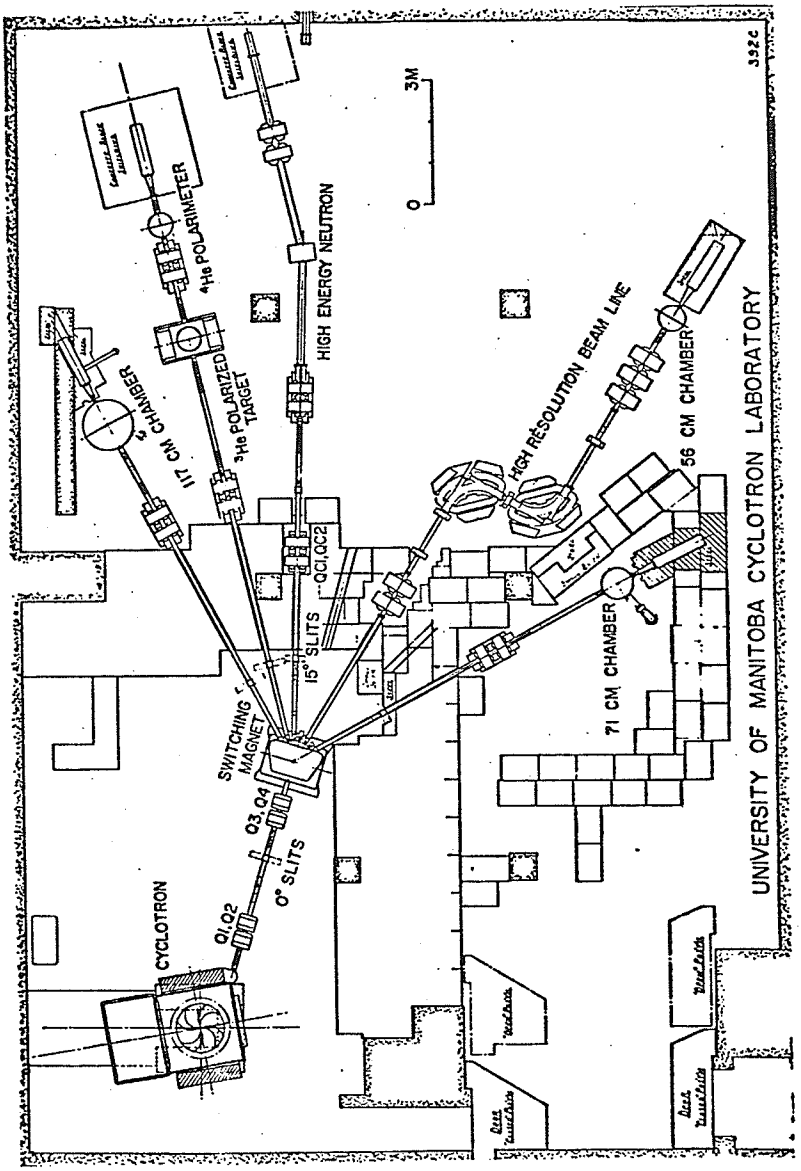
UNIVERSITY OF MANITOBA CYCLOTRON LABORATORY
3926
3M
0
CYCLOTRON
Q1,Q2
0° SLITS
Q3,Q4
SWITCHING MAGNET
15° SLITS
QC1,QC2
117 CM CHAMBER
4He POLARIZED TARGET
4He POLARIMETER
HIGH ENERGY NEUTRON
HIGH RESOLUTION BEAM LINE
56 CM CHAMBER
71 CM CHAMBER

Figure 1-1

.01 PSI . It was found that the pressure transducer generated considerable heat if left on continuously , requiring that it be promptly shut off after a measurement of the pressure . It was assumed that the gas within the cell was at room temperature , which was typically 19-22 degrees Celsius throughout the experiment .

The target gas was contained in a gas cell with 1/3 mil Kapton foil for the side window and beam entry port . The foil was attached to the cell with "Versamid 140" epoxy resin and curing agent .

Gas pressures of .2 - .3 atm. ^{18}O were used . This choice was used to avoid excess strain on the epoxy bond between the Kapton window and target cell , and to avoid excess broadening of the peaks due to straggling (the estimated straggling contributions to the peak at .2 atm. is 40keV FWHM , this will be discussed later) .

When filled with gas , the cell leaked gas at a slow rate . During the first experiment the cell leaked 10% of its gas over several days . During the second experiment the cell pressure decreased rapidly over a few hours . After dismantling the cell , it was found that the rubber "O" rings used in the cell had crumbled into powder . This was probably due to the oxidation of the rubber "O" ring by the oxygen within the cell . This problem had also been observed in other experiments performed at this laboratory.

Four 1mm silcon surface barrier detectors were used

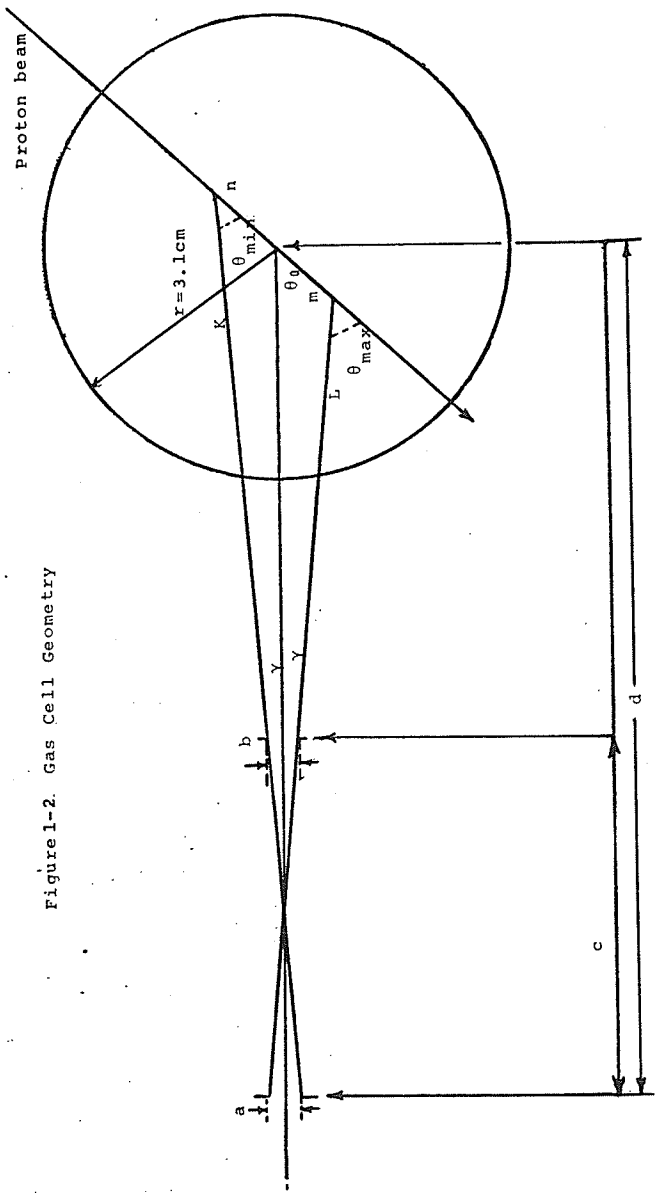

Figure 1-2. Gas Cell Geometry

to detect the alpha particles . This thickness allows the detection of alpha particles in the E_α =26-50 MeV range. Triton particles of energy below 19! MeV will be stopped in 1mm Silicon , while those with an energy greater than 19 MeV will pass through the detector . The $^{18}O(p,He^3)^{16}N$ g.s. reaction has a Q-value of -14.104 MeV , which gives He^3 laboratory energies of approximately 17 MeV in ^{15}N .

The detector setup for the detection of alpha particles was simple . Single detectors were connected to ORTEC pre-amplifiers which in turn were connected to ORTEC spectroscopic amplifiers . The signals from the spectroscopic amplifiers were transmitted to Northern Scientific ADC's , in conjunction with a data accumulation program MIRAD , produced 2048 channel digital spectra . The energy per channel was pre-set to be approximately 22 keV using an Am^{241} alpha source mounted in front of the detectors .

A Faraday cup was used to measure the total charge , and hence the total number of protons which passed through the target cell . This allows an absolute normalization to be assigned to the cross sections .

Two NaI detectors were mounted outside the chamber in order to monitor proton scattering from the target . The ratio of the number of protons scattered into the detector and total counts in the Faraday cup should be constant throughout the experiment .

1-2 Extraction of Cross Sections

In the calculation of differential cross sections measured using a gas target cell , the geometrical aspects of the target and detector system must be taken into account. All of the geometrical properties may be subsumed into one parameter termed the "G-factor" (geometrical factor) . The cross section in terms of the G-factor is defined by:

$$\sigma(\theta_0) = Y\sin(\theta_0)/(nNG) \qquad 1\text{-}1$$

where Y=yield

N=number density of particles in target

n=total number of incident projectiles

θ_0=scattering angle

Silverstein[3] has published an extensive survey concerning the calculation of the G-factor in various geometries . In the experiment described in this thesis , two rectangular slits were used to define the "active area" within the target .

Assuming that the beam is a straight line , Silverstein has developed an expansion giving the G-factor as a function of the cross section and geometrical parameters :

$$G=G_{00}(1+\Delta_0+\Delta_1\, d\sigma(\theta_0)/d\theta_0/\sigma(\theta_0) + \Delta_2 d^2\sigma(\theta_0)/d^2\theta_0/(\sigma(\theta_0))+\ldots) \qquad 1\text{-}2$$

where

$$G_{00}= ab\ell/(R_0h)$$

$$\Delta_0=1/12\ c^2/s^2\ a^2/R_0^2-1/8h^2(a^2+b^2)-1/8\ell^2/R_0^2$$

$$\Delta_1 = 1/2\left(\ell^2/(8R_0^2) - a^2/(4R_0 h)\right)$$

$$\Delta_2 = 1/24(a^2+b^2)/h^2 \quad \text{etc.}$$

where (see figure 1-2)

$c, s = \cos(\theta_0), \sin(\theta_0)$

ℓ = length of backward† slit

b = width of front† slit

a = width of back slit

h = back-front slit separation

R_0 = distance along the centerline of the slit , from the cell center to the detector .

Only the first two terms were used in the calculation, since the higher order corrections are small .

The peak area yields were extracted using a computer program SPECTD which utilizes the fitting method outlined in chapter 2 . Appendix 1 lists tables and graphs of the cross sections for the states analyzed . A program JANUS1 was written which is capable of taking as input the peak areas and geometrical variables , and computing the cross sections in both laboratory and center of mass frames As well, it will plot the center of mass data on a Calcomp plotter. Only the statistical error is quoted.

†The slit furthest from the gas cell is denoted the "backward" slit , while the slit closest to the gas cell is denoted the "front" slit.

1-3 Slit Geometry , Resolution , and Calibration

When a gas cell is used as a container for the target nuclei , a pair of slits must be used to define an "active area " within the target . A detector placed behind the rear slit at an angle θ_0 will detect reactions in which particles emerge through a range of angles $\theta_{min}<\theta<\theta_{max}$, creating a range of energies which will be recorded in the spectrum . Figure 1-2 , displays a schematic representation of the slit - gas target system (the slit widths are normally much narrower , 0.5-2. mm) . In the diagram r is the radius of the gas cell , a and b are the widths of the back and front slits , respectively , c is the separation between the slits , d is the distance between the back slit and cell center , and θ_0 is the scattering angle along the centerline defined by the slits . All other parameters in the diagram can be defined in terms of these variables .

An inspection of figure 1-2 shows that the distances travelled by an emerging particle through the target medium is dependent upon the angle θ_0 and its position of origin within the active area . In traversing the Kapton window and target gas , both the incident protons and scattered particles lose energy . What is ultimately recorded in the spectrum is a reaction occurring throughout a small range of proton energies , the scattered particles subsequently emerging through a range of angles and energies .From figure 1-2 , it is seen that as the scattering angle

within the active area is decreased , the pathlength of the particle through the target is increased . Since the energy of the scattered particle increases with decreasing angle (a result of reaction kinematics) , the particle's energy loss will increase with increasing energy .

The extreme limits of the "kinematic" energy spread occur at the endpoints of the active angle range at θ_{min} and θ_{max} . In order to evaluate the energies of the particles emerging from the Kapton window , the following parameters must be determined : the angles θ_{min} and θ_{max} , the distances K and L , and the distances m and n . From figure 1-2 we have :

$$\gamma = \tan^{-1}((a+b)/(2c)) \simeq (a+b)/(2c) \text{ radians} \qquad 1\text{-}3$$

where the small angle approximation has been used , since the slits are assumed to be narrow , and c>>a+b .

Now ,

$$\theta_{max} = \pi - (\pi - \theta_0 - \gamma) = \theta_0 + \gamma \qquad 1\text{-}4a)$$

and

$$\theta_{min} = \pi - (\gamma + \pi - \theta_0) = \theta_0 - \gamma \qquad 1\text{-}4b)$$

thus the angular spread is ,

$$\theta_{max} - \theta_{min} = 2\gamma = (a+b)/c \qquad 1\text{-}5$$

For the experiment which is the subject of this thesis the angular spread ranged from approximately 1. - 2. degrees . In the evaluation of m and n we have :

$$m = p \cdot \sin(\gamma)/\sin(\theta_{max}) = p \cdot \sin(\gamma)/\sin(\theta+\gamma) \qquad 1\text{-}6a)$$

and

$$n = p \cdot \sin(\gamma)/\sin(\theta_{min}) = p \cdot \sin(\gamma)/\sin(\theta+\gamma) \qquad 1\text{-}6b)$$

where $p = d - ac/(a+b)$

The distance K may be determined from the relations ,

$$r^2=n^2+K^2-2nK\cos(\theta_0-\gamma) \qquad 1\text{-}7$$

which yields ,

$$K=n\cdot\cos(\theta_0-\gamma) \pm \sqrt{n^2\cos^2(\theta_0-\gamma)-(n-r)(n+r)} \qquad 1\text{-}8a)$$

similarly ,

$$L=m\cdot\cos(\pi-\theta_0-\gamma)\pm\sqrt{m^2\cos^2(\pi-\theta_0-\gamma)-(m-r)(m+r)} \qquad 1\text{-}8b)$$

The negative root is ignored since K and L must be positive . Inserting the values of m and n into these expressions yields ,

$$K=p\cdot\sin(\gamma)\cot(\theta_0-\gamma)+\sqrt{r^2-\sin^2(\gamma)\cdot p^2} \qquad 1\text{-}9a)$$

and

$$L=\sqrt{r^2-\sin^2(\gamma)\cdot p^2} \quad -p\cdot\cot(\theta_0+\gamma)\sin(\gamma) \qquad 1\text{-}9b)$$

Thus the energies of particles traversing the gas cell, scattered at angles θ_{min} and θ_{max} will be :

$$E_{\theta_{min}} = E(\theta_{min})_{reaction} - K\cdot(dE/dx)_{gas} - \Delta E_{Kapton} \qquad 1\text{-}10a)$$

and

$$E_{max} = E(\theta_{max})_{reaction} - L\cdot(dE/dx)_{gas} - \Delta E_{Kapton} \qquad 1\text{-}10b)$$

Where $E_{reaction}$ is determined by the kinematics of the reaction of interest .

Figure 1-3 shows the dependence of the difference $\left|E_{max}-E_{min}\right|$ on the scattering angle for a particular slit configuration (the energies are those measured at the detector). Table 1-1 lists several of the variables used

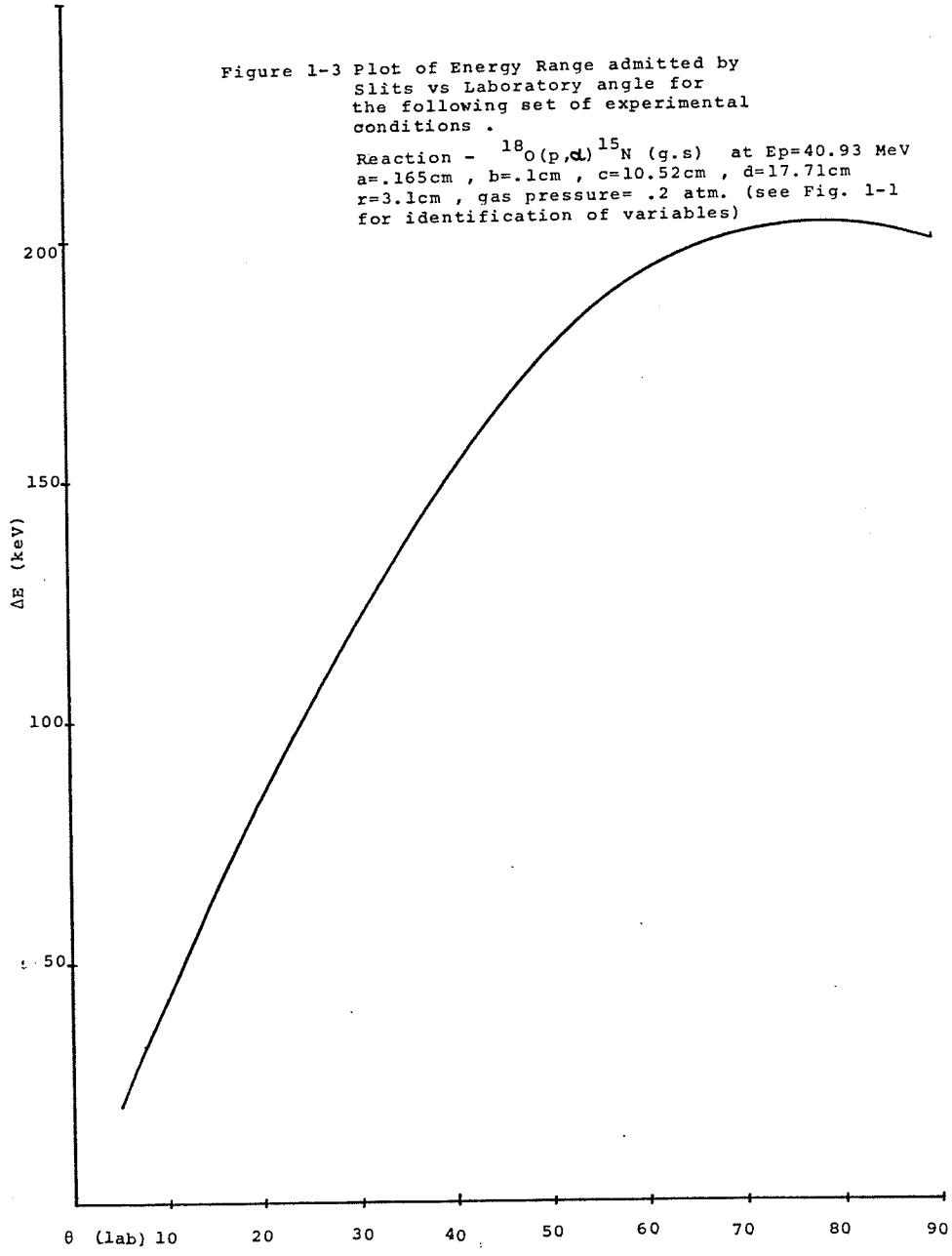

Figure 1-3 Plot of Energy Range admitted by Slits vs Laboratory angle for the following set of experimental conditions .

Reaction - $^{18}O(p,\alpha)^{15}N$ (g.s) at Ep=40.93 MeV
a=.165cm , b=.1cm , c=10.52cm , d=17.71cm
r=3.1cm , gas pressure= .2 atm. (see Fig. 1-1 for identification of variables)

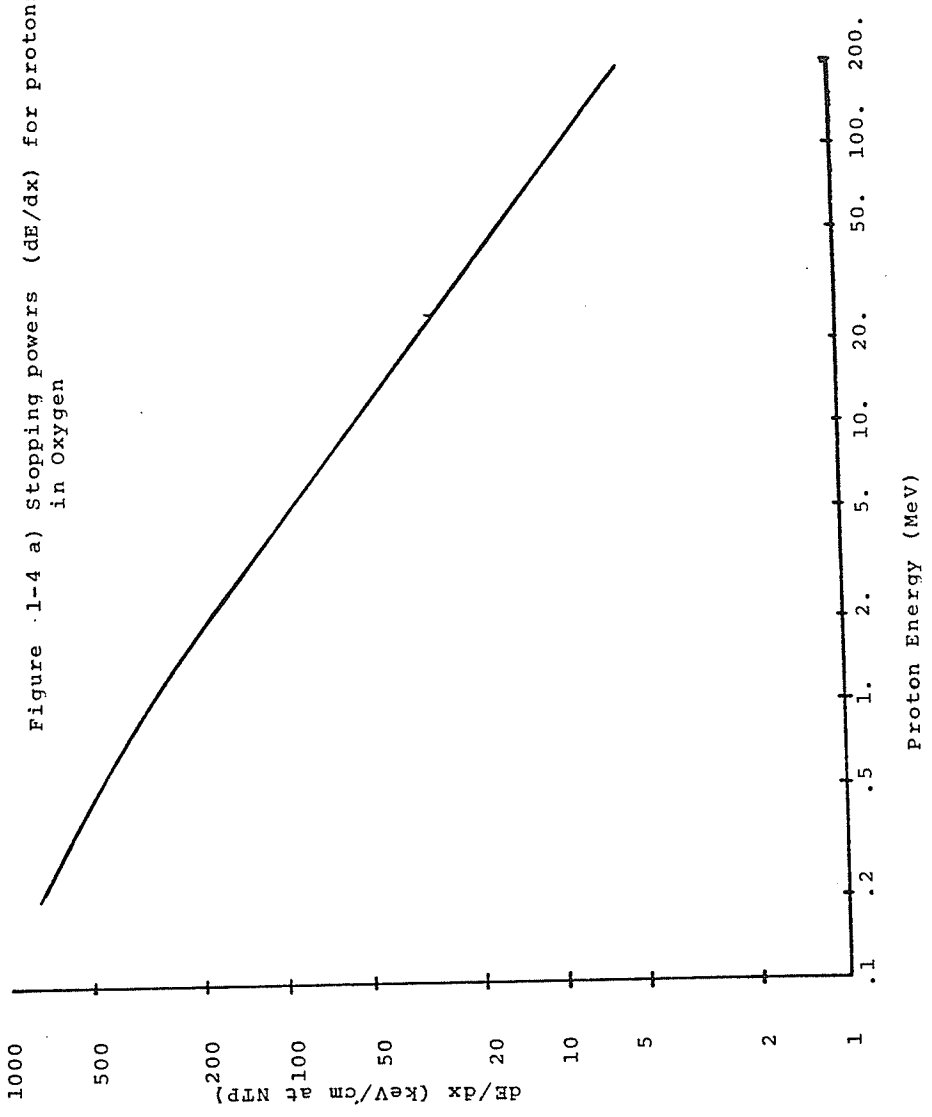

Figure 1-4 a) Stopping powers (dE/dx) for protons in Oxygen

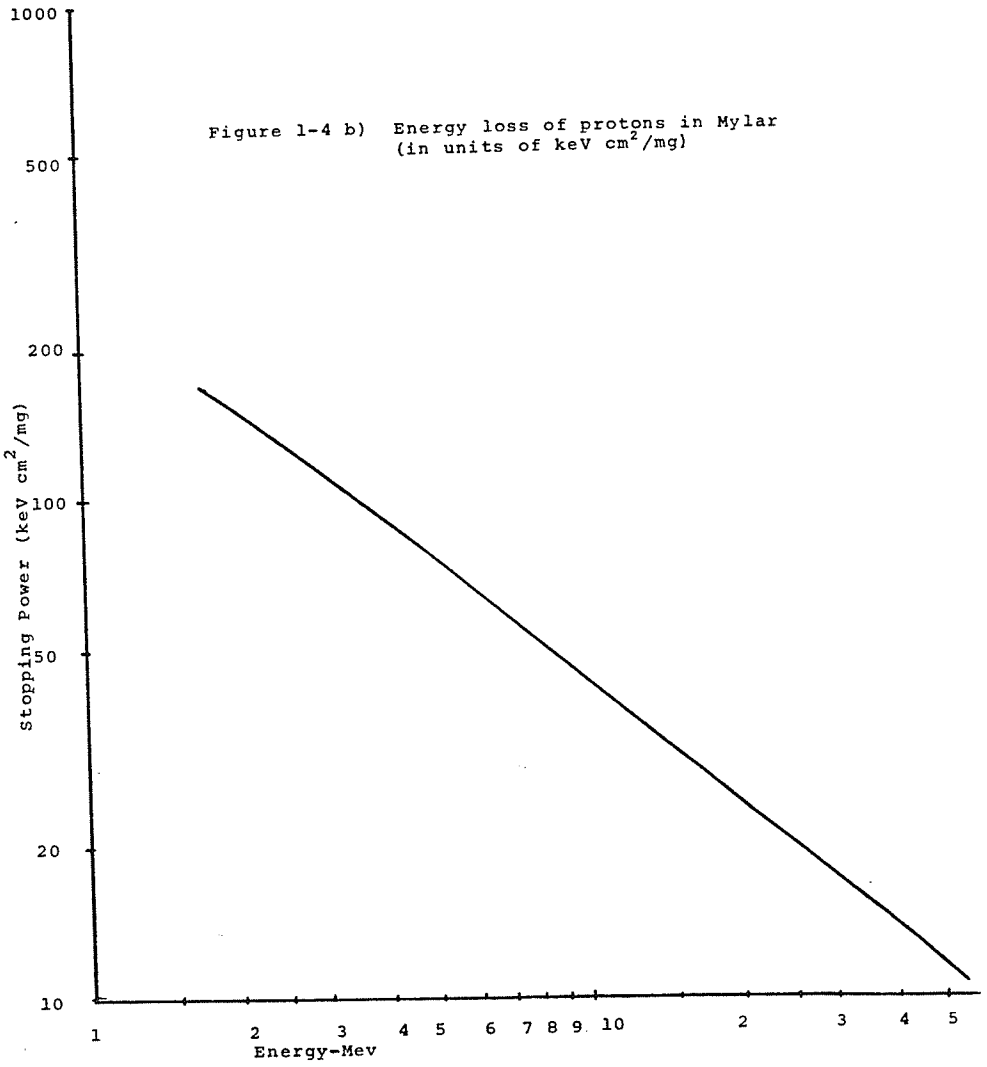

Figure 1-4 b) Energy loss of protons in Mylar (in units of keV cm^2/mg)

in the calculation . The values for the energy loss of the particles in ^{16}O gas were obtained from references 4 and 9 , and are reproduced in fig. 1-4 a) . The energy loss characteristics of Kapton were assumed to be similar to those of Mylar ; fig. 1-4b) shows a plot of the energy loss characteristics of Mylar[10]. In order to transform the proton energy loss to alpha energy losses , use has been made of the approximate expression[4],

$$(dE/dx)_{E_\alpha} = 4(dE/dx)_{E_p}/4 \qquad 1\text{-}11$$

The energy losses were calculated using a computer program RESOL which calculated the energy losses of the proton and alpha particles using the formulae derived previously . The program interpolated values of stopping powers from a set of values stored in the computer . The density of Kapton[4] was taken to be $\simeq 1.11$ gm/cm^3 which gives an energy loss of approximately 13 keV in 1/3 mil Kapton (see fig 1-4b) for 41 MeV protons . The energy loss of 41 MeV protons in ^{16}O gas at NTP is approximately 19 keV/cm , which gives an energy loss of $\simeq$11 keV when the proton travels through 3.1 cm of 0.2 atm. ^{16}O gas . The total loss of the proton to the center of the gas cell is typically 24 keV . The combined energy loss of the alpha particles through the Kapton and 3.1 cm of .2 atm gas ranged from 298 keV at E_α=41 MeV to 410 keV at E_α= 28 MeV . These values were calculated using the program

Table 1-1 Various Slit Geometry parameters
(see bottom of page for description of variables)
Rear slit width=16.5 cm. Front slit width=1.0 cm.
Slit separation=10.52 cm. , distance from cell center to rear slit=17.7cm , cell radius =3.1 cm.
$^{18}O(p,\alpha)^{15}N$ g.s. , E_p=40.93 MeV

θ_0		10	20	30	40	50	60	70	80	90
ΔE_p(K)		0.013	0.013	0.013	0.013	0.013	0.013	0.013	0.013	0.013
E_p(gas)	1	0.010	0.012	0.013	0.013	0.013	0.013	0.014	0.014	0.014
	2	0.018	0.016	0.015	0.015	0.015	0.015	0.015	0.015	0.015
	3	0.014	0.014	0.014	0.014	0.014	0.014	0.014	0.014	0.014
$E_{p'}$	1	40.907	40.905	40.904	40.904	40.904	40.904	40.904	40.904	40.903
	2	40.899	40.901	40.902	40.902	40.902	40.902	40.902	40.902	40.902
	3	40.903	40.903	40.903	40.903	40.903	40.903	40.903	40.903	40.903
θ	1	9.278	19.278	29.278	39.278	49.278	59.278	69.278	79.278	89.278
	2	10.722	20.722	30.722	40.722	50.722	60.722	70.722	80.722	90.722
	3	10.000	20.000	30.000	40.000	50.000	60.000	70.000	80.000	90.000
E_α	1	41.924	41.498	40.803	39.868	38.737	37.461	36.094	34.686	33.289
	2	41.872	41.410	40.678	39.713	38.558	37.266	35.890	34.482	33.090
	3	41.899	41.456	40.741	39.791	38.648	37.364	35.992	34.584	33.189
ΔE_α(gas)	1	0.217	0.193	0.187	0.186	0.188	0.191	0.194	0.199	0.204
	2	0.129	0.151	0.161	0.168	0.175	0.182	0.189	0.197	0.205
	3	0.170	0.171	0.174	0.177	0.181	0.186	0.192	0.198	0.205
ΔE_α(K)	1	0.158	0.159	0.162	0.164	0.167	0.175	0.177	0.179	0.183
	2	0.158	0.160	0.162	0.165	0.167	0.175	0.177	0.179	0.183
	3	0.158	0.159	0.162	0.165	0.167	0.175	0.177	0.179	0.183
$E_{\alpha'}$	1	41.549	41.146	40.454	39.517	38.383	37.096	35.722	34.309	32.903
	2	41.585	41.100	40.356	39.380	38.216	36.909	35.524	34.106	32.701
	3	41.571	41.125	40.406	39.449	38.300	37.003	35.623	34.207	32.802
$(E^1_{\alpha'}+E^2_{\alpha'})/2$		41.567	41.123	40.405	39.449	38.299	37.003	35.623	34.207	32.802

For each of the variables , Row 1 corresponds to θ_{min}

Row 2 " " " θ_{max}

Row 3 " " " θ_0

ΔE_p(K)= Energy loss of proton in Kapton (MeV)

ΔE_p(gas)= Energy loss of proton in gas (MeV)

$E_{p'}$= Proton energy involved in (p,α) reaction (MeV)

θ = Scattering angle of alpha (lab. , deg.)

E_α = Energy of alpha emitted in reaction (MeV)

ΔE_α(gas)= Energy loss of alpha in gas (MeV)

ΔE_α(K) = Energy loss of alpha in Kapton (MeV)

$E_{\alpha'}$ = Energy of alpha at detector (MeV)

Note: The superscripts denoting the variables in the last row refer to rows 1 and 2 of $E_{\alpha'}$.

RESOL .

The previous considerations were derived solely from the kinematic properties and geometry of the slit and target configuration . There exist two other major sources of peak broadening which are statistical in nature . They arise from the spread in the incident proton energy , and spreading inherent in the electronics and data accumulation equipment , and energy loss straggling of the particles travelling through the gas and Kapton . The spread due to the beam energy and electronics is assumed to be gaussian in nature , with halfwidths of approximately 20 keV and 35 keV respectively [1,7] .

The straggling distributions for the target thickness used in this experiment follow a Landau distribution , which has been discussed at length in the literature [5,6] . The energy spread (FWHM) of the alpha particles for a typical target thickness (0.2 atm.) used in the experiment described by this thesis was calculated by the computer code STRAGL [8] , available at the University of Manitoba . The FWHM ranged from 42 keV at E_α= 26 MeV to 39.9 keV at E_α=40 MeV . For the Kapton foil , the FWHM was similar with a typical value of 41 keV FWHM . Assuming the distributions contributing to the energy spread from statistical processes are approximately gaussian , the FWHM arising from these may be obtained by summing the individual FWHM's

in quadrature . This yields ,

$$\sigma \simeq \sqrt{\sigma^2_{\text{beam}} + \sigma^2_{\substack{\text{detector} \\ \text{electronics}}} + \sigma^2_{\substack{\text{straggling} \\ \text{(gas)}}} + \sigma^2_{\substack{\text{straggling} \\ \text{(Kapton)}}}}$$

$$\simeq \sqrt{20^2 + 35^2 + 40^2 + 41^2} = 70\text{keV}$$

This is the best resolution that can be obtained with the given conditions . When this is folded with the kinematic spread (see fig. 1-3) it is evident that the expected resolution will be much worse . In the actual experiment the best resolution obtained was roughly 100 keV FWHM .

1-4 Energy Calibration of the Spectra using known energy states

The excited states were identified by calibration of the spectra using the energies and channel centroids of the known states present in the spectra . The energies were calculated by taking the average values of the extreme energies calculated as discussed in the previous section . This average energy only differed by 1 or 2 keV from that calculated at θ_0. A spectrum was taken with .074 atm. ^{16}O added to the 0.23 atm. ^{18}O in the gas target for calibration purposes . The cross sections for the $^{16}O(p,\alpha)^{13}N$ reaction are greater than the $^{18}O(p,\alpha)^{15}N$ reaction , resulting in large , well defined peaks corresponding to known low-lying states of ^{13}N . It is important that the calibration is carried out for two different angles . The rate of change of alpha energy with respect to angle

Table 1-2 Results of Calibration

Proton Energy = 41.217 MeV
Barred quantities are the result of calculations using the calibration line .
The calibration line was obtained from a least square fit of the detector energy to the channel centroids .

1-2 a) $\theta = 13.45^{\circ}$, $\bar{E}_{detector} = \bar{x} \cdot 2.261407 \times 10^{-2} - .346684$ MeV .

State (J ,E)	Channel centroid	E at detector	E at gas cell centre	$\bar{E}$ at detector	$\bar{E}$ at gas cell centre	$E-\bar{E}$ keV	Q^{*}	$\bar{Q}^{*}$	$Q-\bar{Q}$ keV	Q literature
$1/2^{-}$,g.s	1858.3	41.688	42.067	41.677	42.056	11	3.973	3.961	12	3.9799
$3/2^{-}$,6.32	1610.4	36.064	36.489	36.071	36.496	-7	-2.351	-2.343	-8	-2.344
$7/2^{+}$,7.57	1561.6	34.954	35.386	34.967	35.399	-13	-3.594	-3.58	-14	-3.588
0^{+};g.s.†	1483.9	33.212	33.659	33.210	33.656	3	-5.224	-5.227	3	-5.218
$3/2^{-}$,3.51†	1346.1	30.088	30.572	30.094	30.577	-5	-8.74	-8.73	-1	-8.729
$5/2^{-}$,7.38†	1191.3	26.605	27.144	26.593	26.132	12	-12.601	-12.614	13	-12.594

$\sigma_{E-\bar{E}} = 9.3$ keV $\sigma_{Q-\bar{Q}} = 9.9$ keV $\sigma_{\bar{Q}-Q_{literature}} = 9.5$ keV

1-2 b) $\theta = 23.43^{\circ}$, $\bar{E}_{detector} = \bar{x} \cdot 2.2498 \times 10^{-2} - .339334$ MeV

State	Channel centroid	E at detector	E at gas cell centre	$\bar{E}$ at detector	$\bar{E}$ at gas cell centre	$E-\bar{E}$ keV	Q^{*}	$\bar{Q}^{*}$	$Q-\bar{Q}$ keV	Q literature
$1/2^{-}$,g.s.	1843.8	41.144	41.527	41.143	41.526	1	3.975	3.975	0	3.9799
$3/2^{-}$,6.32	1595.4	35.555	35.983	35.555	35.983	0	-2.347	-2.347	0	-2.344
7/2+,7.57	1546.1	34.452	34.888	34.445	34.881	7	-3.589	-3.589	8	-3.588
0^{+},g.s.†	1466.7	32.652	33.104	32.659	33.111	-7	-5.221	-5.213	-8	-5.218
$3/2^{-}$,3.51†	1328.8	29.549	30.039	29.556	30.047	-7	-8.733	-8.724	-9	8.729
$5/2^{-}$,7.38†	1174.5	26.091	26.639	26.085	26.633	6	-12.597	-12.604	7	-12.594

$\sigma_{E-\bar{E}} = 6.1$ keV $\sigma_{Q-\bar{Q}} = 6.6$ keV $\sigma_{\bar{Q}-Q_{literature}} = 6.6$ keV

† These states arise from the $^{16}O(p,\alpha)^{13}N$

* Q-values were calculated using E at the gas cell centre, and relativistic kinematics.

Table 1-3 Identification of some ^{15}N states in the spectra (from the 23.43 spectra, see Table 1-3). Energies are given in units of MeV .

$\bar{x}$	$\bar{E}$	$\bar{E}_{reaction}$	$\bar{Q}$	$\bar{E}_{ex}$(MeV)	E_{table}
1636.96	36.49	36.912	-1.291	5.266	(5.2704) *
1546.09	34.445	34.881	-3.597	5.572	(7.567)
1556.39	34.677	35.111	-3.337	7.312	(7.301)
1483.27	33.032	33.48	-5.183	9.158	(9.152 , 9.155)
1457.24	32.446	32.900	-5.839	9.814	(9.829)
1421.44	31.641	32.104	-6.737	10.712	(10.693 , 10.702)
1400.02	31.159	31.628	-7.273	11.248	(11.235)
1392.44	30.989	31.46	-7.463	11.438	(11.438)
1365.61	30.385	30.864	-8.133	12.108	(12.095)
1348.56	30.001	30.486	-8.558	12.533	(12.522 , 12.559)
1285.82	28.59	29.095	-10.119	14.094	(14.09 , 14.1)
1279.02	28.437	28.945	-10.287	14.262	(14.24)
1193.41	26.510	27.051	-12.403	16.378	(16.39)
1186.07	26.345	26.889	-12.584	16.559	(16.576)

* Bracketed quantities refer to nearby states taken from the literature .

The relativistic formula for the Q-value is given by[4)]

$$Q=M_1+M_2-M_3-(M_1^2+M_2^2+M_3^2+2M_2E_1-2E_3(E_1+M_2)+2P_1P_3\cos(\psi))^{\frac{1}{2}}$$

where ,

M_1= proton mass (938.304 MeV)

M_2= target (^{18}O) mass (16766.289 MeV)

M_3=alpha mass (3727.413 MeV)

E_1= total proton energy

E_3=total alpha energy

P_1= proton momentum

P_3= alpha momentum

ψ = laboratory scattering angle of alpah particle .

$(dE/d\theta)$ depends on the particular reaction taking place ; it may be termed the "signature " of the reaction . Thus if a particular state , assumed to be the result of a particular reaction , yields the same excitation energy at two different angles , it is fairly certain that its identity was not mistaken .

The centroids of these peaks were calculated and a least-square straight line of the form E=mx+b was fitted to these points , giving the measured spectrum energy as as function of the spectrum channel number . The difference between the energy values calculated from the line and those used for the fit averaged about 8 keV or about .03% of the actual energy . Table 1-2 shows the results of the calibration . Table 1-3 shows the energy values of the unknown peaks in the spectra as well as their associated excitation energies . These were calculated by adding the energy losses in the gas and foil to the spectrum energies and subsequently calculating the Q-values for the reactions using relativistic kinematics . Several peaks from nuclei other than ^{18}O are present , most notably the ^{16}O states , and a small contribution from ^{17}O. Although the calibrated spectra yielded many identifiable states , their angular distributions were not all extractable due to poor statistics and resolution in spectra of higher angles . Figure 1-5 shows a comparison of the ^{16}O enriched spectrum with a normal ^{18}O spectrum , the ^{16}O peaks are evident in the diagram .

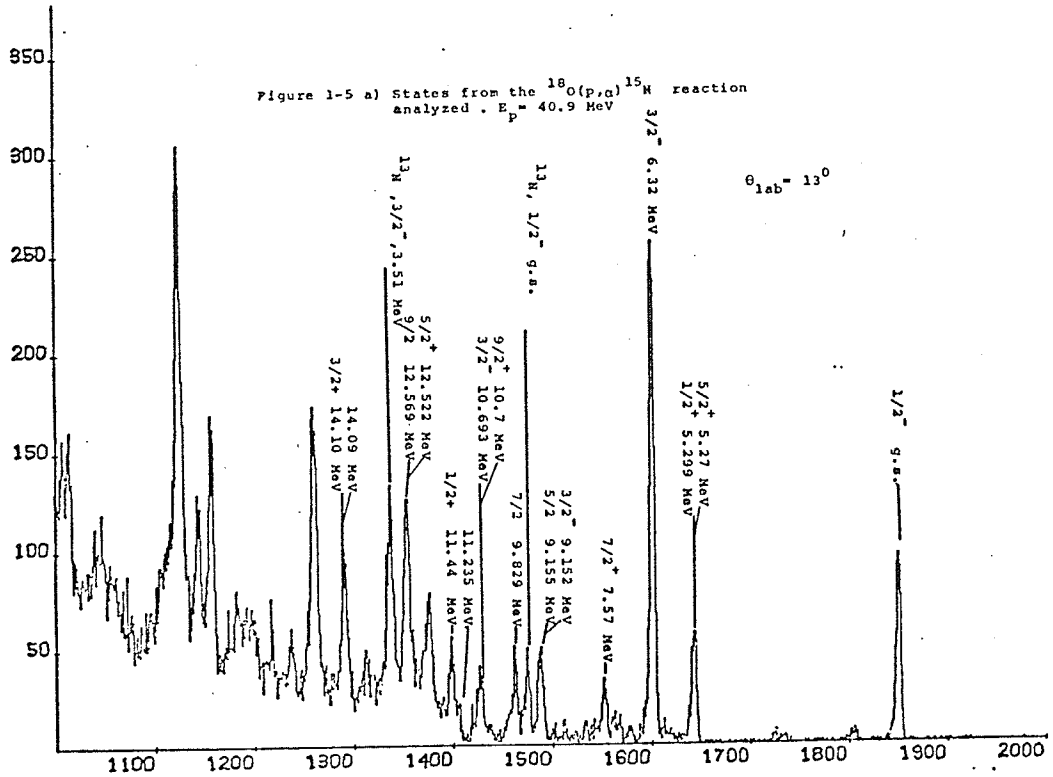

Figure 1-5 a) States from the ^{18}O(p,α)^{15}N reaction analyzed . E_p = 40.9 MeV

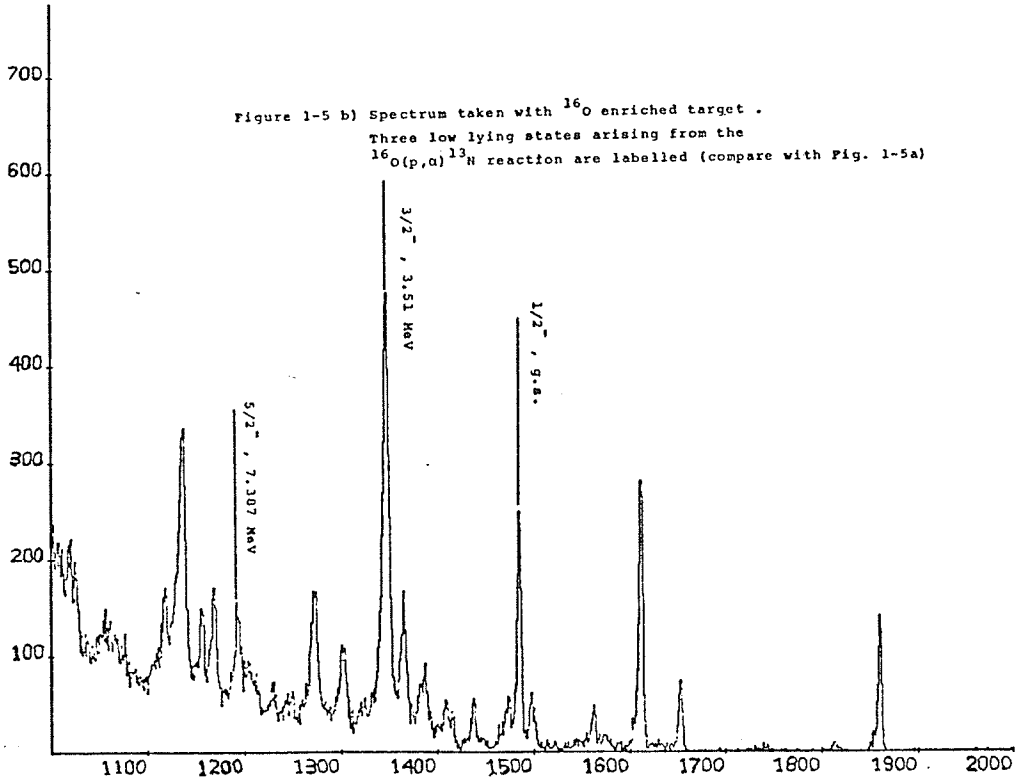

Figure 1-5 b) Spectrum taken with ^{16}O enriched target .
Three low lying states arising from the
^{16}O(p,α)^{13}N reaction are labelled (compare with Fig. 1-5a)

Chapter Two-Spectrum Analysis

The data accumulated in digital multichannel analyzers consists of histograms representing the number of electronic pulses (generated by the energy loss of particles in detectors) , accumulated in specific voltage ranges determined by the MCA . The spectra , when considered as continuous functions of energy , may be described by the equation:

$$\sum_i C_i f(E-E_i) + B(E) \qquad 2\text{-}1$$

where the C_i are peak areas, f_i are normalized peak functions , B(E) is a background function, and the E_i are the positions (relative to some definite point of the peak function) of the various peaks . Let the boundaries of the channel n be denoted by $(n-1)\Delta E$ and ΔE . Furthermore , let the position of peak i be expressed as an integral multiple of ΔE, plus a small quantity ε_i . Thus $E_i = m_i \Delta E + \varepsilon_i$, m an integer . Then the quantity measured in channel n of the histogram will be given by,

$$H_n = \int_{(n-1)\Delta E}^{n\Delta E} \left(\sum_i (C_i f(E-m_i \Delta E-\varepsilon_i)) \right) dE \qquad 2\text{-}2$$

The histogram peak shape is determined by the location of the E_i relative to thr channel boundaries . The problems of analysis of spectra of the type measured in this experiment fall into two categories :

a) Defining an appropriate model containing adjustable variables pertinent to the data measured .

b) Finding the set of adjustable variables such that the probability of measuring the data set with respect to the model function is maximized .

The remainder of this chapter will be concerned with the problems outlined in a) and b) .

2.1 The Peak Model

The underlying peak function which determines the shape of the peaks in the spectra is a superposition of various probability distributions considered in Chapter 1 . The distribution arising from purely kinematic and geometric aspects of the measurement is strongly affected by the particular angle at which the spectra is measured . As a result of this , each spectrum has its own distinctive peak shape . Due to the difficulty in defining a model for the " theoretical " peak shape , a model can be generated using an actual histogram peak taken from individual spectra , using an area-true quintic spline interpolation developed by Spath [11].

An interpolating spline function S(x) to a set of n points (x_k, y_k) k=1,n , is a set of n-1 polynomials of order 2m+1 , $S_k(x)$, defined on the intervals (x_k, x_{k+1}) , k=1,...,n-1 , such that the function passes

through the points (x_k, y_k) and is always 2m times differentiable at these points . A commonly used form of spline interpolation are natural splines , which have the property $(d^i S/dx^i)_{x=x_1} = (d^i S/dx^i)_{x=x_n} = 0$, $(i=m+1,\ldots,2m)$.

The conditions stated supply the $2(m+1)(n-1)$ equations necessary to calculate the coefficients of the n-1 polynomials of order $2m+1$ [11] . The conditions are listed to convince the reader :

$S_k(x_k) = y_k$	$k=1,n-1$	(n-1) conditions	2-3a)
$S_k(x_{k+1}) = y_{k+1}$	$k=1,n-1$	(n-1) conditions	2-3b)
$(d^i S_k/dx^i)_{x=x_{k+1}} = (d^i S_{k+1}/dx^i)_{x=x_{k+1}}$	$i=1,2m$ $k=1,n-2$	2m(n-2) conditions	2-3c)
$(d^i S_1/dx^i)_{x=x_1} = (d^i S_{n-1}/dx^i)_{x=x_n} = 0$	$i=m+1,2m$	2m conditions	2-3d)
		2(m+1)(n-1) Total	

These functions have the property that they minimize the quantity :

$$\int_{x_1}^{x_n} \left| d^{m+1} S(x)/dx^{m+1} \right|^2 dx \qquad 2\text{-}4$$

For cubic splines this property approximately minimizes the " strain energy " of a curve . The proof is given by Spath [11] , whose book gives an extensive survey of spline techniques . The major area of interest in splines in this section lies in the fact that quintic splines may

be used to generate an area true interpolation to a histogram . The term "area true " has the meaning that the integral of the function over a particular channel interval is equal to the value recorded in the channel .

The interpolating function , of order five , to the points (x_k, y_k) may be written as :

$$\bar{f}(x)=\bar{f}_k(x)=A_k z^5+B_k z^4+C_k z^3+D_k z^2+E_k z+F_k \qquad 2\text{-}5$$

where $z=(x-x_k)$ and $x_k \leqslant x \leqslant x_{k+1}$. For the situation at hand $0 \leqslant z \leqslant 1$, since the channel width is one . If the points (x_k, y_k) which the spline function is to interpolate are defined by :

$$y_1=0 \qquad 2\text{-}6a)$$

and $$y_{k+1}=y_k+\Delta x_k H_k=y_k+H_k \qquad 2\text{-}6b)$$

where H_k = histogram value

Then the difference ,

$$\bar{f}_{k+1}(x_{k+1})-\bar{f}_k(x_k)=y_k+H_k-y_k=H_k \qquad 2\text{-}7$$

is the area of the histogram in the interval (x_k, x_{k+1}).

The polynomial $\bar{f}(x)$ represents the area of the histogram in the interval (x_1, x) $x_1 \leqslant x \leqslant x_n$. The actual peak shape will thus be the derivative of this polynomial ,

$$d\bar{f}_k/dx= 5A_k z^4+4B_k z^3+3C_k z^2+2D_k z+E_k \qquad 2\text{-}8$$

a fourth degree polynomial . Figure 2-1 a) displays the general form the fifth order spline takes for a particular peak , Figure 2-1 b) displays the underlying peak function formed from the derivative . The spline coefficients were calculated from an input histogram using a Fortran program

Figure 2-1
Spline Interpolation used to generate histogram distribution .

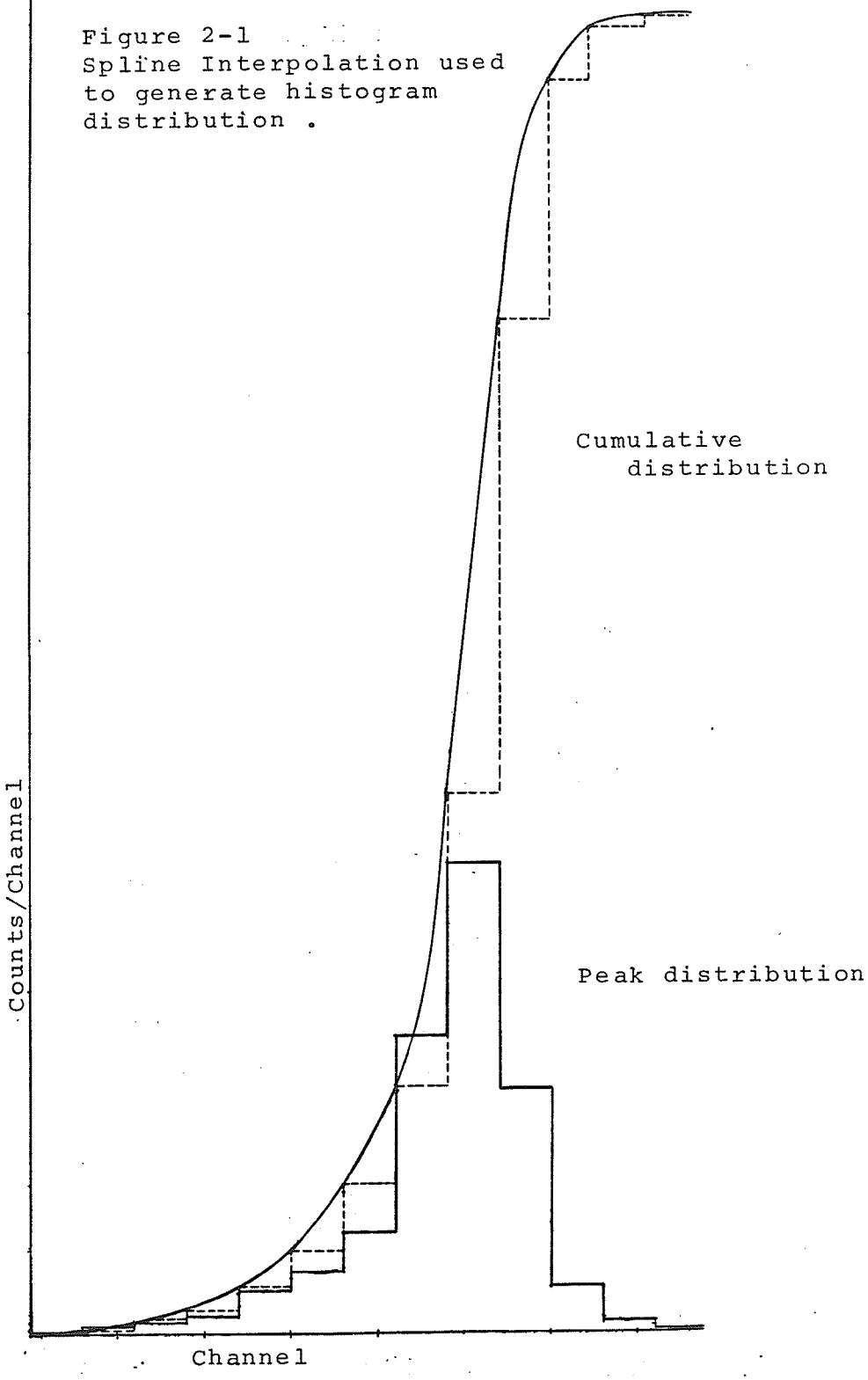

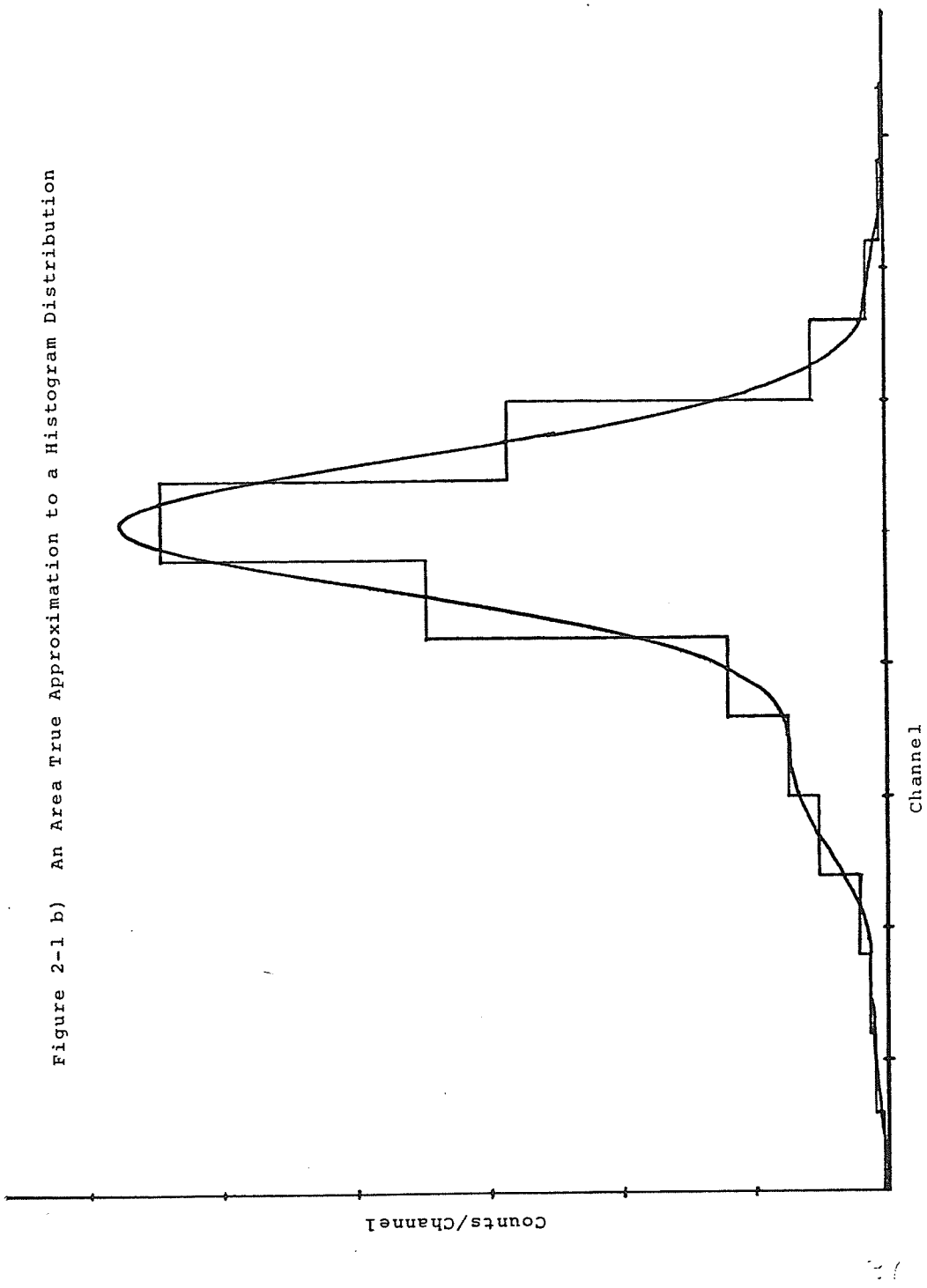

Figure 2-1 b) An Area True Approximation to a Histogram Distribution

QUINTP given by Spath in his book[11]. The calculation was performed on the PDP-15 facilities existing in the Cyclotron Laboratory . All other peak histograms measured in the spectra may be generated by insertion of the "ε" parameter when integrating the interpolation , explicitly the histogram will have the values :

$$H_i(\varepsilon_i) = \int_{x_i}^{x_{i+1}+\varepsilon} d\bar{f}(x) = \bar{f}(x_{i+1}+\varepsilon) - \bar{f}(x_i+\varepsilon) \qquad 2\text{-}9$$

$$= (A_{i+1}-A_i)\varepsilon^5 + (B_{i+1}-B_i)\varepsilon^4 + (C_{i+1}-C_i)\varepsilon^3 + (D_{i+1}-D_i)\varepsilon^2 + (E_{i+1}-E_i)\varepsilon + (F_{i+1}-F_i)$$

with $F_{i+1}-F_i = f_{i+1}(x_{i+1}) - f_i(x_i) = A_i+B_i+C_i+D_i+E_i$,

where use has been made of the relations stated in the previous section . Figure 2-2 shows a set of histograms generated from an underlying peak function for values of $\varepsilon = .0,.1,.2,\ldots,.9$, for a very narrow peak distribution and a very wide peak distribution (note the strong variation in the narrow distribution). When the method described is applied to a peak taken directly from a spectrum, the spline interpolation can generate approximations to the measured histograms within the spectrum and thus be used in a statistical fitting procedure . The fact that $H_i(\varepsilon)$ is differentiable with respect to the parameter ε allows its use as a fitting parameter in the system of simultaneous equations that must be solved in order to maximize the probability that the model describes the measured data .

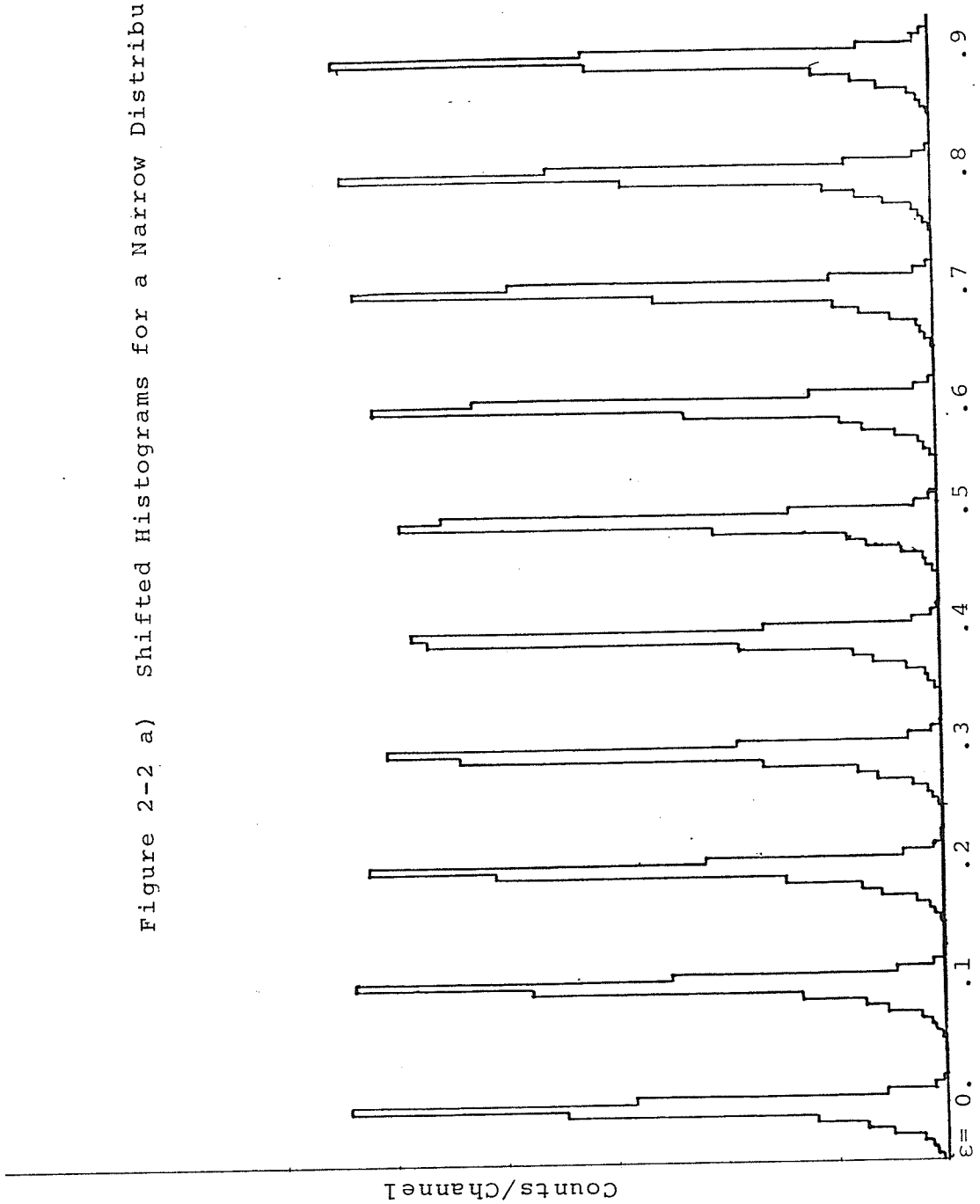

Figure 2-2 a) Shifted Histograms for a Narrow Distribution

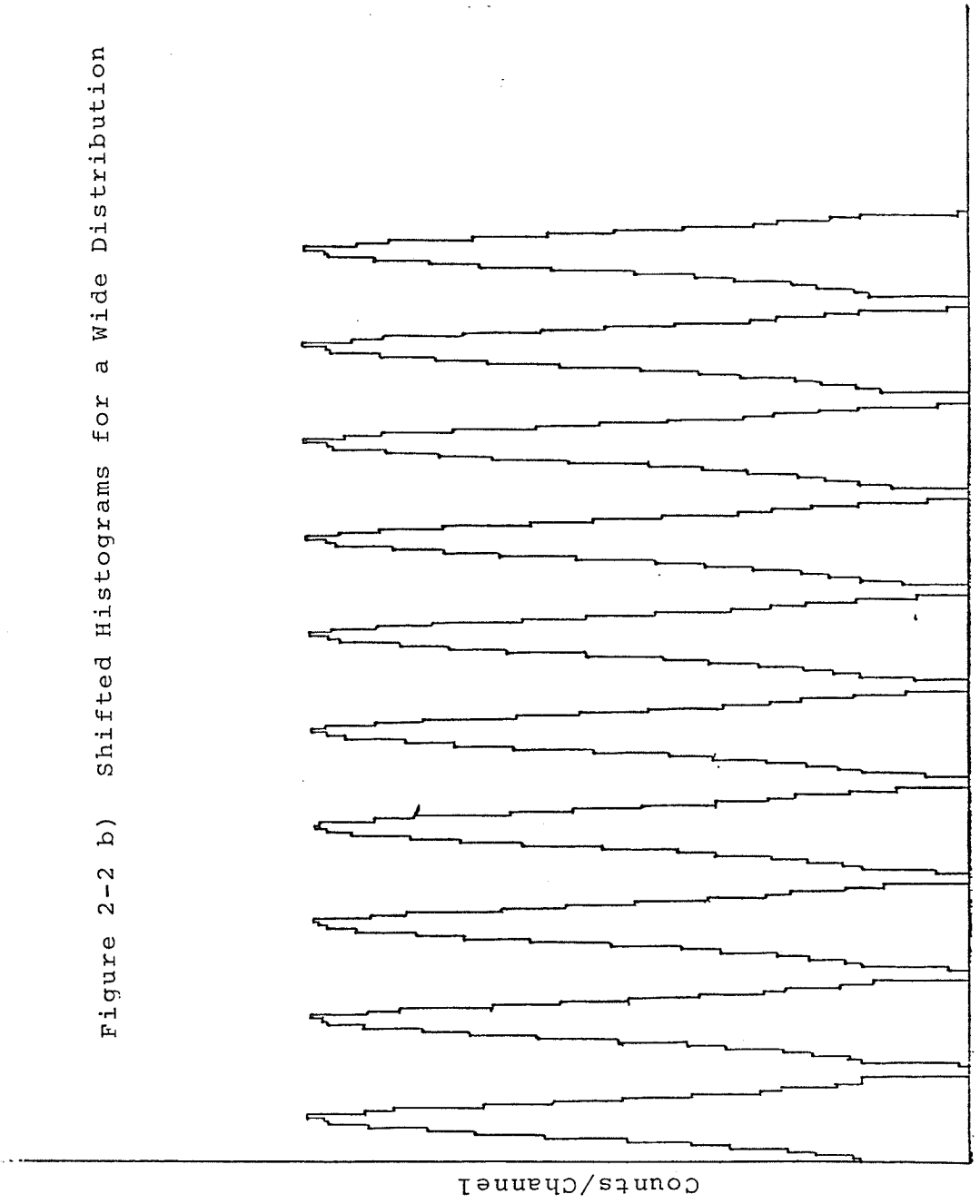

Figure 2-2 b) Shifted Histograms for a Wide Distribution

2-2 Solution of Peak Fitting Equations

In nuclear scattering experiments , what is often measured is the probability p that a specific event will occur in n trials (ie. , n protons passing through the target resulting in pn alpha particles being scattered into a solid angle) . Generally n is very large while p is very small . Under these limiting conditions (lim $p \to 0$) the statistical distribution governing a particular channel measurement is given by the Poisson distribution :

$$P(N,Y) = Y^N e^{-Y}/N! \qquad 2\text{-}10$$

which gives the probability that an integer value N will be measured when the average expected value is Y . The value Y is identified as the product of n and p described previously . The probability that an ordered set of channels is measured (ie. a peak distribution) will be the product of the individual channel probabilities ,

$$P = \prod_i Y_i^{N_i} e^{-Y_i}/N_i! \qquad 2\text{-}11$$

The aim of peak fitting analysis is to find a set of coefficients describing the mean value Y which maximizes this probability . To this end a meaningful model which contains parameters describing the peak areas and background function existing in the spectrum must be ascribed to Y . A region containig a multiplet (overlapping peaks) may be described by :

$$Y_x = \sum_j C_j H(x, x_j, \varepsilon_j) + B(x) \qquad 2\text{-}12$$

where C_j = area of the j^{th} peak

$H(x, x_j, \varepsilon_j)$ = histogram peak value described previously , with extreme left channel boundary x_j .

$B(x)$ = background function .

The maximization of the probability P is equivalent to maxmizing the logarithm of P . Since the logarithm is a sum over the channels of the region being fit it is much more convenient to use this formulation , thus the function to be maximized is given by :

$$W = \ln(P) = \sum_x (N_x \ln(Y_x) - Y_x - \ln(N_x !)) \qquad 2\text{-}13$$

For any fitting parameter "β" it is necessary that the equation :

$$\partial W/\partial \beta = \sum_x (N_x/Y_x - 1)\, \partial Y_x/\partial \beta = 0 \qquad 2\text{-}14$$

be satisfied . If there are n parameters describing the model Y , then there exist n equations of this type that must be satisfied simultaneously . The model chosen for this particular analysis was :

$$Y_x = \sum_j C_j H(x, x_j, \varepsilon_j) + bA_1 + (A_2 x + A_3 x^2 + A_4 x^3) \qquad 2\text{-}15$$

The polynomial background function $\sum_i A_i x^{(i-1)}$ was generated using the following procedure :

a) A large range of the spectrum (1000 channels) was subdivided into ordered groups of ten channels each .

b) The point (x,y) corresponding to the lowest y-valued point in each ten channel segment was chosen .

c) A monotonically decreasing sequence (with respect to the y value) was chosen from the set picked from step b) .

d) A least-squares cubic polynomial was fit through the sequence chosen in c) and used for the background function .

An example of such a fit is shown in Figure 2-3. This algorithm underestimates the background . To correct this , the parameter b in equation 2-15 is included in the constant portion of the polynomial background . The inclusion of only one adjustable parameter b in the constant portion of the background assumes that the x-dependant portion of the background fit is good enough to be used "as is" . Since points are chosen over a large range of the spectrum the estimate of the curvature should be satisfactory and a local adjustment of the constant portion of the background should be all that is required .

Using the model for a multiplet containing m peaks described previously, the following set of simultaneous equations are arrived at :

$$g_j = \partial W/\partial C_j = \sum_x (N_x/Y_x - 1) H(x, x_j, \varepsilon_j) = 0 \qquad 2\text{-}16a)$$

$$g_{m+1} = \partial W/\partial b = \sum_x (N_x/Y_x - 1) A_1 = 0 \qquad 2\text{-}16b)$$

$$g_{m+1+j} = \partial W/\partial \varepsilon_j = C_j \sum_x \partial H(x, x_j \varepsilon_j)/\partial \varepsilon_j (N_x/Y_x - 1) = 0 \qquad 2\text{-}16c)$$

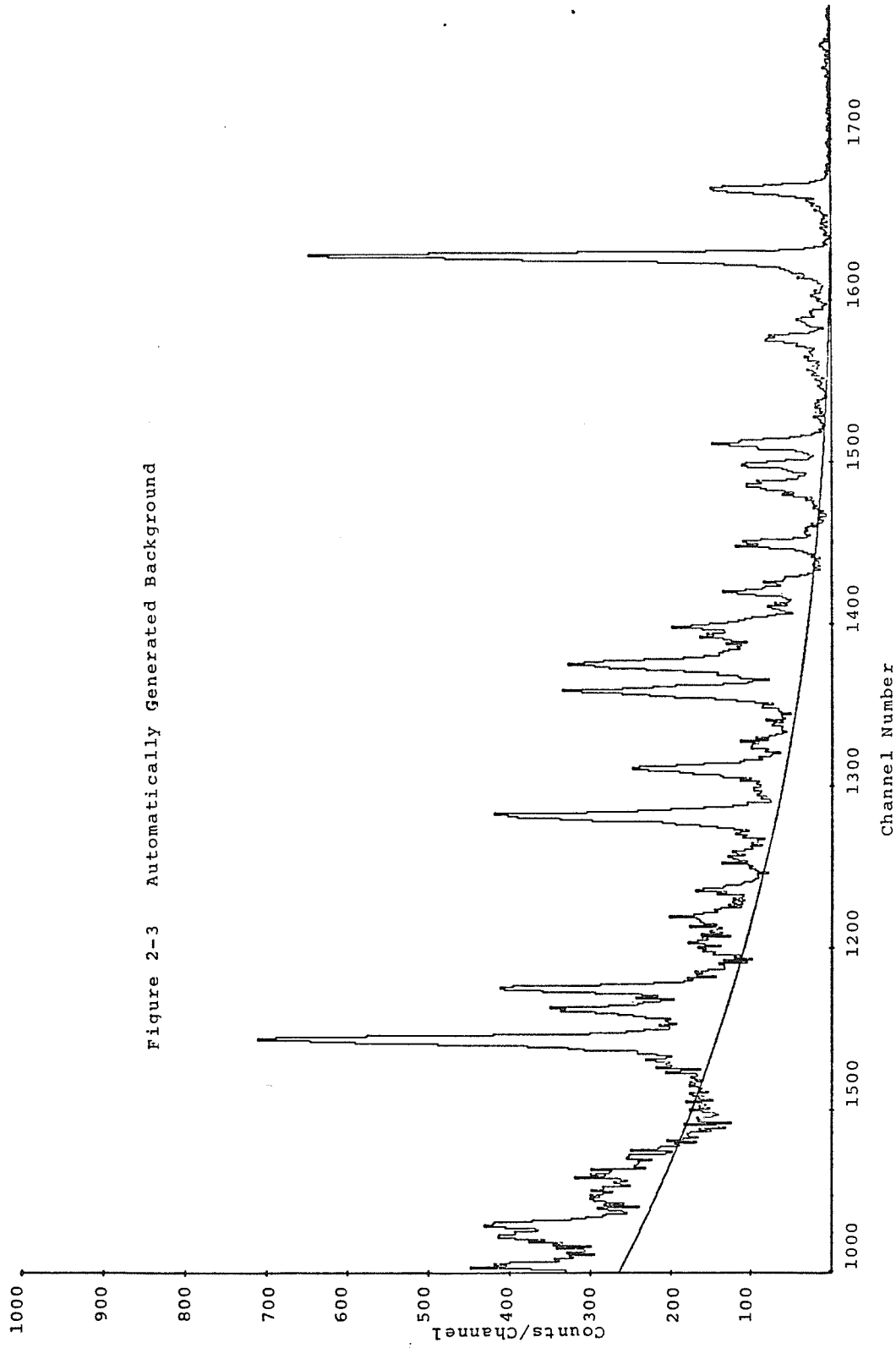

Figure 2-3 Automatically Generated Background

Where the fitting parameters are contained in a 2m+1 dimensional vector $<C_1, C_2, \ldots, C_m, b, \varepsilon_1, \varepsilon_2, \ldots, \varepsilon_m>$, where ε_i corresponds to the member of the multiplet having peak area C_i . The equations stated above are non-linear and therefore require an iterative procedure for their solution. A commonly used procedure is the Newton-Raphson Method [12] which involves a first order Taylor expansion of the equations 2-16 . The iterative formula for this method is:

$$<\beta>_{i+1} = <\beta>_i - (J^{-1} <g>)_{<\beta>=<\beta>_i} \qquad 2\text{-}17$$

J is the Jacobian of the set of functions g_i taken with respect to the coefficients β_i , and is given by :

$$J = \begin{pmatrix} \partial g_1/\partial C_1 & \cdots & \partial g_1/\partial \varepsilon_m \\ \vdots & & \vdots \\ \partial g_{2m+1}/\partial C_1 & \cdots & \partial g_{2m+1}/\partial \varepsilon_m \end{pmatrix} \qquad 2\text{-}18$$

This iterative procedure has the advantage that it converges rapidly to a solution if the initial estimate $<\beta_0>$ is close to the actual value $<\beta>$. The drawback of this method is that for estimates of $<\beta>$ which are far from the actual value the iterations may diverge . This should not be a major difficulty for this particular problem , since a least- squares fit , where the shift parameter ε is held constant , is linear in its equations

and thus readily and rapidly solvable . The least - squares values should be reasonably close to the value $<\beta>$ to be used as an initial estimate . It is fortunate that the Jacobian matrix J is symmetric , making computation of the inverse Jacobian simpler than the non-symmetric case . The terms of J will be denoted by : $J_{ij}=\partial g_i/\partial\beta_i$ where $<\beta>=<C_1,\ldots,C_m,b,\varepsilon_1,\ldots\varepsilon_m>$, thus ,

$$J_{j,j'}=\partial^2 W/\partial C_j\,\partial C_{j'}$$
$$=-\sum_x N_x/Y_x^2 H(x,x_j,\varepsilon_j)H(x,x_{j'},\varepsilon_{j'}) \qquad j,j'=1,m \qquad 2\text{-}19a)$$

$$J_{j,m+1}=\partial^2 W/\partial C_j\,\partial b$$
$$=-A_1\sum_x N_x/Y_x^2 H(x,x_j,\varepsilon_j) \qquad j=1,m \qquad 2\text{-}19b)$$

$$J_{j,\ell}=\partial^2 W/\partial C_j\,\partial\varepsilon_{j'} \qquad 2\text{-}19c)$$
$$=\delta(j,j')\{\sum_x \partial H(x,x_j,\varepsilon_j)/\partial\varepsilon_j(N_x/Y_x-1)\} \qquad \ell=m+2,2m+1,\ j'=\ell-m-1$$
$$-C_{j'}\sum_x N_x/Y_x^2\,\partial H(x,x_{j'},\varepsilon_{j'})/\partial\varepsilon_{j'}H(x,x_j,\varepsilon_j) \qquad j=1,m$$

$$J_{m+1,\ell}=\partial^2 W/\partial b\,\partial\varepsilon_j \qquad 2\text{-}19d)$$
$$=-C_j A_1\sum_x N_x/Y_x^2\,\partial H(x,x_j,\varepsilon_j)/\partial\varepsilon_j \qquad \ell=m+2,2m+1,\ j=\ell-m-1$$

$$J_{\ell,\ell'}=\partial^2 W/\partial\varepsilon_j\,\partial\varepsilon_{j'} \qquad 2\text{-}19e)$$
$$=\delta(j,j')C_j\sum_x\partial^2 H(x,x_j,\varepsilon_j)/\partial^2\varepsilon_j(N_x/Y_x-1)$$
$$-C_jC_{j'}\sum_x N_x/Y_x^2\,\partial H(x,x_j,\varepsilon_j)/\partial\varepsilon_j\,\partial H(x,x_{j'},\varepsilon_{j'})/\partial\varepsilon_{j'}$$
$$\ell,\ell'=m+2,2m+1,\ j=\ell-m-1,\ j'=\ell-m-1$$

where $\delta(i,j)$ is a Kronecker delta function .

2-3 Application of the Method

A Fortran program using the fitting method described was written for use on the PDP-15 facilities at the Cyclotron Laboratory . A least square fit with $\varepsilon = 0$ was used as an initial estimate for the peak areas and background coefficient . In order to accurately determine the position of the multiplet a region of 5 to 10 channels above and below the positions calculated from the calibration was scanned , and a least - square calculation performed on each position. The position which yielded maximum peak area with no negative peaks in the multiplet was chosen as the position at which to start an iterative calculation. The code was tested on doublets using known values of parameters inserted in a test spectrum . Nominal values of 5000 and 1000 counts were used for the left and right peak areas respectively . Respective shift parameters of .4 and .7 were used for the left and right peaks . The areas are nominal since real numbers are rounded off to create an integer array . This probably explains the fact that the sum of the extracted areas is about 14 counts high . Figure 2-4 shows the results of the test. The program failed to converge for peak separations of 3 channels or less . This is probably due to the inability of the fitting procedure to distinguish two strongly overlapping peaks . However the program fit the doublets of peak separation greater than 3 channels quite well.

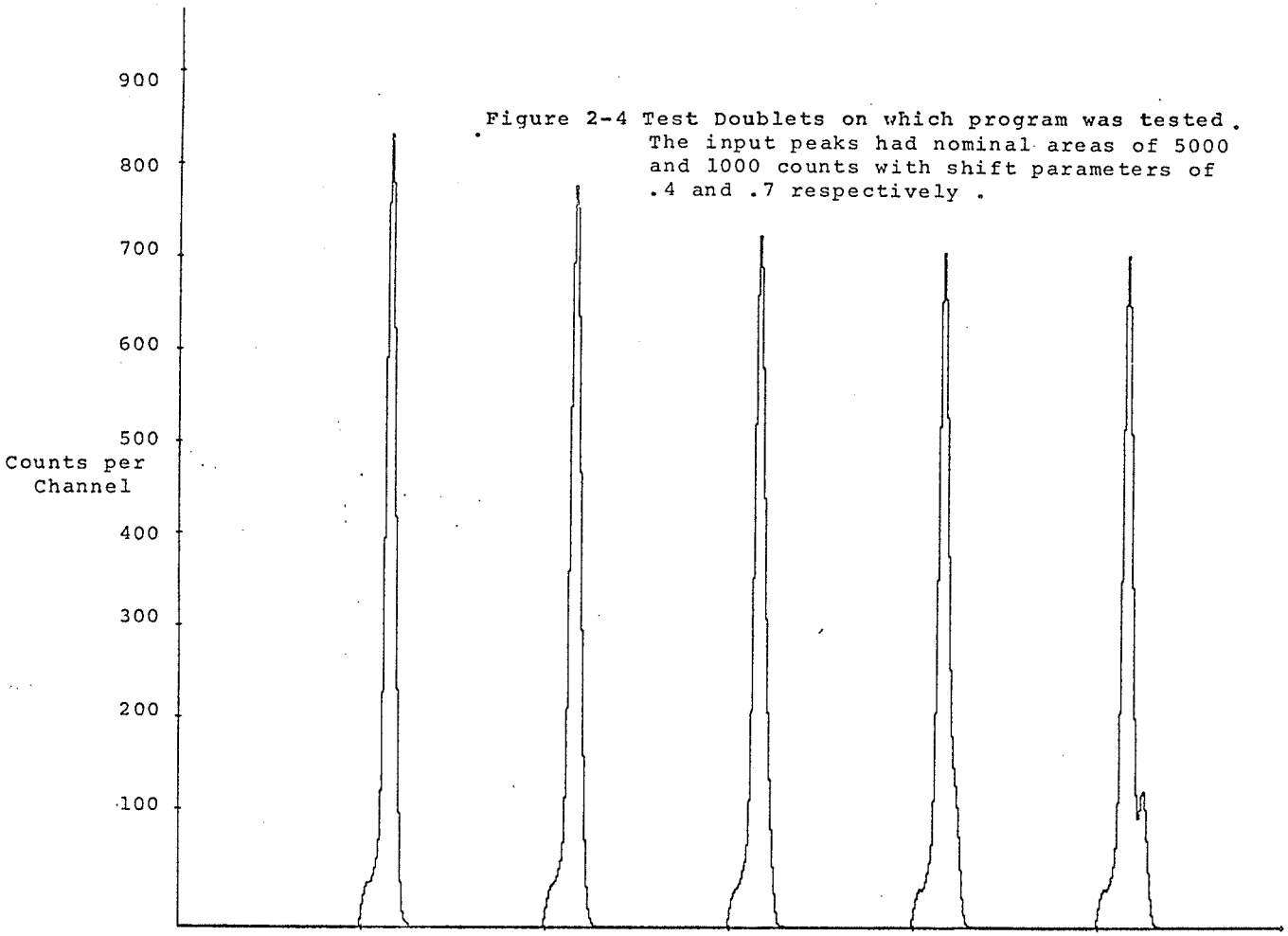

Figure 2-4 Test Doublets on which program was tested. The input peaks had nominal areas of 5000 and 1000 counts with shift parameters of .4 and .7 respectively .

Results of Calculation						
Area and Shift .	Left Peak	No Fit	No Fit	4998, .41	5008 , .406	5010, .40
	Right Peak	"	"	1015, .72	1006 , .71	1004, .70

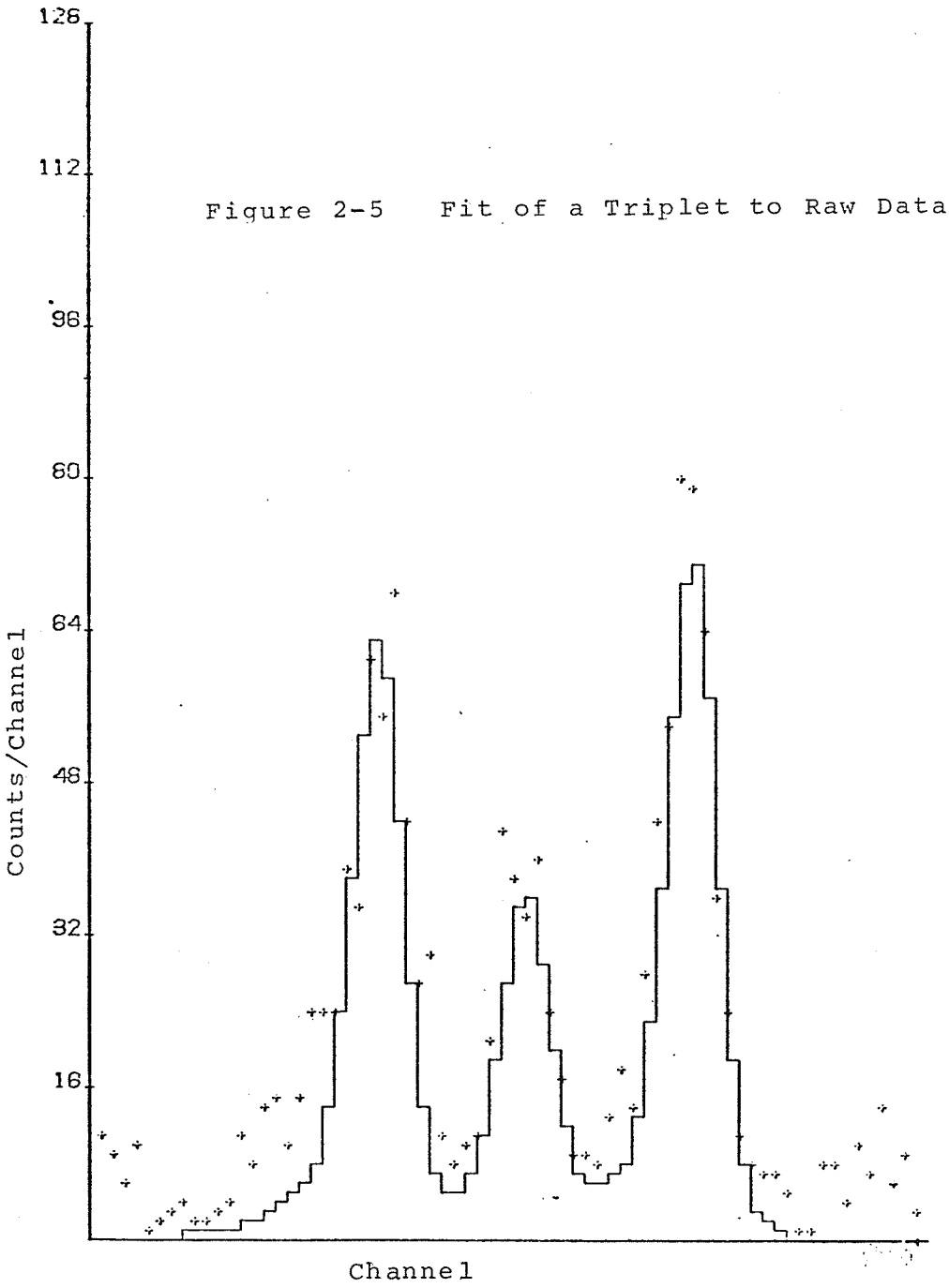

Figure 2-5 Fit of a Triplet to Raw Data

Figure 2-6 A Smoothed Peak Distribution

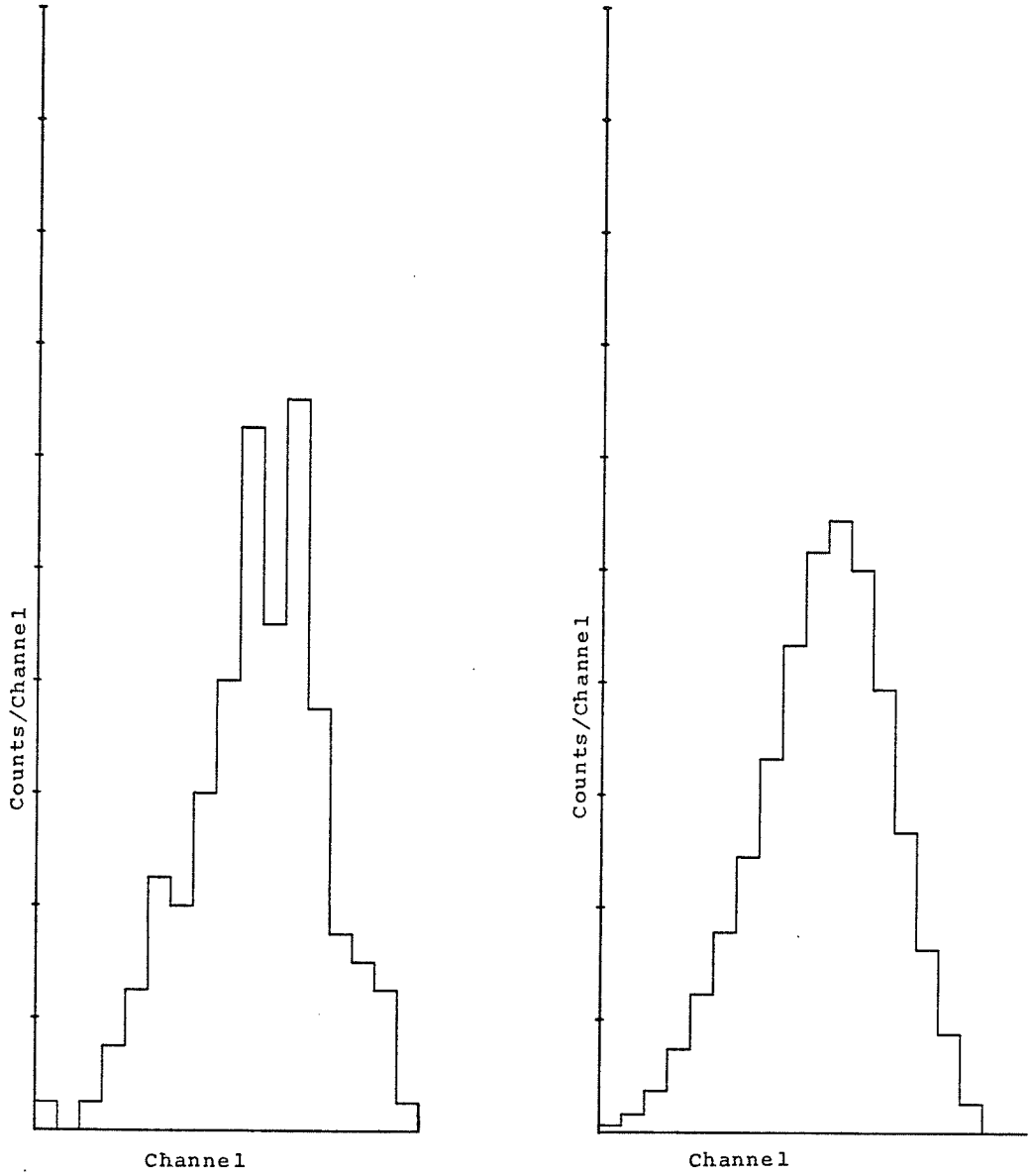

Figure 2-5 shows fits extracted from an actual spectrum for a triplet .

One of the problems encountered with a spectrum which has counts with very poor statistics is that it does not contain a peak which does not have gross fluctuations for use as a fitting function . In order to alleviate this problem a cubic spline smoothing process described by Spath[11] can be applied to peaks with gross fluctuations . It is possible using the program FLATC given by Spath to calculate a set of points (x_k, y_k) such that the value of the third derivative of the spline at x_k is proportional to the difference between the actual data point u_k and y_k at x_k; ie. , $p_k(u_k-y_k)=r_k$ where r_k is the third derivative and p_k is the proportionality constant This procedure was only applied in order to define a model peak function and was not applied to the actual data. Figure 2-6 shows the application of this method to a peak.

2-4 Conclusion

A fitting method which attempts to describe rigourously the model and statistical distributions present in nuclear spectra has been outlined . Its applicability to spectra containing narrow 'histogram-like' peak distributions with smooth background is apparent . The shortcomings of the method lie mainly in the time consuming solution of the set of nonlinear equations ,which often fail to converge to a proper solution.

Chapter 3 - DWBA Analysis of Cross Sections

The term " direct transfer reaction " refers to a process in which a transfer of nucleons occur between the incident projectile and target nucleus . Such a reaction is assumed to occur in one step over a short period of time ($\simeq 10^{-22}$ sec.) , hence the term direct reaction . The symbolic notation for reactions is ,

$$A + a \rightarrow B + b \text{ or } A(a,b)B$$

where a and b are the incident and exiting projectiles respectively , and A and B are the target and residual nucleus respectively .

The mechanisms describing the reaction can be classified under four seperate processes [16] :

1) Direct pick-up - The incident projectile a " picks-up " a nucleon cluster x from the target A to form a+x=b , leaving the residual nucleus B .

2) Knock-out - The incident projectile a "knocks-out " the particle b from A and is captured into the target nucleus to form B .

3) Heavy particle pick-up - The projectile "captures " the bulk portion of A to form B , leaving a light particle b .

4) Heavy particle Knock-out - The incident projectile knocks B out of A and combines with nucleons left over from A to form b .

Kinematic considerations have been used [16] to argue that heavy particle pickup and knock-out processes have maximum cross sections at backward angles . Since the data measured in this experiment are at angles less than 90 degrees , these mechanisms are not expected to contribute appreciably to a description of the data presented in this thesis .

The purpose of this analysis is to compare the measured cross sections for (p,α) reactions from the ^{18}O ground state to various states of ^{15}N with Distorted Wave Born Approximation (DWBA) calculations using a cluster model for the transferred group of nucleons . These calculations are carried out using the conputer code DWUCK5 [13], a DWBA code capable of performing a full finite range calculation of differential cross sections for transfer reactions . The derivation and formalism of the DWBA theory has been treated extensively [14,15,16]. A statement of some of the ideas and results of the theory follows .

3-1 Direct reactions and DWBA Theory

The starting point of reaction theory is concerned with a meaningful interpretation of the transition matrix . The transition matrix is the operator which connects the initial and final states of a system undergoing a reaction. Formally the transition matrix may be defined by [16]:

$$T_{fi} = \langle\phi|U|\chi^+\rangle + \sum_{n=0} \langle\chi^-|W_1(G_1^+W_1)^n|\chi^+\rangle \qquad 3\text{-}1$$

In this formalism , the potential V which describes the interactions in the system is separated into two parts: V=U+W . It is assumed that scattering solutions to the potential U are known , they are denoted by χ^+ and χ^- in equation 3-1 . The symbol ϕ in equation 3-1 represents a plane wave state , while G_1^+ is a Green function defined by [16]:

$$G_1^{\pm} = 1/(E-H_0-U\pm i\varepsilon) \qquad 3\text{-}2$$

where H in eqn. 3-2 is the kinetic energy operator . Each of the terms in the summation over n in equation 3-1 represents successive scattering processes[16,26]. The DWBA theory assumes that only one interaction takes place (ie n=0).

In the conventional form of the DWBA theory it is assumed that the potential U of equation 3-1 describes the elastic scattering of the projectile a from the target nucleus A [16]. These potentials may be determined by fits of the parameters of , for instance , the Optical Model to

experimental angular distributions . Using this assumption the transition matrix element becomes [16] :

$$T_{ba}=\langle \chi_b^- \phi_b \Phi_B | V_{aA}-U_{aA} | \chi_a^+ \phi_a \Phi_A \rangle \qquad 3\text{-}3$$

where $\chi^{\pm}$ represent the distorted wave functions calculated from optical potentials and , ϕ_a, ϕ_b, Φ_A and Φ_B are eigenfunctions of the internal Hamiltonian operator for particles a , b , A and B respectively . The potential U_{aA} is the elastic scattering optical potential while V_{aA} is the potential which describes the complete interaction of the particle and nucleus . The first term of eqn. 3-1 disappears since the initial and final states are not connected by the potential U .

For a pick-up reaction where a certain number of nucleons are picked up out of A , the interaction potential may be written :

$$V_{aA} = V_{aB} + V_{ax}$$

where V_{aB} and V_{ax} describe the interaction of particle a with particles B and x respectively , thus :

$$T_{ba}=\langle \chi_b^- \phi_b \Phi_B | V_{ax}+(V_{aB}-U_{aA}) | \chi_a^+ \phi_a \Phi_A \rangle \qquad 3\text{-}4$$

It is usually assumed in the DWBA formalism that the inelastic effect of V_{aB} is small relative to the elastic process . Furthermore it is assumed that the proportion of the nucleons contained in A that are removed in x is small . This leads to the approximation taht the elastic scattering processes of the projectile on A or B are equivalent . This approximation is considered valid for heavy nuclei al-

though it becomes questionable for light nuclei, where the proportion of nucleons taken out of x is greater[16].

Using this approximation the matrix element becomes :

$$T_{ba}=\langle \chi_b^- \ \phi_b \Phi_B | V_{ax} | \chi_a^+ \ \phi_a \ \Phi_A \rangle \qquad 3\text{-}5$$

When expanded over the z projections of the total angular momenta of A and B and the spins of a and b , the T-matrix element becomes[14,15,16] :

$$T_{ba}= \sum_{m'_b, m'} \int d\vec{R}_b \int d\vec{R}_a \ \chi^{-*}_{m'_b, m_b}(\vec{k}_b, \vec{R}_b) \qquad 3\text{-}6$$

$$\langle \psi_{J_B M_B} \ \psi_{s_b m'_b} \ | V_{ax} | \psi_{J_A M_A} \ \psi_{s_a m'_a} \rangle \chi^{+}_{m_a, m'_a}(\vec{k}_a, \vec{R}_a)$$

The matrix element $\langle \psi_{J_B M_B} \ \psi_{s_b m_b} \ | V_{ax} | \psi_{J_A M_A} \ \psi_{s_a m_a} \rangle$ in equation 3-6 may be expanded over the orbital angular momentum, spin and total angular momentum that are transferred during the reaction. The expression may then be written:

$$\langle \psi_{J_B M_B} \ \psi_{s_b m'_b} \ | V_{ax} | \psi_{J_A M_A} \ \psi_{s_a m'_a} \rangle$$

$$\sum_{L,S,J} (-1)^{s_b - m_{b_i} - L} \langle s_a m_a s_b, -m_b | S, m_a - m_b \rangle \langle J_A M_A J, M_A - M_B | J_B M_B \rangle$$

$$\langle L, m, S, m_a - m_b | J, M_B - M_A \rangle \ A_{LSJ}(\xi) \ f^{m}_{LSJ}(\vec{R}_a, \vec{R}_b) \qquad 3\text{-}7$$

The functions A_{LSJ} and f^{m}_{LSJ} are called the spectroscopic strength factor and spectroscopic form factor respectively. The strength factor contains information concerning the

strength of the reaction and the overlap of the initial and final nuclear states . The form factor $f^{m}_{LSJ}(\vec{R}_a,\vec{R}_b)$ describes the interactions of the incident and exiting particles and will thus describe any measurements made of particles b . Both of these functions depend upon the model which is chosen to describe the nucleus .

The differential cross section of a reaction may be directly related to the T matrix by the summation

$$d\sigma/d\Omega = \mu_a\mu_b/(2\pi\hbar^2)^2 k_b/k_a \sum_{\substack{m_a m_b \\ M_A M_B}} |T|^2/(2J_A+1)/(2s_a+1) \qquad 3\text{-}8a)$$

where μ_a,μ_b are the reduced masses of the incident and outgoing particles , and the sum is over the J_z projections M_A,M_B,m_a,m_b. The expression for the differential cross section in this formulation may be written :

$$d\sigma/d\Omega = \mu_a\mu_b/(2\pi\hbar^2)^2 k_b/k_a \ (2J_B+1)/(2J_A+1)/(2s_a+1)$$
$$\sum_{J,m,m_a,m_b} \Big| \sum_{L,S} A_{LSJ}\ \beta^{L,m,m_a,m_b}_{SJ} \Big|^2 \qquad 3\text{-}8b)$$

where β^{L,m,m_a,m_b}_{SJ} is the reduced amplitude :

$$\beta^{L,m,m_a,m_b}_{SJ} =$$

$$(2J+1)^{-\frac{1}{2}}(i)^{-L} \sum_{\substack{m' m_a' \\ m_b'}} \langle s_a,m_a',-m_b'|S,m_a'-m_b'\rangle\langle L,m',S,m_a'-m_b'|J,m-m_b+m_a\rangle$$

$$(-1)^{s_b-m_b'} \iint \chi^{-}_{m_b' m_b}(\vec{k}_b,\vec{R}_b)\, f^{m}_{LSJ}(\vec{R}_b,\vec{R}_a)\, \chi^{+}_{m_a' m_a}(\vec{k}_a,\vec{R}_a)\, d\vec{R}_a d\vec{R}_b \qquad 3\text{-}9$$

where $m'=M_B-M_A-m_a'+m_b'$.

3-2 Selection Rules

The conservation of angular momentum and parity leads to various selection rules in the population of states of the residual nucleus via a direct reaction[17]. For a (p,α) reaction these are :

$$\vec{L}=\vec{L}_{\alpha}-\vec{L}_{p}=\vec{l}_{n1}+\vec{l}_{n2}+\vec{l}_{p1} \qquad 3\text{-}10a)$$

$$\vec{S}=\vec{S}_{\alpha}-\vec{S}_{p}=\vec{s}_{n1}+\vec{s}_{n2}+\vec{s}_{p1} \qquad 3\text{-}10b)$$

$$\vec{J}=\vec{L}+\vec{S}=\vec{J}_{f}-\vec{J}_{i}=\vec{j}_{n1}+\vec{j}_{n2}+\vec{j}_{p1} \qquad 3\text{-}10c)$$

$$\vec{T}=\vec{T}_{\alpha}-\vec{T}_{p}=\vec{T}_{f}-\vec{T}_{i} \qquad 3\text{-}10d)$$

Where p,α,i and f refer to the proton , alpha and initial and final nuclear states respectively . The symbols L,S,J and T represent the transferred orbital , spin , total angular momenta , and isospin respectively . The lower case symbols such as $\vec{l}_{n1}$ and $\vec{s}_{p1}$ refer to the orbital and spin angular momentum quantum numbers of the individual nucleons residing in their initial nuclear state .

The following rules apply to a (p,α) reaction :

$$|\vec{S}| = 1/2 \qquad 3\text{-}11a)$$

$$|\vec{T}| = 1/2 \qquad 3\text{-}11b)$$

$$|\vec{J}| = |\vec{L}| \pm 1/2 \qquad 3\text{-}11c)$$

The parity of the initial and final states of the nucleus is assumed to be given by :

$$\Pi_{i}\Pi_{f} = (-1)^{L} \qquad 3\text{-}12$$

This assumption is valid only if the relative angular momenta of the nucleons involved in the transfer is assumed to be zero .

The selection rules 3-11 and 3-12 uniquely specify the values for the L and S transfer for a given J^{Π} transfer . This allows the removal of the sum over L and S in equation 3-8 , yielding :

$$d\sigma/d\Omega = \mu_a \mu_b/2(2\pi\hbar^2)^2 \; k_b/k_a \sum_J |A_{LSJ}|^2 \sum_{m,m_b} |\beta^{L,m,m_a}|^2 \qquad 3\text{-}13$$

where the value $m_b=0$, $s_a=1/2$, and $(2J_B+1)=(2J+1)$ have been inserted for a (p,α) reaction . This reduction in complication allows the shape of the differential cross section for a particular J transfer to be calculated via the summation over the β_{SJ}^{L,m,m_a} parameters .

3-3 The Cluster Form Factor and the $^{18}O(p,\alpha)^{15}N$ Reaction

The cluster form factor assumes that the nucleons transferred in the reaction form a triton cluster which is bound in a Woods-Saxon potential [27]. This cluster is treated as a single particle with quantum numbers N,L,S and J , where N is the radial quantum number for a particle state described by the shell model . A discussion of how this type of calculation can be implemented may be found in reference 18 .

Energy conservation requires that the N and L values of the triton satisfy :

$$2N+L = 2(n_{n1}+n_{n2}+n_{p1})+l_{n1}+l_{n2}+l_{p1} \qquad 3\text{-}14$$

where the subscripted values denote the nuclear shell model

orbitals of the transferred nucleons . This condition restricts the possible states of the residual nucleus reached by the (p,α) reaction .

The ^{18}O , $J^{\Pi}=0^{+}$ ground state is believed to consist of a closed ^{16}O core plus two neutrons in a $(1d5/2)^2$, $(2s1/2)^2$ or $(1d3/2)^2$ plus a small core excited $(sd)^4$ particle configuration[19] . According to equation 3-14 there is an upper limit to the value of J which the ^{15}N residual nuclei can possess following a (p,α) pick up reaction . Setting N=0 , and applying equation 3-14 , the maximum value L can take on is L=6 , yielding states of $13/2^+$ or $11/2^-$ total angular momenta and parity . These states would arise from a pick up of two s-d neutrons plus an s-d proton from the ^{18}O nucleus .

3-4 DWBA calculations using DWUCK5

DWBA calculations were performed using optical potentials to describe the incident proton wavefunctions χ_a and outgoing alpha wavefunctions χ_b . The form of the potentials required by the DWUCK5 codes is of the form :

$$V=V_c+V_v\ f(x_0,a_0)+iW_v f(r_{iv},a_{iv})+iV_I df(x_i,a_i)/dx_i$$
$$+V_s 1/r\ df(x_s,a_s)/dx_s\ \vec{L}\cdot\vec{S} \qquad 3\text{-}15$$

where x and a are the "radius" and diffuseness" parameters of the optical model . The function f(x,a) is given by:

$$f(x,a)=(1+\exp((x-x_i)/a_i))^{-1} \qquad 3\text{-}16$$

3-4 a) Proton Potentials

There is plentiful information concerning optical parameters for proton elastic scattering from ^{18}O at the energy at which this experiment was performed . Table 3-1 lists the various potentials found in the literature . The potential P5[21] is an energy dependant fit which used data through the proton energy range of this experiment (40.9 MeV) . Potential P1 to P4 lacked data between 29.8 and 66.5 MeV . On this basis P5 is preferable .

3-4b) Alpha Potentials

The paucity of appropriate elastic scattering potentials for the $^{15}N(\alpha,\alpha)^{15}N$ reaction made it necessary to calculate an optical potential using the parameter search computer code SEEK [25]. Cross section data for $^{15}N(\alpha,\alpha)^{15}N$ at E = 40.5 MeV was obtained from the Lawrence Berkely Laboratory [22]. An elastic scattering potential with a well depth of approximately 279 MeV was calculated for this data previously by Wozniak et al. [23], for use in $(\alpha,^{9}Be)$ studies . Real well depths of approximately 50 MeV per nucleon [24] are expected for elastic scattering of composite particles . On this basis a depth of approximately 200 MeV would be desirable for an alpha potential .

Table 3-2 list two potentials calculated using the SEEK code . The potential A1 has a well depth of approximately 180 MeV which corresponds well with 200 MeV . The potential A2 is much deeper and compares with potential A3

Table 3-1 Proton Optical Potentials† for $^{18}O(p,p)^{18}O$

Set	$E_{particle}$	Ref.	V	W	W_D	V_{so}	r_v	a_v	r_w	a_w	r_{so}	a_{so}
P1	13.04-66.5	20	57.6-.2E	.15E-4.5	7.2-.06E	4.9	1.07	.74	1.34	.64	.9	.57
P2	" " "	20	52.1-.21E	.36E-10.7	7.42-.067E	5.1	1.16	.66	1.29	.65	1.0	.62
P3	Ref. 20	20	56.-.22E	1.2+.09E	5.92-.05E	6.04	1.16	.75	1.37	.85-.008E	1.064	.78
P4	" " "	20	56.	" " "	" " "	6.2	1.17	.75	1.32	.588	1.01	.75
P5	14.7-44.1	21	59.5-.29E	.38E-9.5	10.4-.17E	4.4	1.1	.7	1.3	.67	1.00	.60

Table 3-2 Alpha Optical Potentials† for $^{15}N(\alpha,\alpha)^{15}N$

Set	$E_{particle}$	V	r_v	a_v	W	r_w	a_w	r_c
A1	40.5	180.17	1.338	.651	17.01	1.563	.644	1.25
A2	40.5	285.27	1.203	.652	20.43	1.397	.727	1.25
A3	40.5	279.	1.22	.65	17.6	1.35	.65	1.2

†Note: The potentials listed in Tables 3-1 and 3-2 are of the form :

$$V_c - Vf(x) - iWf(x) + 4iW_D a_w f'(x) - (E/mc)^2 V_{so} (1/r) f'(r) \sigma \cdot l$$

As such , the calculated parameters are not suitable for the DWUCK5 code (see eqn. 3-15) They are compatible if we set $V_{DWUCK} = -V_{Table}$, $W_{DWUCK} = -W_{Table}$, $V_{so_{DWUCK}} = -4\ V_{so_{Table}}$

Table 3-3 Bound State Parameters

	Separation Energy	r_0	a_0	V_{so}
$t+^{15}N$	15.832*+E^{xn}	1.24	.47	8
p+t	19.812	1.488	.144	-

*Separation energy of triton in ^{18}O , E^{xn}=excitation energy of ^{15}N state

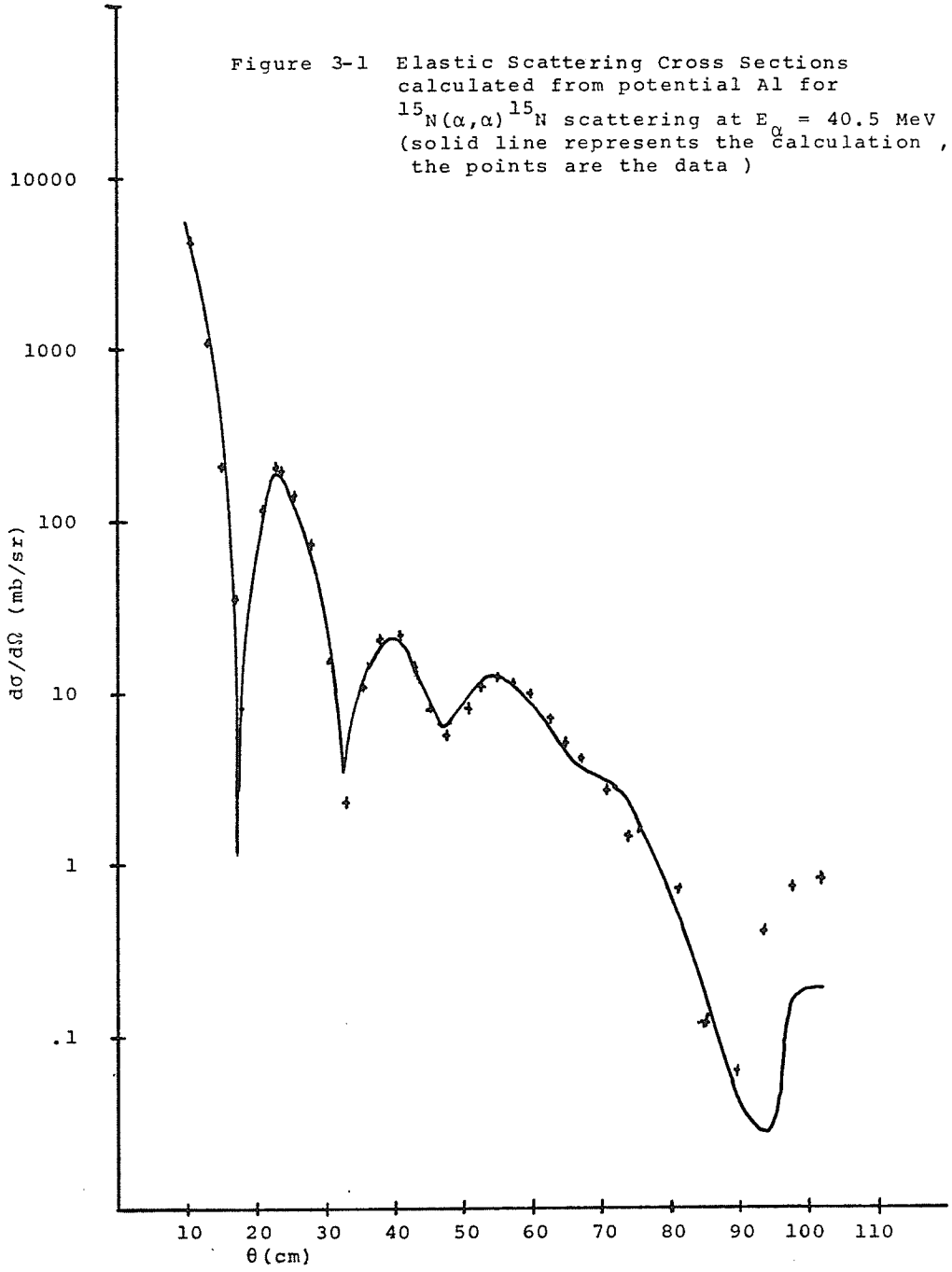

Figure 3-1 Elastic Scattering Cross Sections calculated from potential A1 for $^{15}N(\alpha,\alpha)^{15}N$ scattering at E_α = 40.5 MeV (solid line represents the calculation , the points are the data)

which was calculated by Wozniak et al using a different computer code (GENOA) . The quality of the fit for the 285 MeV well was somewhat superior to that of the 180 MeV well . However , as noted the 180 MeV well is preferable on physical grounds . Figure 3-1 displays a plot of the experimental cross sections and the differential cross sections calculated from Al .

3-4 c) Bound State Parameters

The finite range computer code DWUCK5 calculates form factors for the triton cluster bound in the nucleus , and the incident proton bound to the triton . The potential used to describe the interaction is of the Woods-Saxon form . The code must be supplied with values of the radius , diffuseness , and spin-orbit depths for the respective bound states . It also requires that the binding energies of the bound particles be supplied . The code then calculates a potential well depth which matches the binding energy of the triton or proton bound to the nucleus or the triton respectively .

Values of 1.488 fm. for the radius and .144 fm. for the diffuseness of the p+t system were used [35]. No spin-orbit potential for the p+t system was employed [35]. The triton bound state parameters were obtained by varying the radius and diffuseness until the calculated cross sections from DWUCK5 resembled the data extracted for the $1/2^-$ ground state of ^{15}N . These parameters were kept fixed in subse-

quent calculations of other cross sections . Values which gave good agreement were 1.24 fm . for the radius and 0.47 fm for the diffuseness . These values were within the range of parameters used by Maples[36] in a study of (p,α) reactions on light nuclei . Maples used values ranging between 1.03 fm. to 1.6 fm. for the bound state triton radius and 0.20 fm. to 0.87 fm. for the bound state diffuseness . A spin-orbit depth of 8 MeV was employed [35].

3-5 States Accessible via a Pick-up Process

The assumption that a transfer reaction proceeds via a simple one step process induces a high degree of selectivity in the expected states to which the residual nucleus is excited . The transferred nucleons are assumed to be transferred directly to the proton from their shell states in the target nucleus . The remaining nucleons within the residual nucleus are assumed not to be disturbed from the shells which they filled in the target nucleus . Furthermore , in the simple triton cluster transfer model , it is assumed that the correlation among the three transferred nucleons can be well represented as a single triton "particle " existing in an appropriate potential well (Woods-Saxon for this case) .

The ^{18}O g.s. is believed to be composed of a predominantly 2p-0h configuration with respect to ^{16}O with neutrons spread over the $(1d5/2)^2$, $(2s1/2)^2$ and $(1d3/2)^2$ shells , and more complicated 4p-2h core excited states[19,37].

The 2p-0h configuration for the ground state will allow access to 0p-1h,1p-2h, and 2p-3h states in ^{15}N . The core-excited ground states may lead to 1p-2h,2p-3h,3p-4h and 4p-5h states .

In contrast to a pickup reaction , the states accessible via stripping reactions can be considerably different Here , nucleons are deposited onto the target nucleus by the projectile . Assuming that these reactions occur as a one step , direct process , the stripped nucleons can populate shell model levels above those of the target nucleus , which must remain intact if the reaction occurrs in one step . By comparing the results of stripping reactions to ^{15}N (refs. 28,29,30,34,39) with a pick up reaction to the same final state , some information concerning the structure of the nucleus may be gained .

Tables 3-4 and 3-5 list the various quantum numbers corresponding to the single particle shell orbitals and transferred triton clusters , respectively . Table 3-6 lists the nature of the residual states when a 2N+L triton cluster is removed .

3-6 Cluster Form Factor Calculations compared with Experimental results

In view of the simplification of the triton single particle cluster model for the pickup (p,α)reaction process , an agreement between a DWBA calculation using this model and experimental data would suggest that there exists

Table 3-4 Quantum Number Contributions of Shell Nucleons to transferred Cluster

Nucleon Orbit	n	l	Number of Quanta (=2n+l)
1p3/2	0	1	1
1p1/2	0	1	1
1d5/2	0	2	2
2s1/2	1	0	2
1d3/2	0	0	2

Table 3-5 Quantum Numbers of transferred Cluster

No. from 2s-1d Shell	No. from 1p Shell	$\sum_{i=1}^{3}(2n_i+l_i)=2N+L$
3	0	6
2	1	5
1	2	4
0	3	3

Table 3-6 Final State Characteristics arising from (N,L) transfer

2N+L	Possible (N,L) Combinations	Parity	Particle-Hole Nature of final state *
6	(3,0),(2,2),(1,4),(0,6)	+	1p-2h
5	(2,1),(1,3),(0,5)	-	(0p-1h) or (2p-3h)
4	(2,0),(1,2),(0,4)	+	(1p-2h) or (3p-4h)
3	(1,1),(0,3)	-	(2p-3h) or (4p-5h)

* with respect to ^{16}O core .

a strong correlation that the three nucleons are well represented as a triton cluster within the target nucleus. An agreement would also state something about the structure of the residual nucleus , since the nucleons in the triton are transferred out of specific levels in the target nucleus , leaving the residual nucleus in a definate state.

The following pages present some full finite range DWBA calculations using DWUCK5 , for several states of the $^{18}O(p,\alpha)^{15}N$ reactions at incident proton energy 40.9 MeV. The calculations represent the reduced amplitudes , as such they say nothing about the absolute normalization of the calculation . Only the shape of the cross section is reflected in the calculations . Figure 3-2 shows a spectrum with the ananlyzed states . The error bars of the cross sectional data reflect only the statistical spread calculated from the peak area .

Note : In the data presented those points with darkened circular centers represent data from the second experiment , those without are from the first experiment .

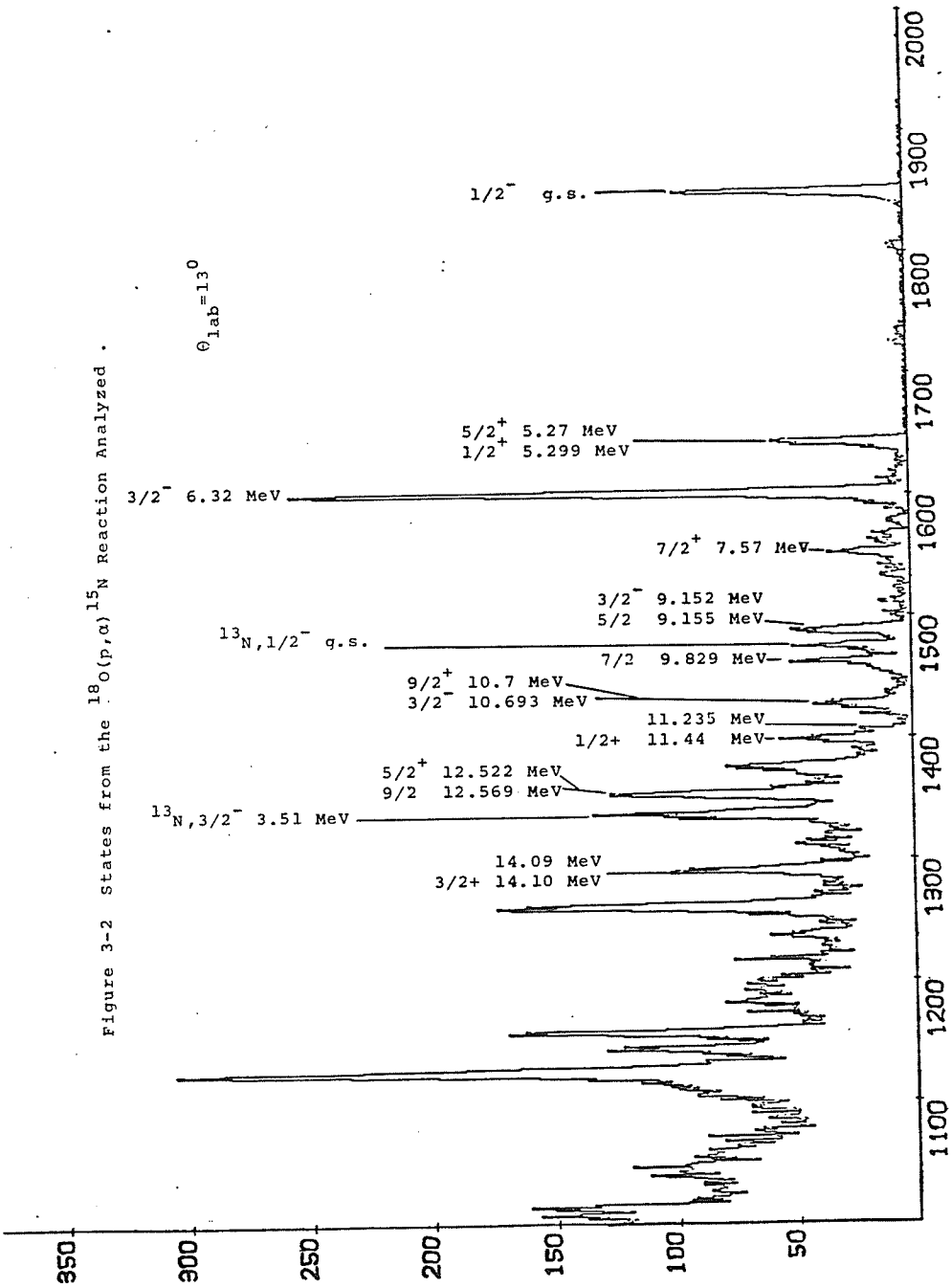

Figure 3-2 States from the $^{18}O(p,\alpha)^{15}N$ Reaction Analyzed .

$J^{\Pi} = 1/2^-$ Ground State

This state is believed to be predominantly a $p_{\frac{1}{2}}$ hole. The state has been observed in various stripping reactions to ^{15}N (ref. 28,29,30,31,34,38) . Falk et al [28] found that it was neccesary to assume a 2p-3h component in order to explain their results of a $^{12}C(\alpha,p)^{15}N$ reaction.

As noted previously , the bound state parameters used in the DWBA calculations were adjusted to agree with the cross sections for this state . Figure 3-3 displays the calculations and extracted data .The shape of the calculated distribution (N=2) appears to agree well with the extracted data . The calculation for N=1 is also shown . The DWBA distribution falls more rapidly in value than the experimental values , this problem was also noted by Maples [36].

The good agreement implies that the three nucleons transferred from the ^{18}O ground state are well represented as a single particle triton cluster .

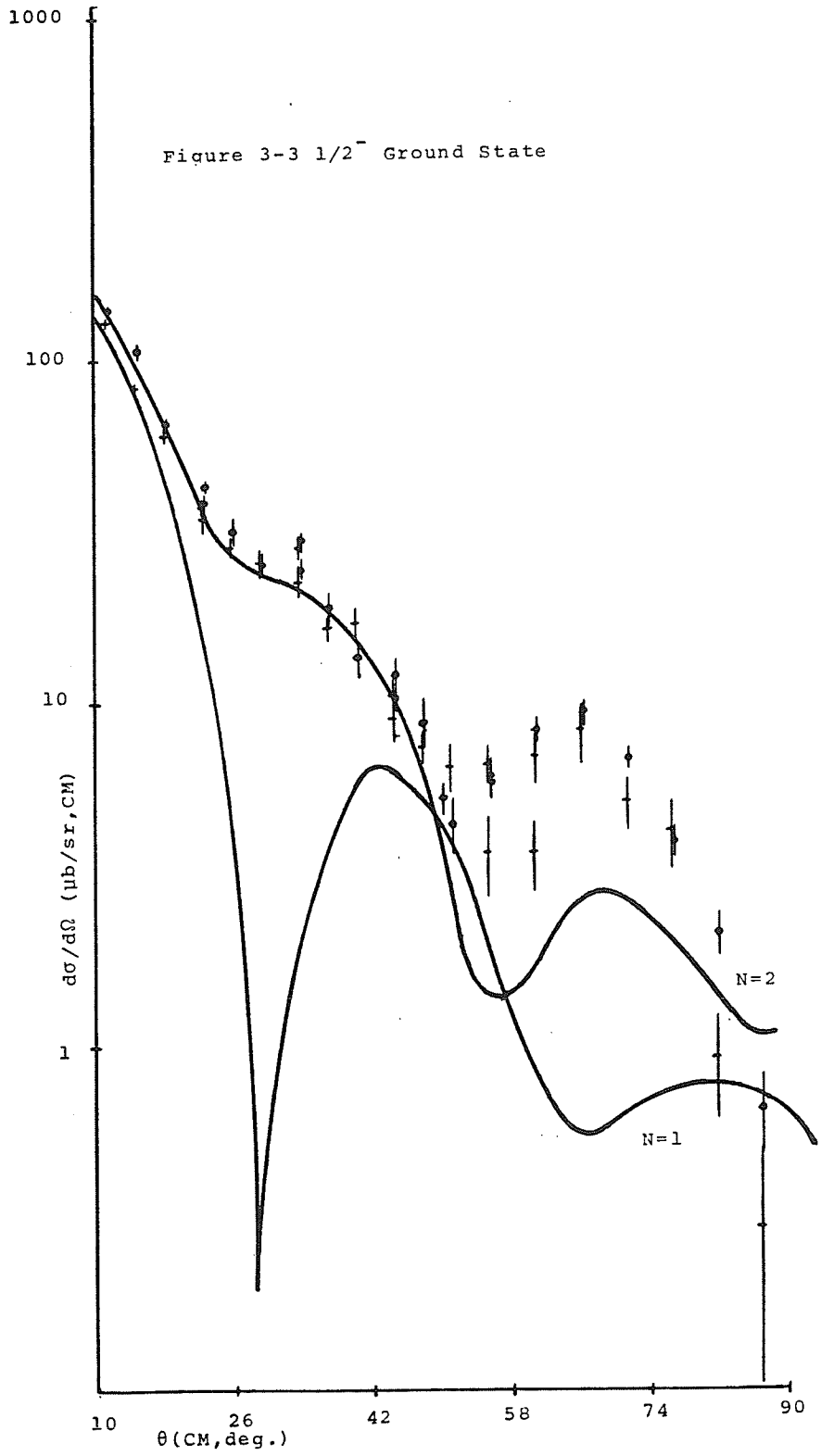

Figure 3-3 $1/2^-$ Ground State

$J^{\Pi} = 5/2^{+}$, 5.27 MeV and $J^{\Pi} = 1/2^{+}$, 5.299 MeV

These states are believed to be composed of 1p-2h and 3p-4h configurations [28,34]. These states, which are not resolved in this experiment or other experiments on stripping reactions [28,34], are strongly excited in the $^{12}C(\alpha,p)^{15}N$ reaction as well as the pick-up experiment discussed here. Figures 3-4 a) and 3-4 b) show cluster transfer calculations for the $5/2^{+}$, (N=1,2), and the $1/2^{+}$ (N=1,2,3) states. Also shown (fig. 3-4 c) is a linear combination of the $5/2^{+}$, (N=1) plus the $1/2^{+}$(N=2) states. The broken line is the linear superposition, which was found by matching the sum of the two theoretical calculations to experimental data at two arbitrary angles. The superposition appears to match the shape of the data well, below 58 degrees, falling off rapidly at larger angles.

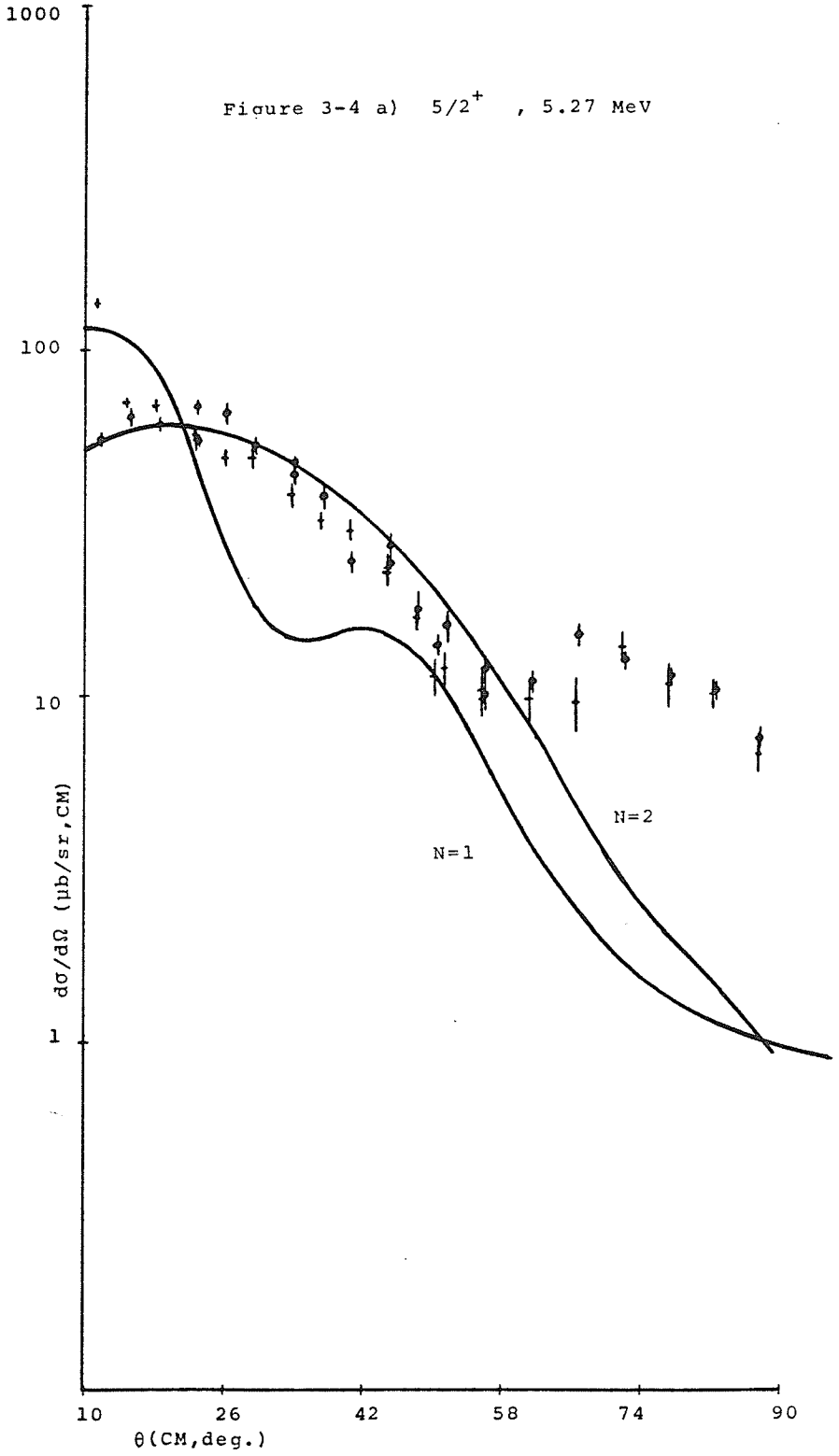

Figure 3-4 a) $5/2^+$, 5.27 MeV

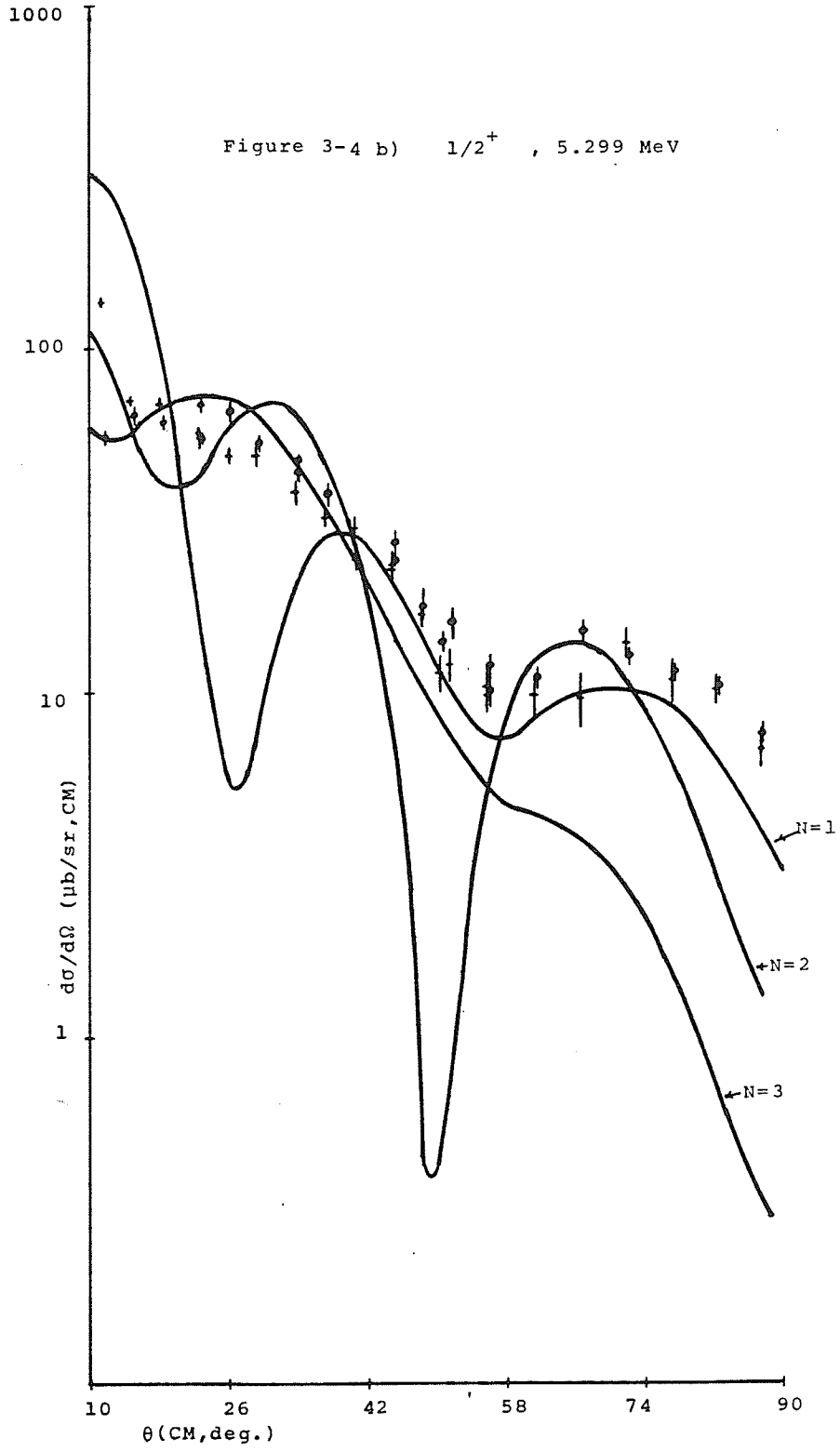

Figure 3-4 b) $1/2^+$, 5.299 MeV

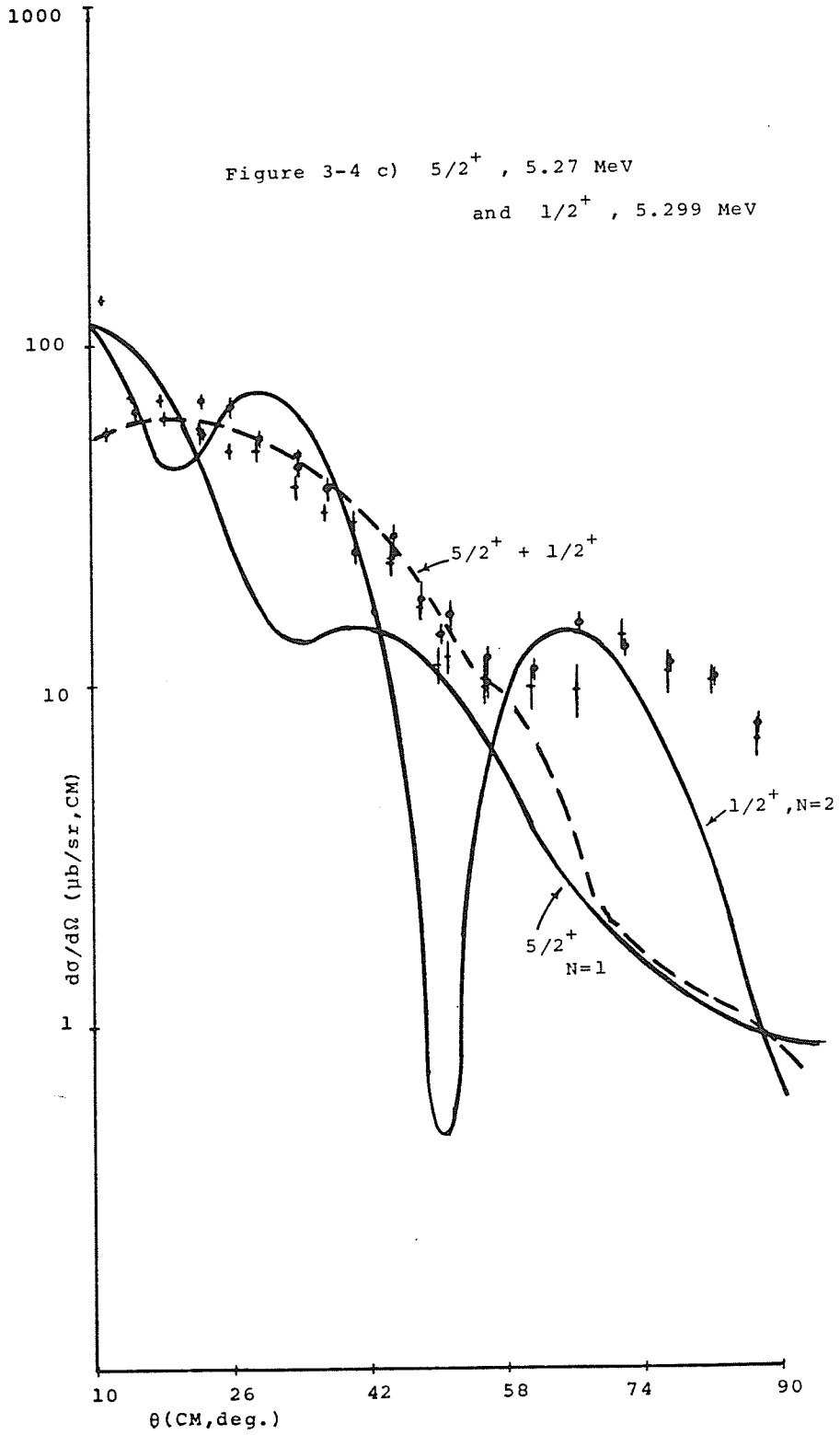

Figure 3-4 c) $5/2^+$, 5.27 MeV
and $1/2^+$, 5.299 MeV

$J^{\Pi} = 3/2^-$, 6.32 MeV State

This state is believed to consist predominantly of a $p_{3/2}$ hole . It is only weakly excited by stripping reactions leading from ^{12}C to ^{15}N (ref. 28,29) implying that the dominant configuration of the ^{12}C target has filled $p_{3/2}$ levels . This state is strongly excited by the $^{18}O(p,\alpha)^{15}N$ reaction. The cluster transfer calculations do not reproduce the shape of the measured distributions satisfactorily (Fig. 3-5 a) . An attempt was made to reconcile the shape of this calculation with that of the experiment , still yielding poor results (Fig. 3-5 b). This was carried out by making small adjustments to the triton bound state radius and diffuseness .

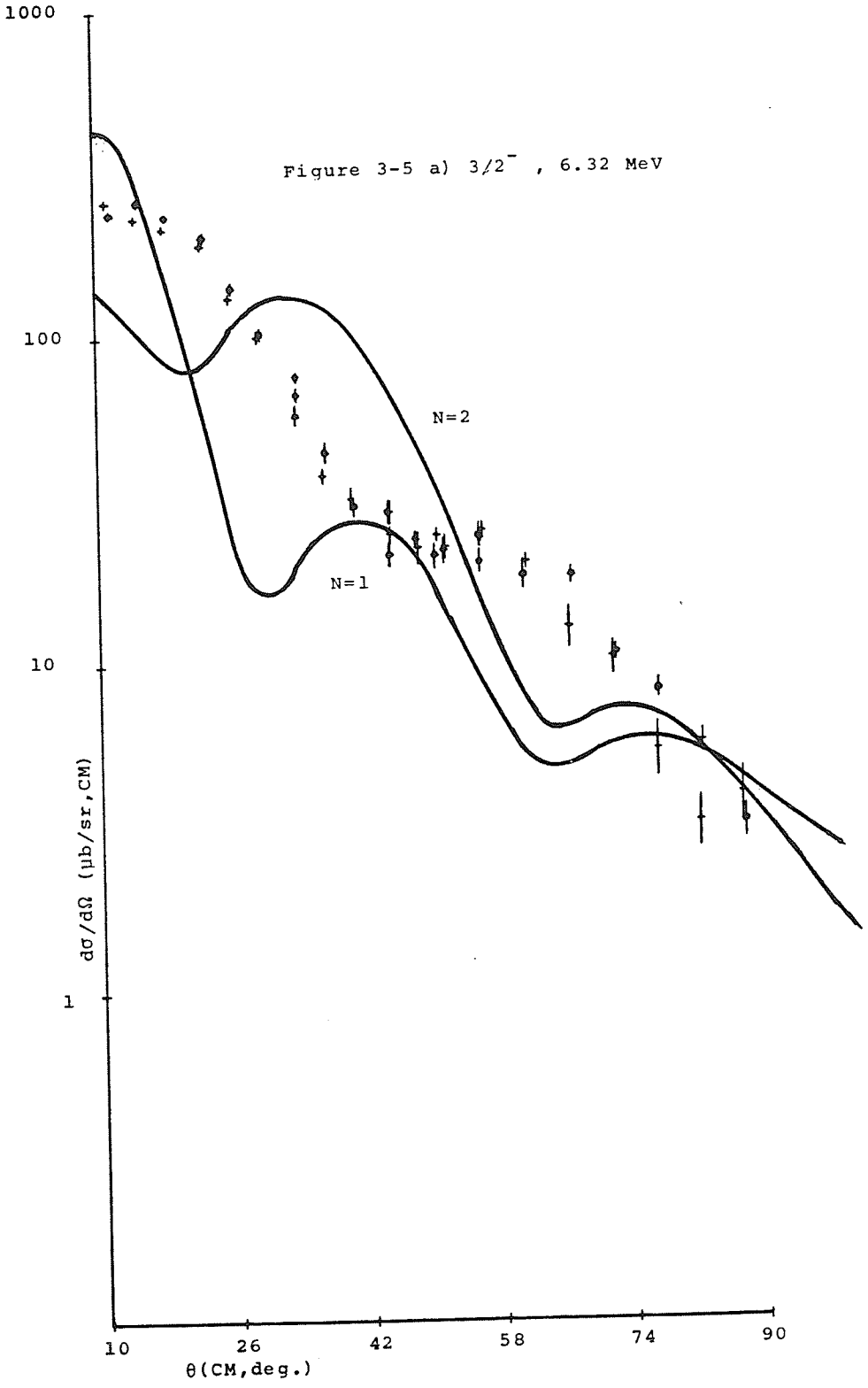

Figure 3-5 a) $3/2^-$, 6.32 MeV

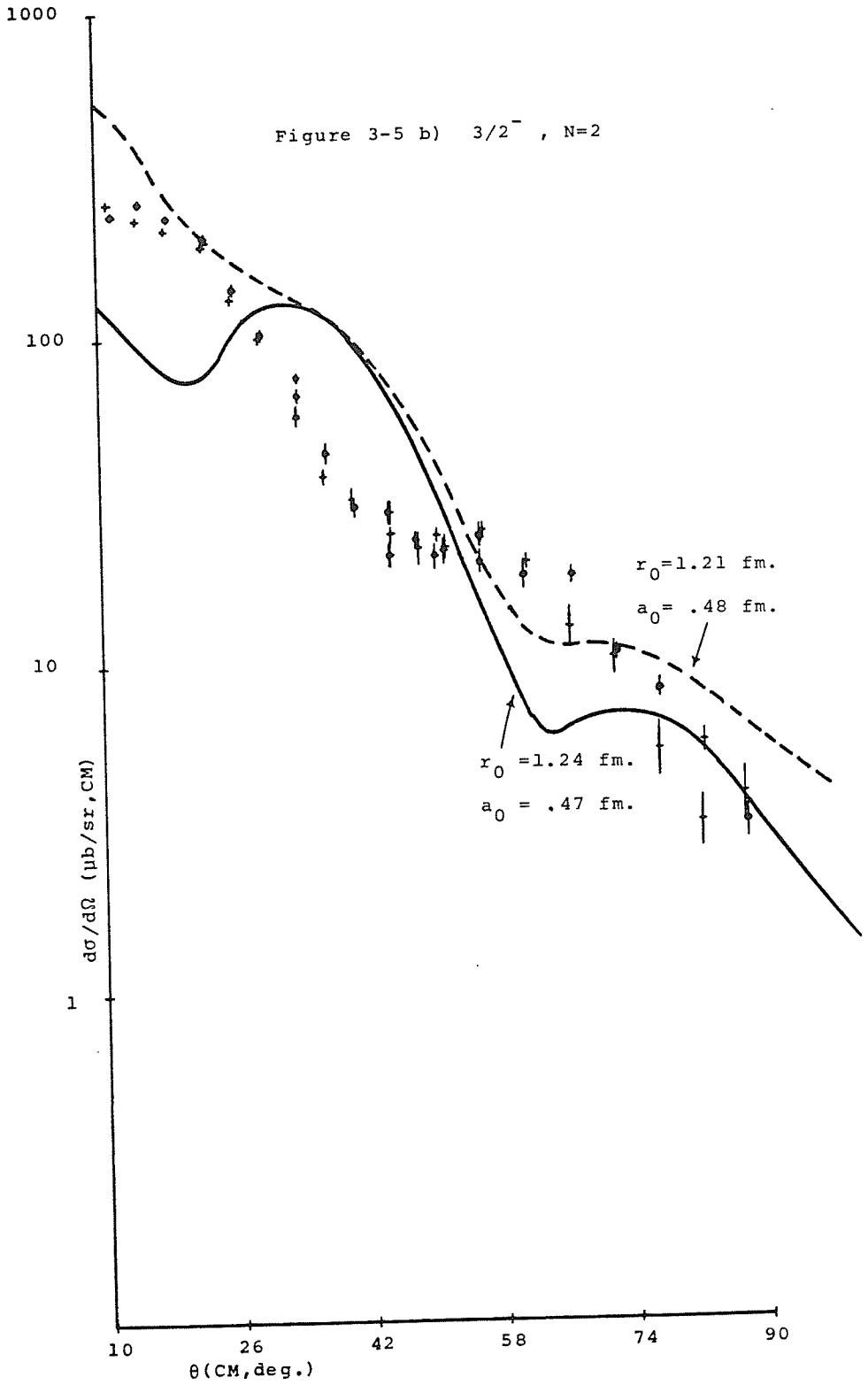

Figure 3-5 b) $3/2^-$, N=2

$J^{\Pi} = 7/2^{+}$, 7.57 MeV State

This state is excited in both the $^{12}C(\alpha,p)^{15}N$ and $^{18}O(p,\alpha)^{15}N$ reactions . It is believed to have a dominant 1p-2h nature [28]. The shape of the N=2 cluster transfer calculation bears a resemblance to the extracted data (Fig. 3-6) , although the pathological drop in magnitude is present .

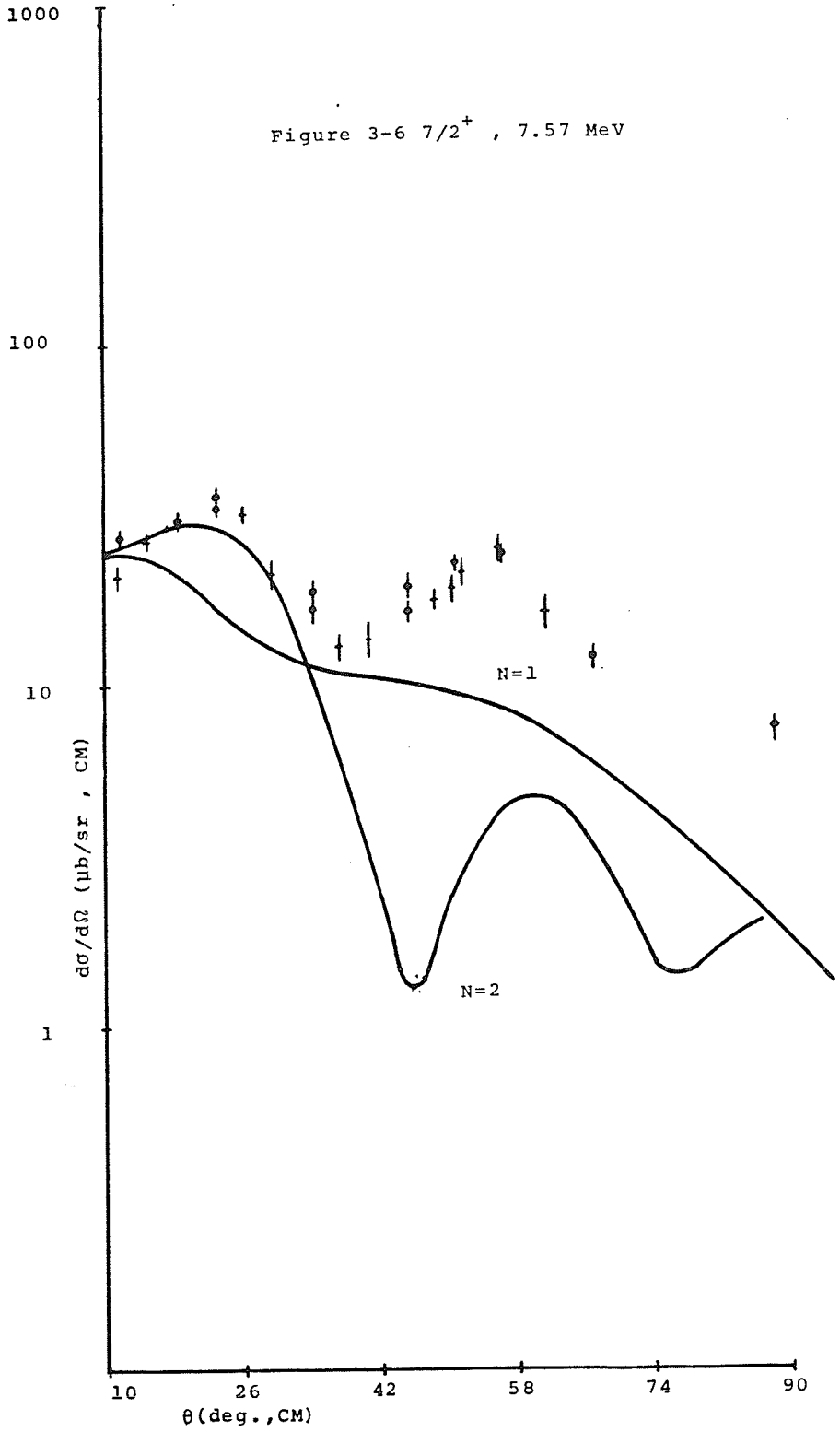

Figure 3-6 $7/2^+$, 7.57 MeV

$J^{\Pi} = 3/2^-$, 9.152 MeV and 9.155 MeV ($5/2^+$) States

The parity of the 9.155 MeV state is unknown. Shell model calculations [28] suggest that it has positive parity The $J^{\Pi} = 3/2^-$ state is believed to have a dominant 2p-3h configuration, while the $J = 5/2^{(+)}$ state has large 3p-4h components. Figures 3-7 a) and b) show the cluster transfer calculations for the two states . Figure 3-7 a) shows a linear combination of the two (broken line) for the $5/2^+$, N=1 and $3/2^-$,N=2 curves . The shape of this curve resembles the data at lower angles , however , at higher angles the curve exhibits a sharp drop .

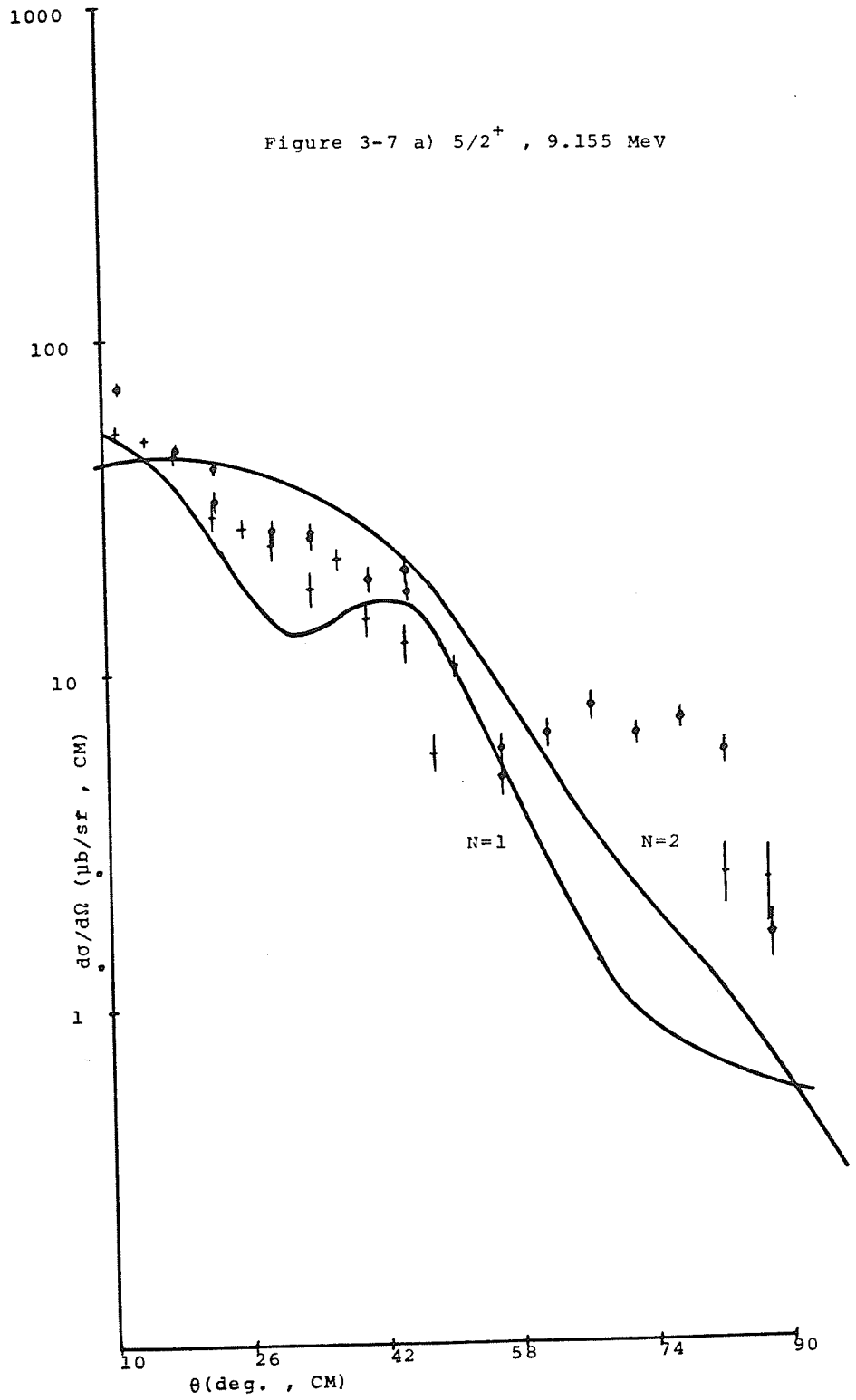

Figure 3-7 a) $5/2^+$, 9.155 MeV

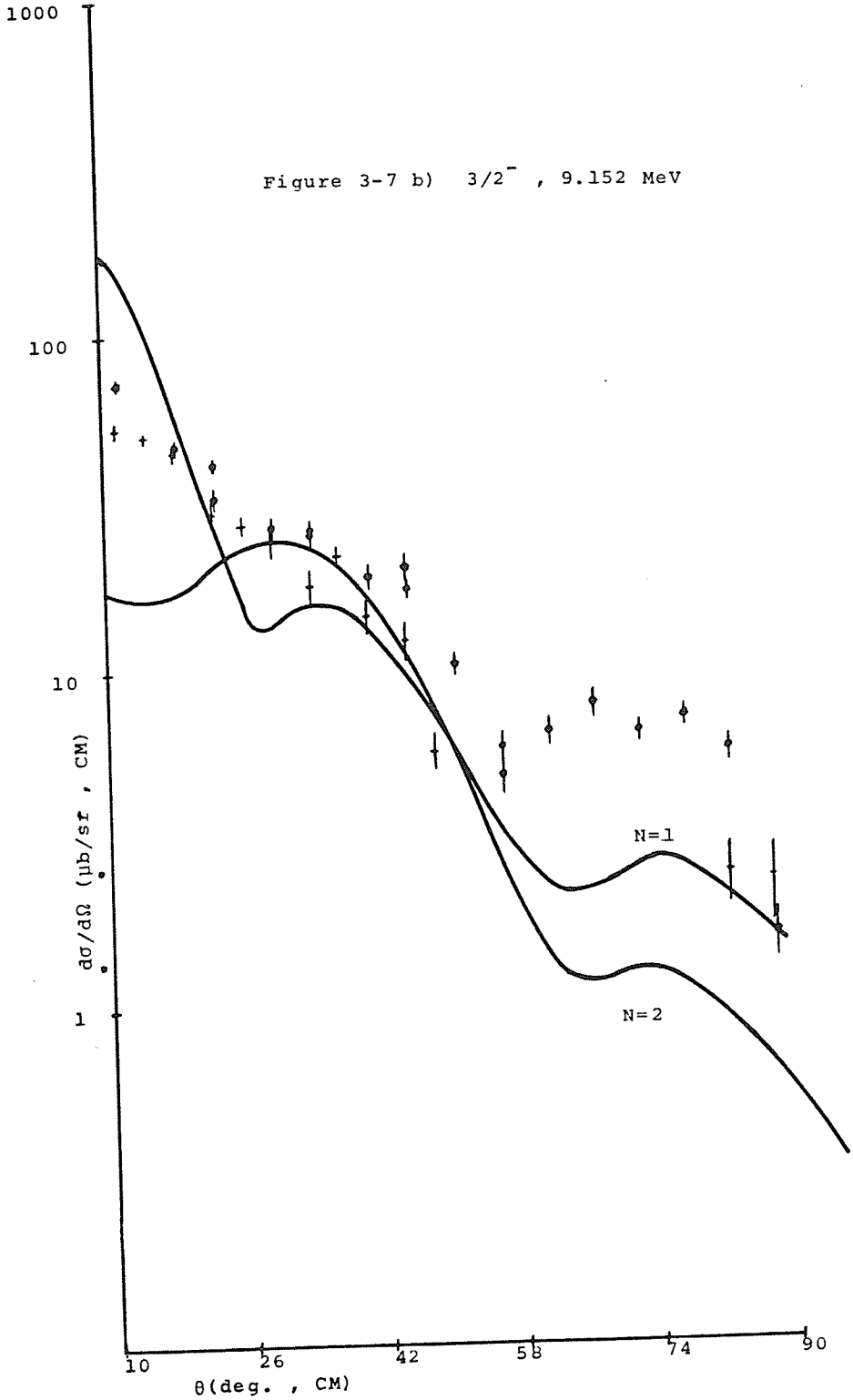

Figure 3-7 b) $3/2^-$, 9.152 MeV

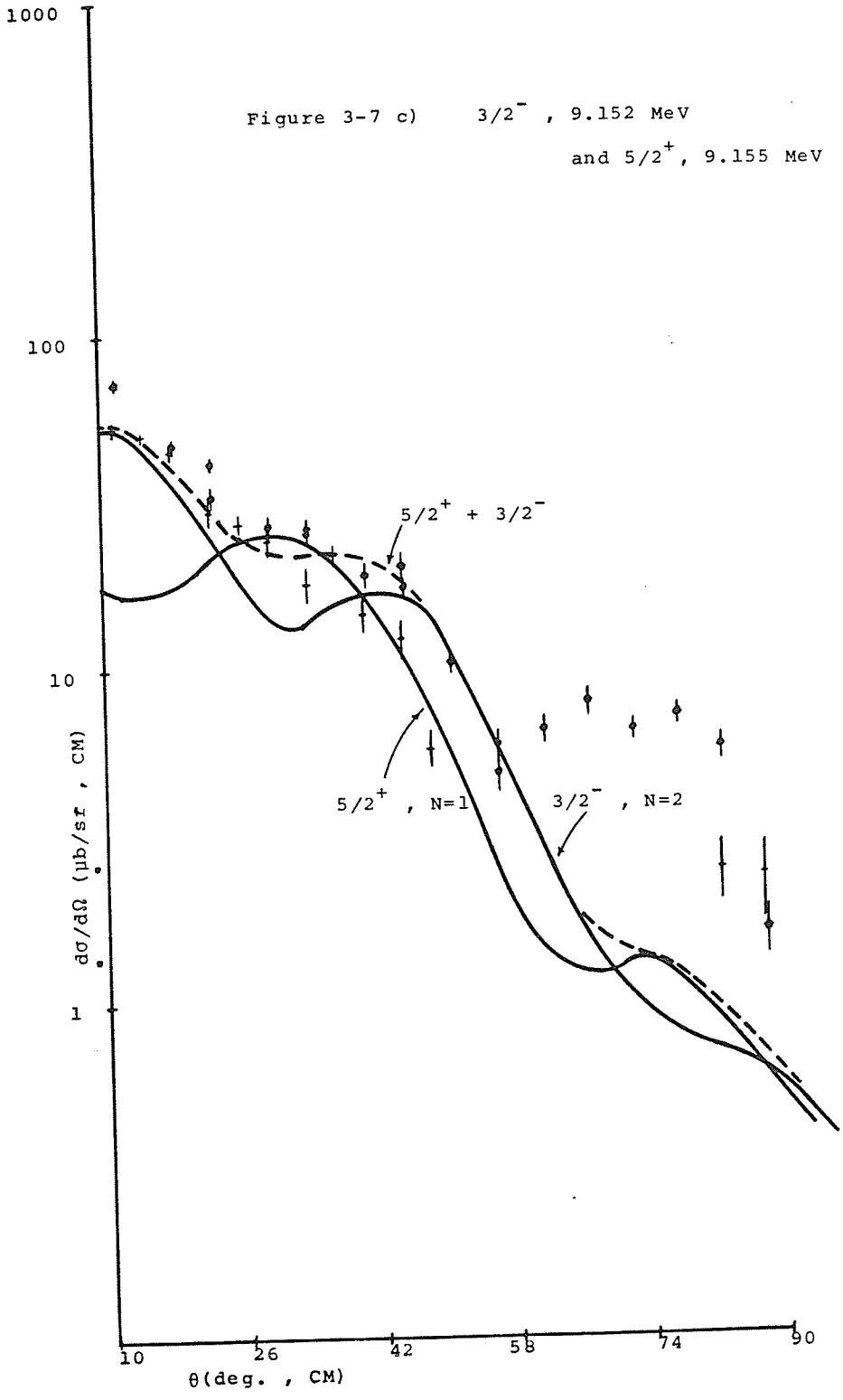

Figure 3-7 c) $3/2^-$, 9.152 MeV
and $5/2^+$, 9.155 MeV

J = 7/2 9.829 MeV State

This state is excited by stripping reactions to ^{15}N and is moderately excited in the $^{18}O(p,\alpha)^{15}N$ reaction . Philips et al[32] have assigned a negative parity to this state . Figures 3-8 a) and b) show cluster transfer calculations for the $7/2^+$ and $7/2^-$ states .

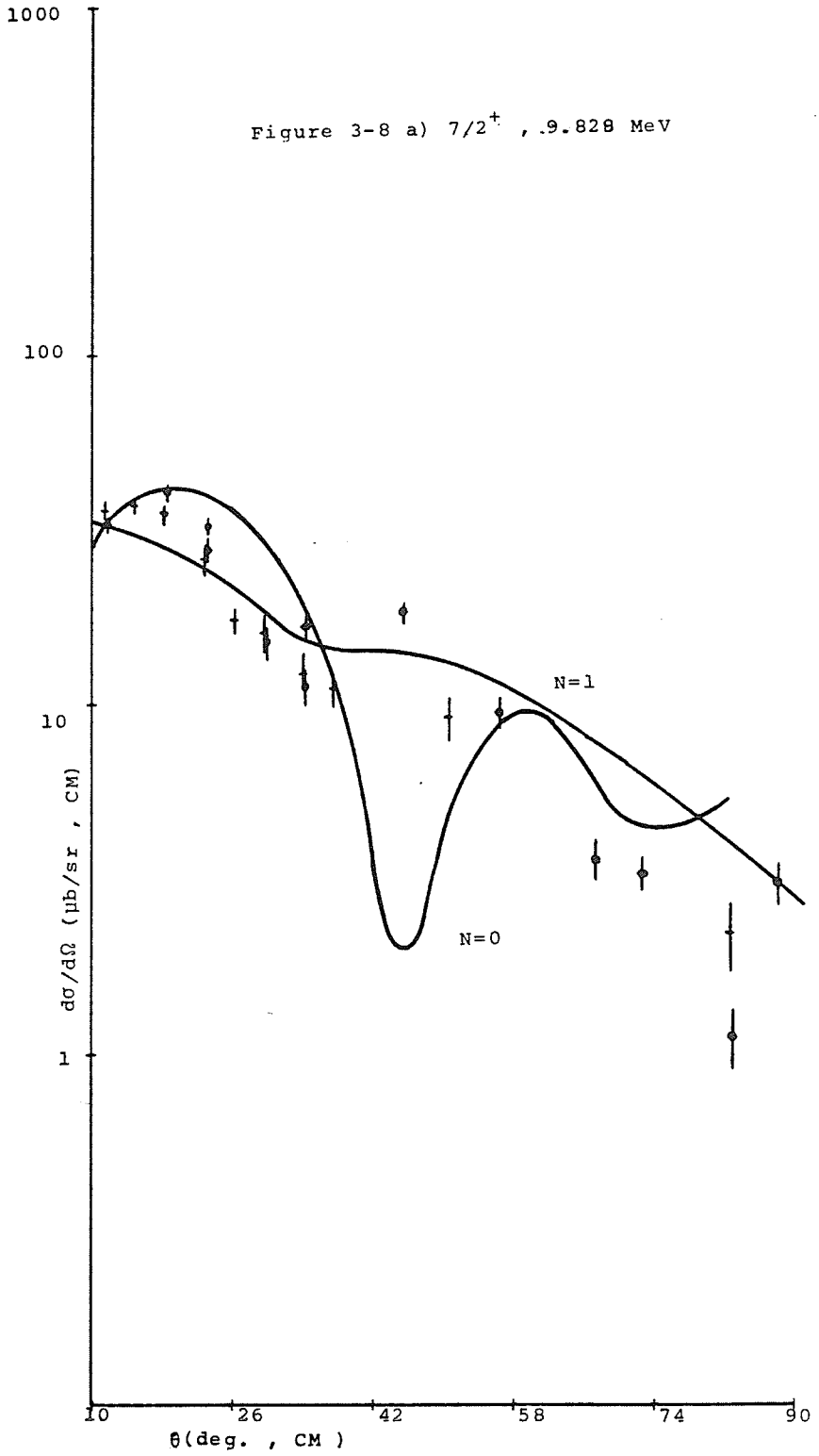

Figure 3-8 a) $7/2^+$, 9.828 MeV

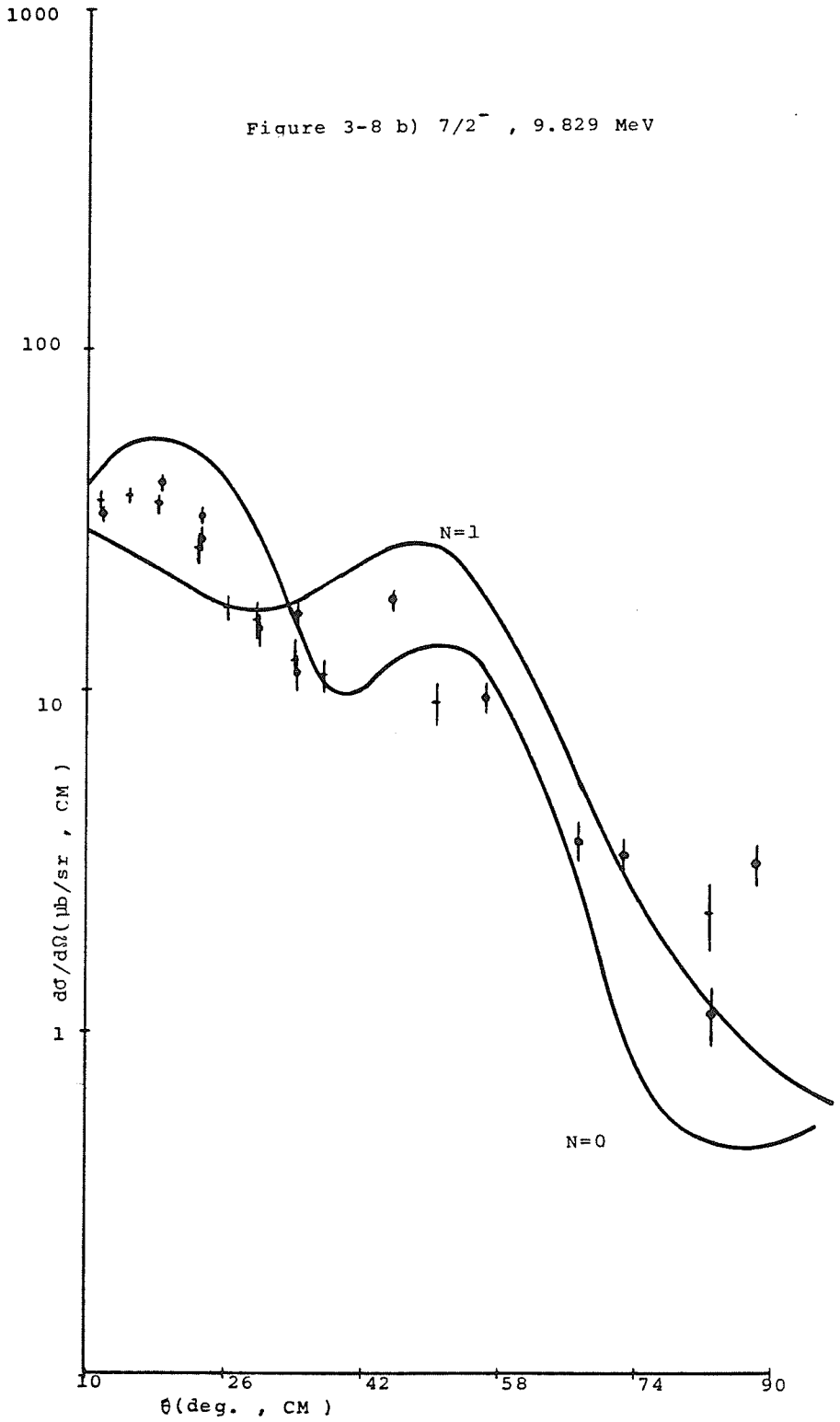

Figure 3-8 b) $7/2^-$, 9.829 MeV

$J^{\Pi} = 9/2^{+}$, 10.7 MeV and $J^{\Pi} = 3/2^{-}$, 10.693 MeV

This doublet is observed in stripping experiments to ^{15}N (ref 28) . It was assumed in these studies that the $9/2^{+}$ state (Fig. 3-9 a) was being excited . The cluster transfer calculations for the $9/2^{+}$ state (Fig. 3-9 a) appears to follow the trend of the data , while the $3/2^{-}$ state (Fig. 3-9 b) does not .

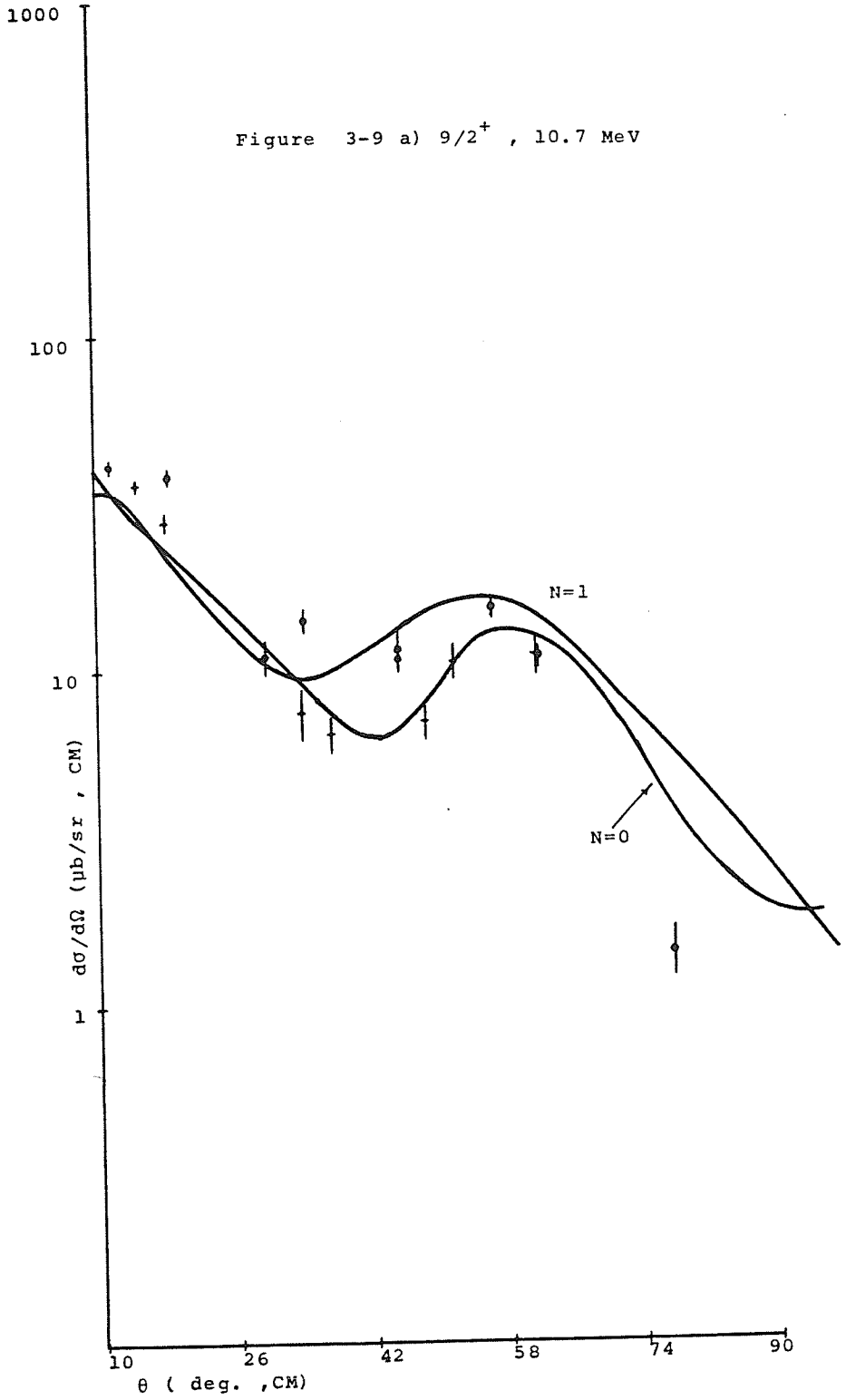

Figure 3-9 a) $9/2^+$, 10.7 MeV

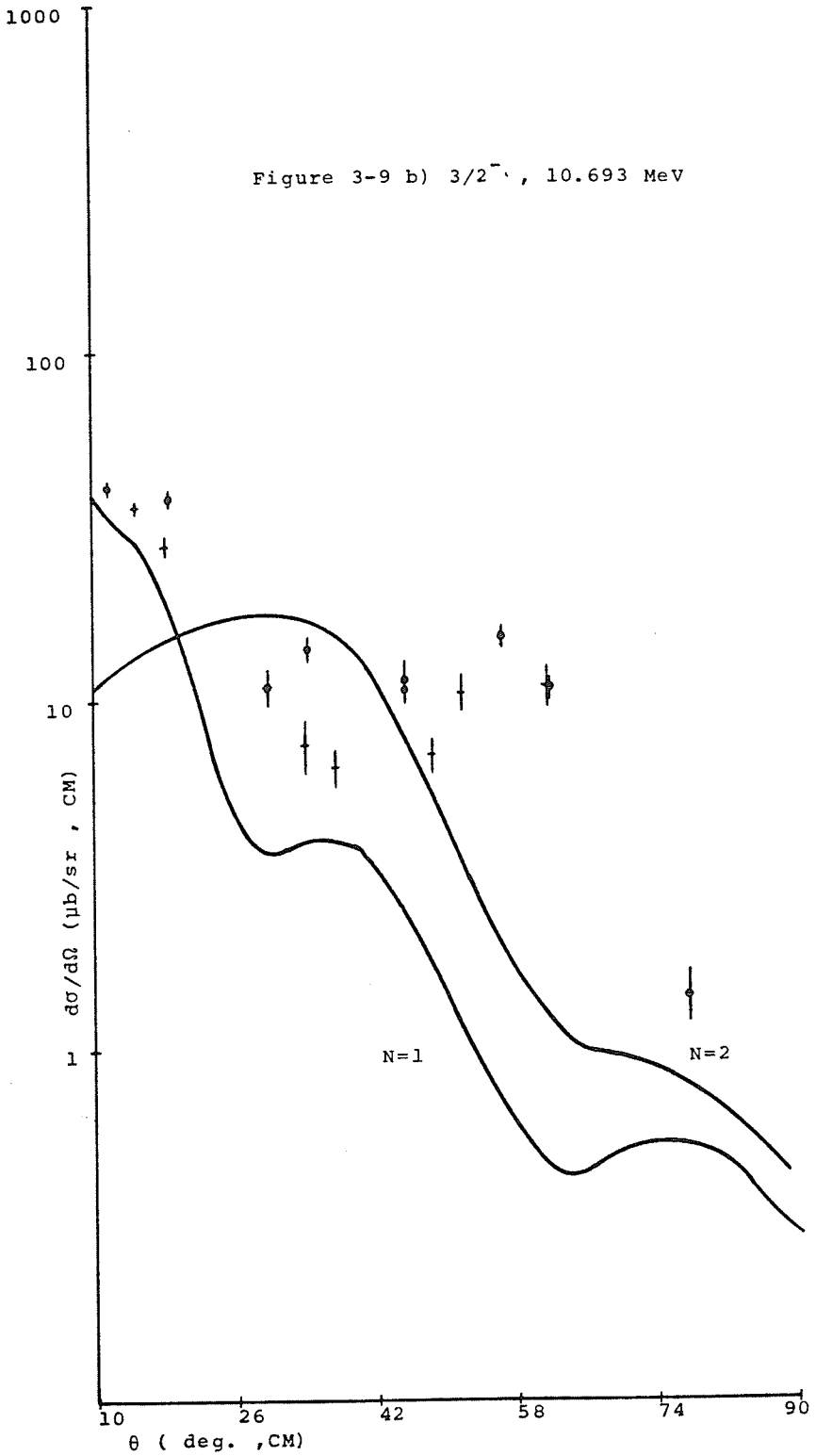

Figure 3-9 b) $3/2^-$, 10.693 MeV

$J > 3/2$, 11.235 MeV State

This state , along with the $J^{\Pi} = 1/2^{+}$ 11.44 MeV state is not reported in the $^{12}C(\alpha,p)^{15}N$ stripping studies [28,34) , implying that it has hole configurations in the (s-p) ^{12}C core . Figures 3-10 a) to i) , show cluster transfer calculations for $J^{\Pi} = 3/2\pm$, $5/2\pm$,$7/2\pm$, $9/2\pm$ and $11/2\pm$.

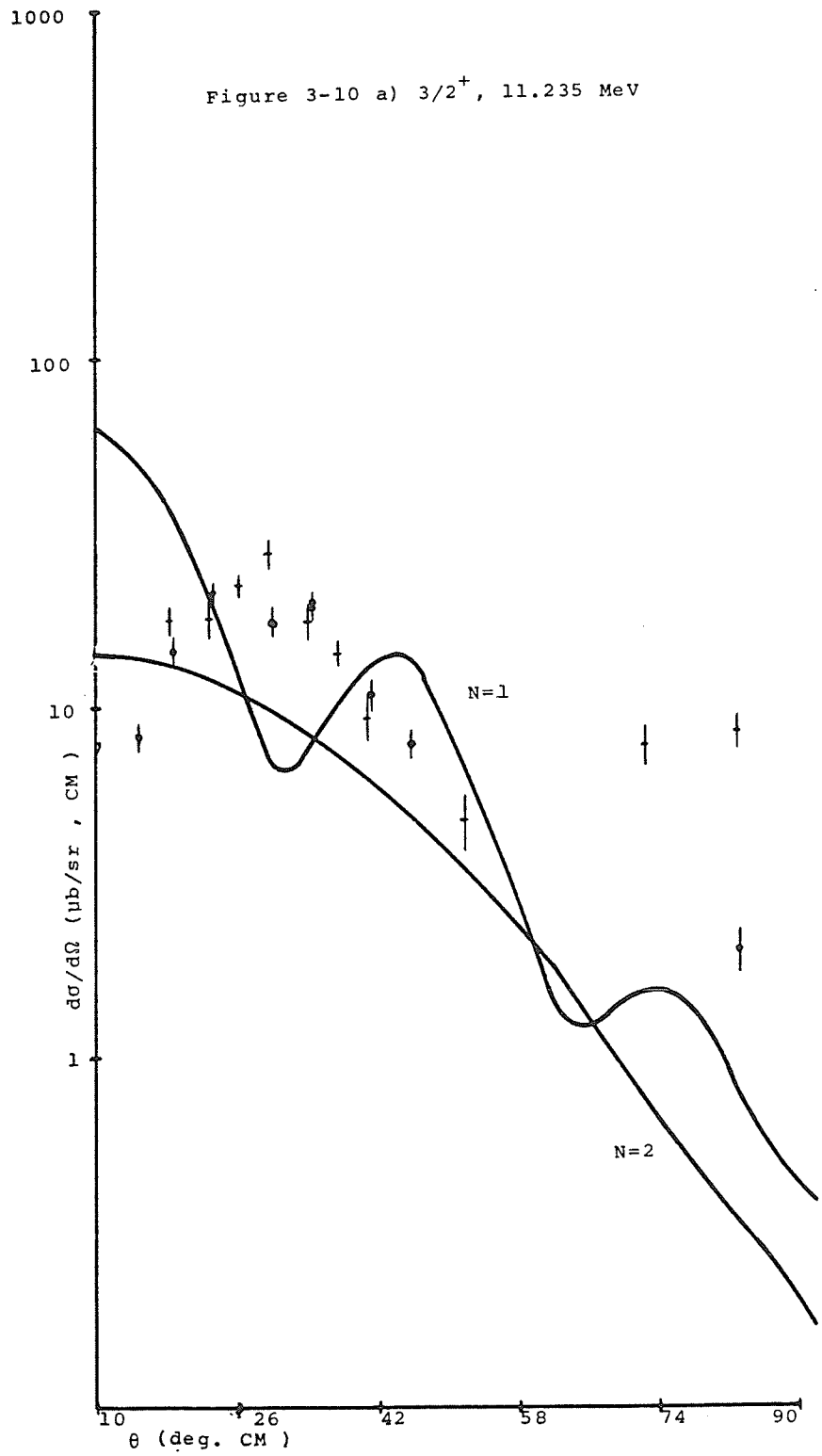

Figure 3-10 a) $3/2^+$, 11.235 MeV

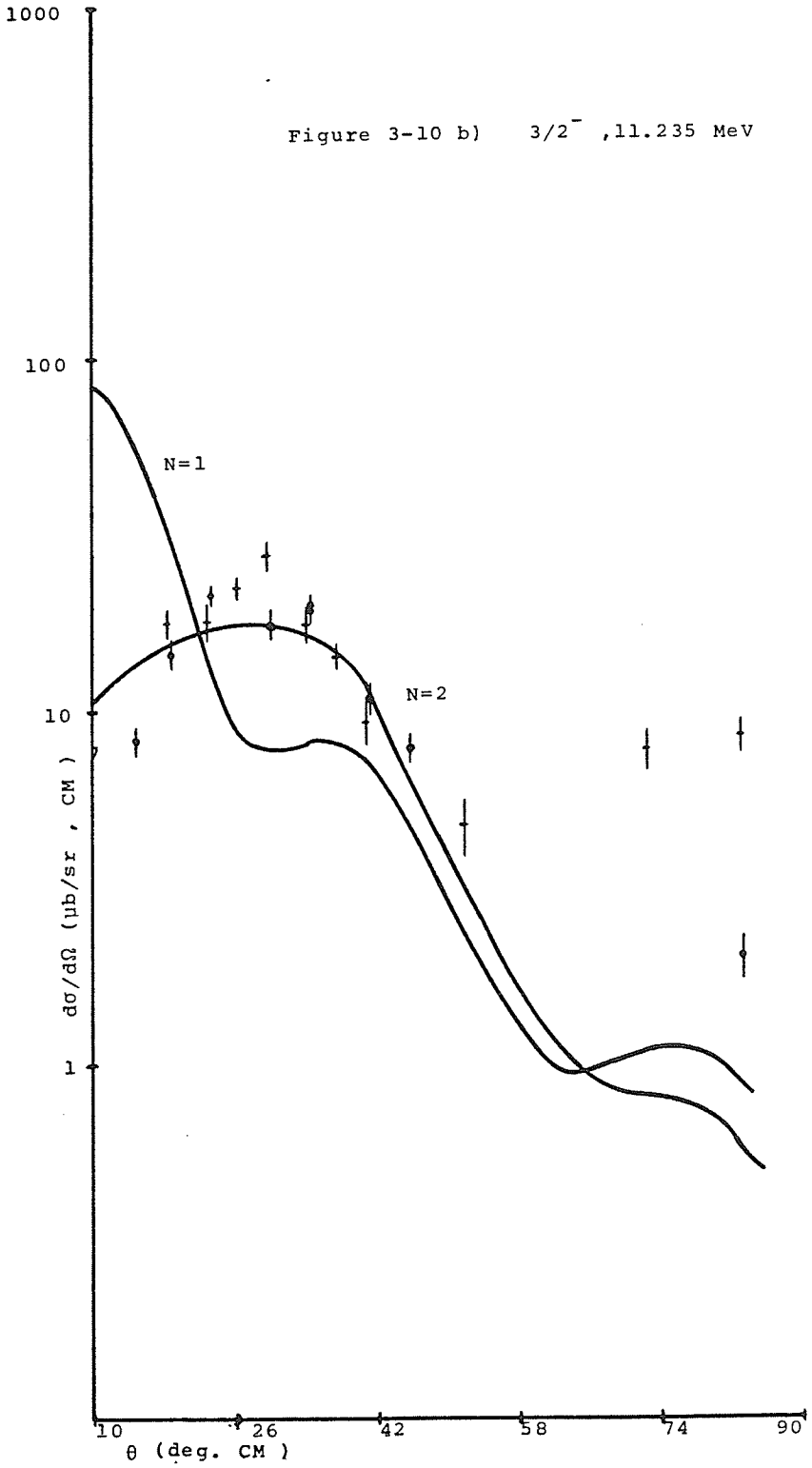

Figure 3-10 b) $3/2^-$,11.235 MeV

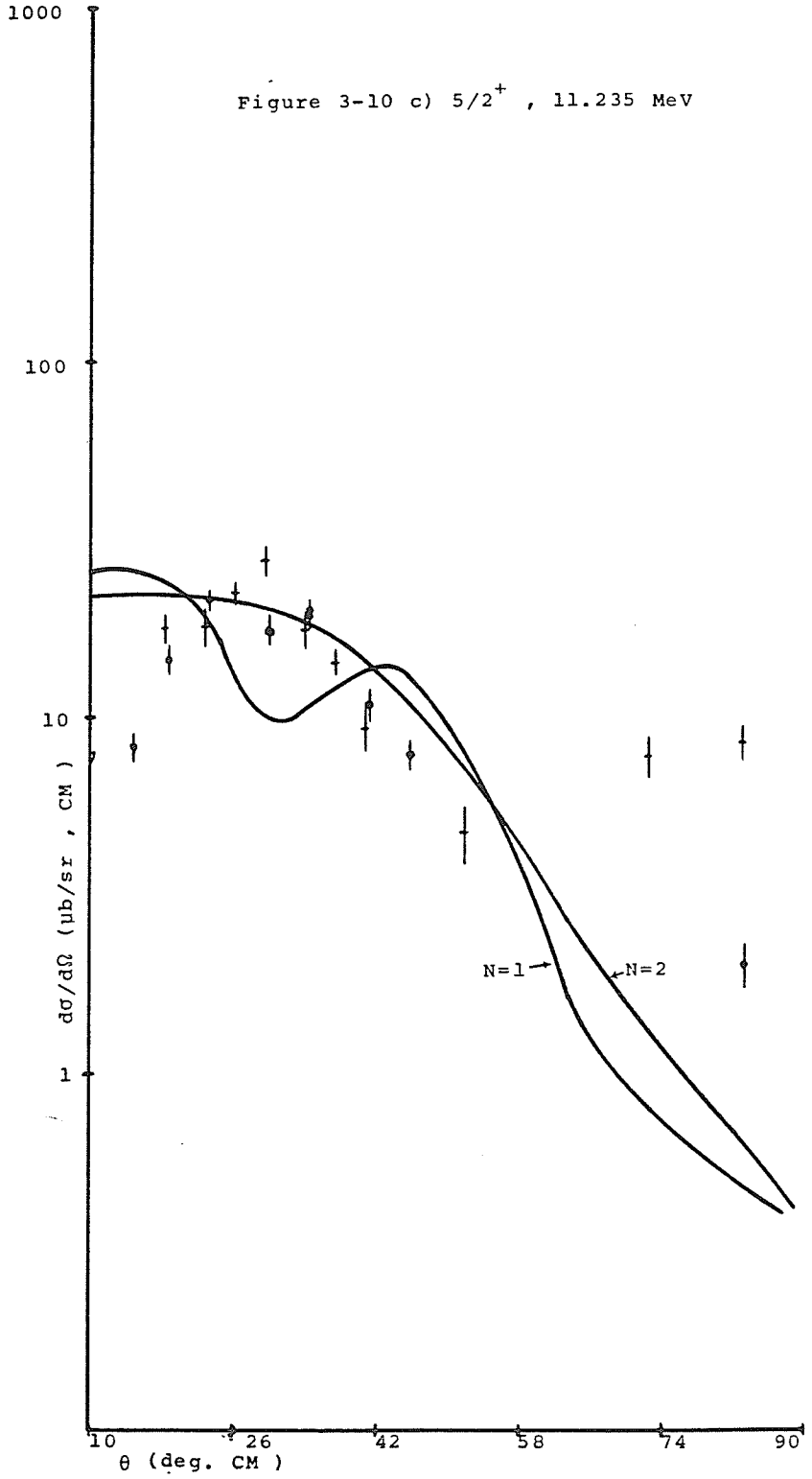

Figure 3-10 c) $5/2^+$, 11.235 MeV

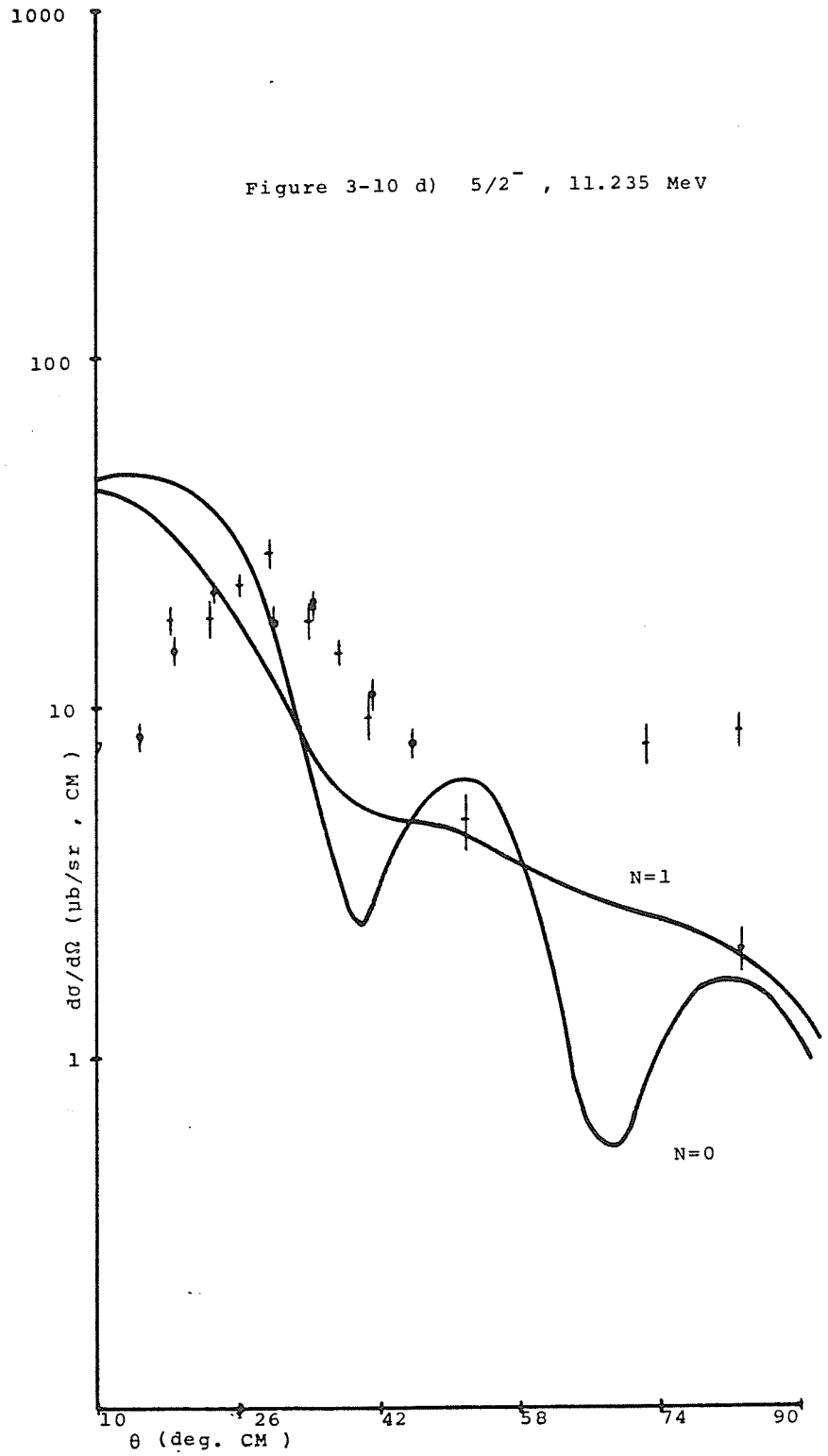

Figure 3-10 d) $5/2^-$, 11.235 MeV

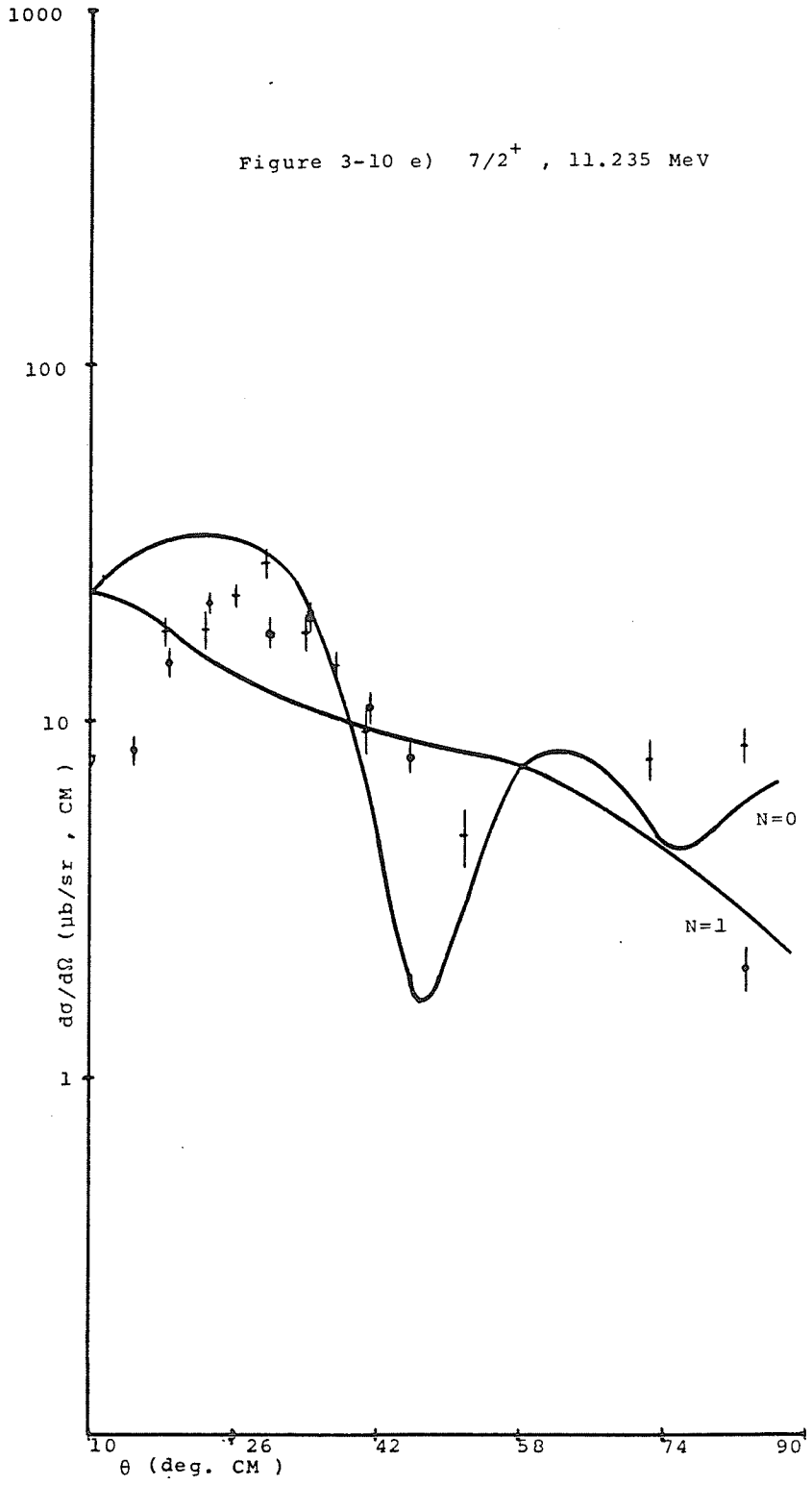

Figure 3-10 e) $7/2^+$, 11.235 MeV

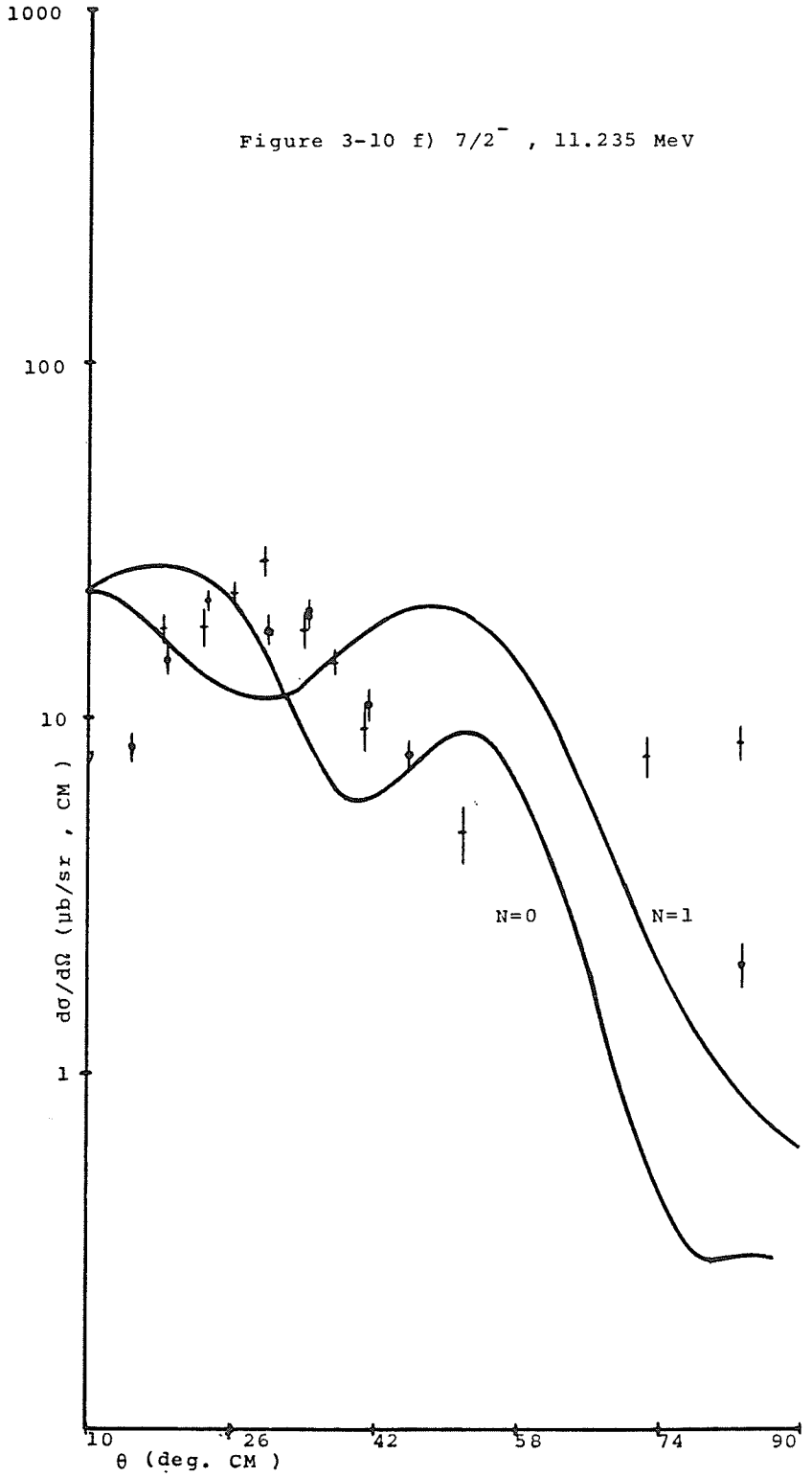

Figure 3-10 f) $7/2^-$, 11.235 MeV

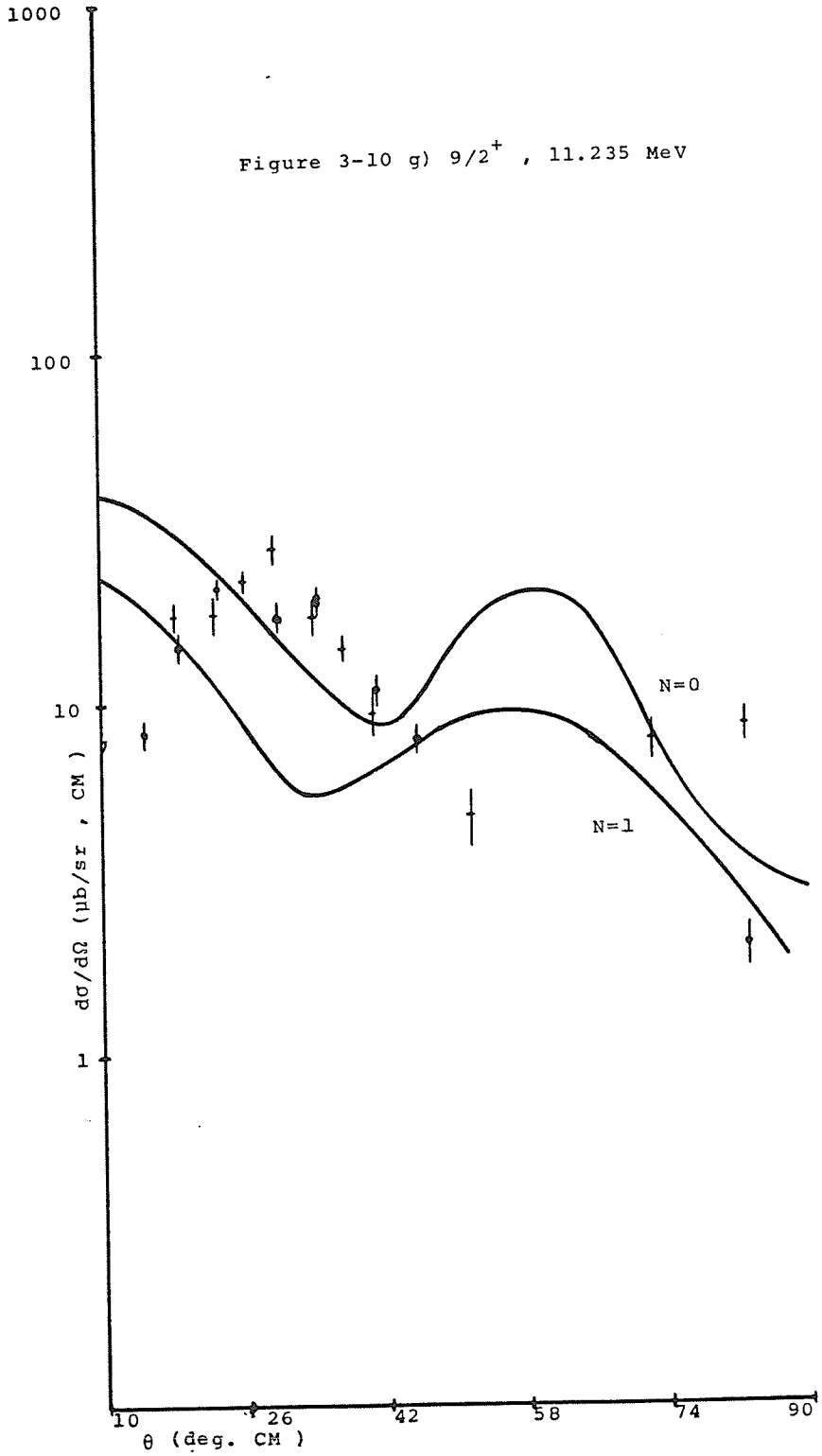

Figure 3-10 g) $9/2^+$, 11.235 MeV

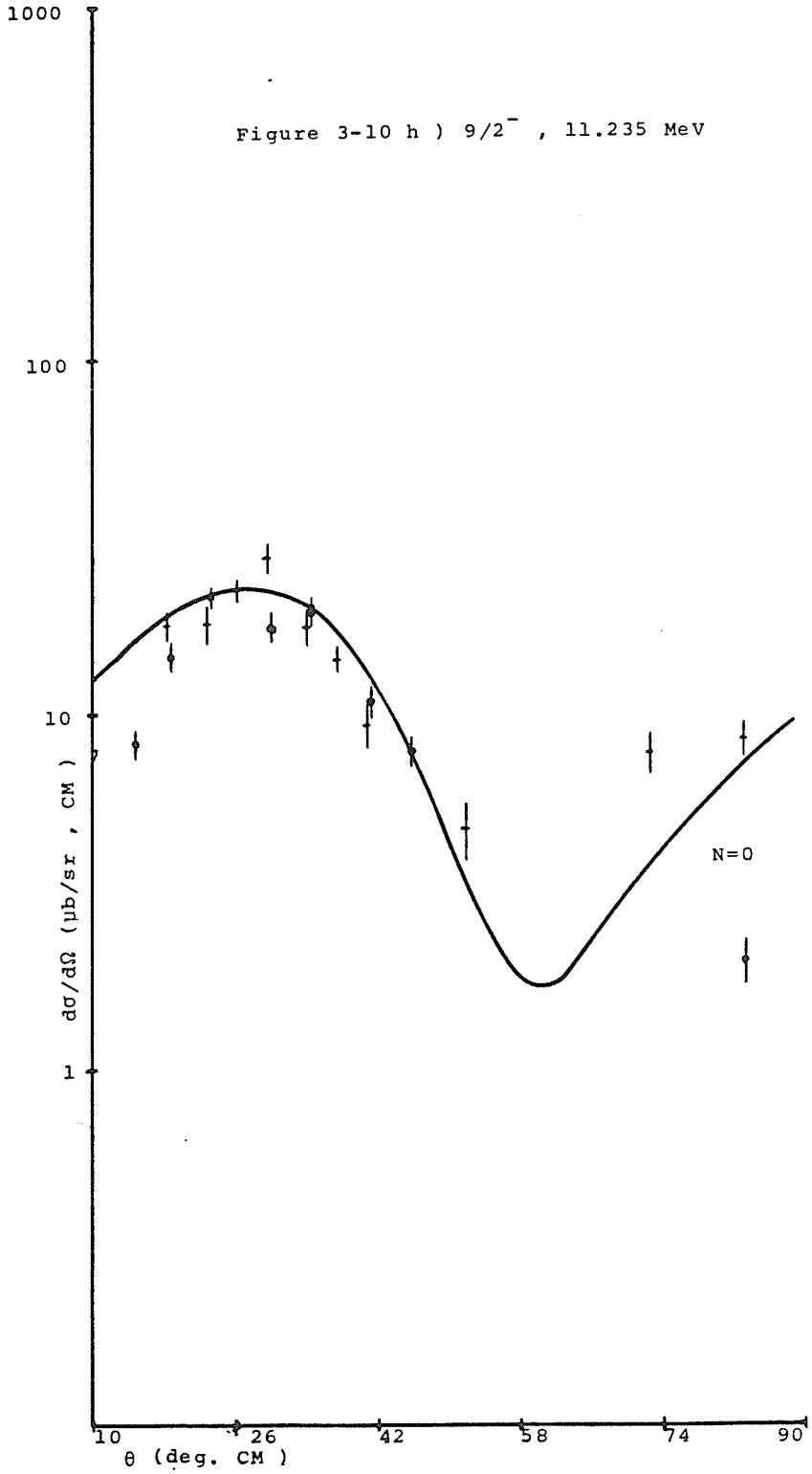

Figure 3-10 h) $9/2^-$, 11.235 MeV

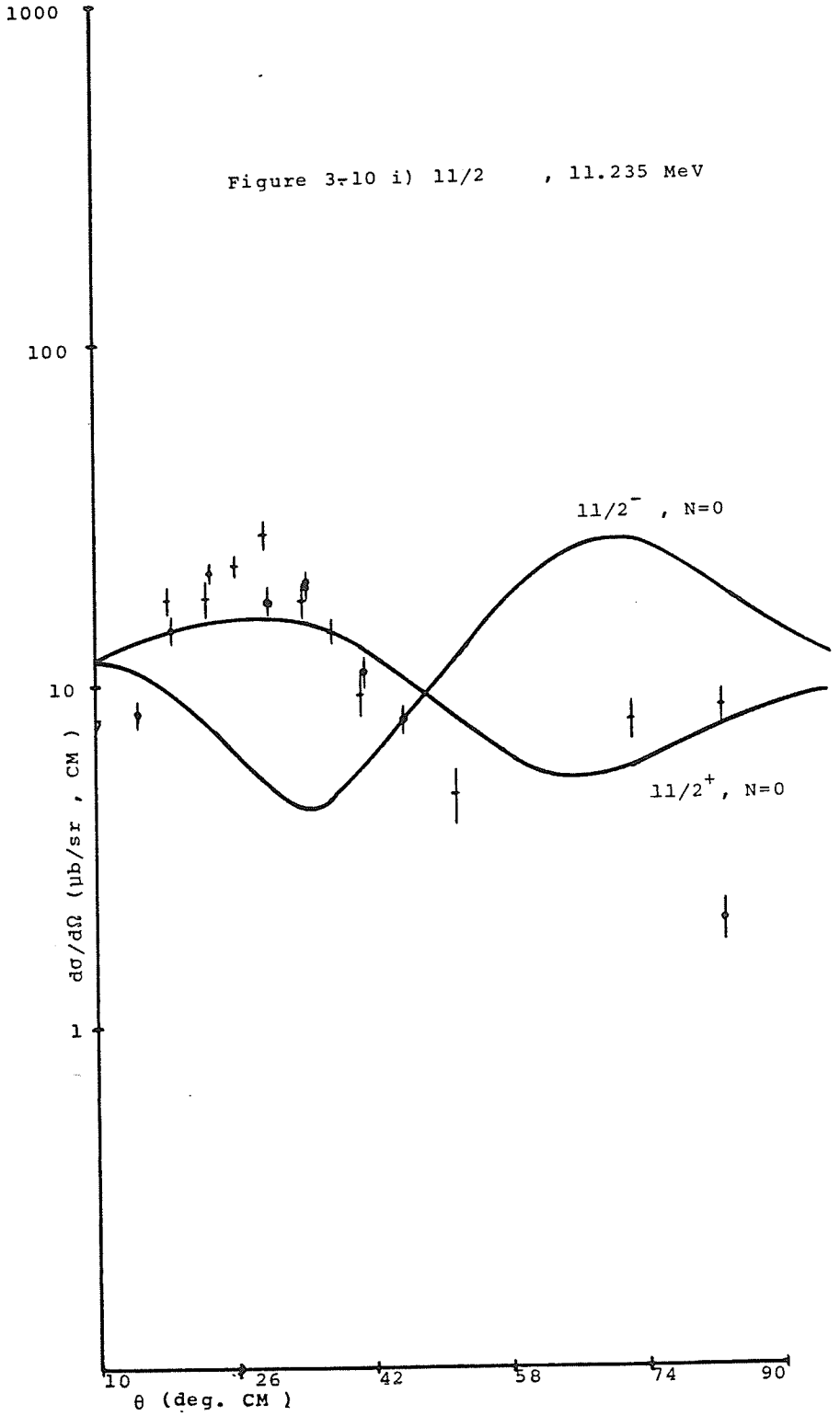

Figure 3-10 i) 11/2 , 11.235 MeV

$J^{\Pi} = 1/2^{+}$ 11.44 MeV State

This state is not reported in the $^{12}C(\alpha,p)^{15}N$ stripping studies[28,34], but is relatively strong in the $^{18}O(p,\alpha)^{15}N$ pick-up reaction. This would appear to imply that this state contains hole configurations in the (sp) ^{12}C core , which would not be excited in a $^{12}C(\alpha,p)^{15}N$ reaction . The cluster transfer calculations (fig. 3-11) do not appear to reproduce the salient features of the extracted data .

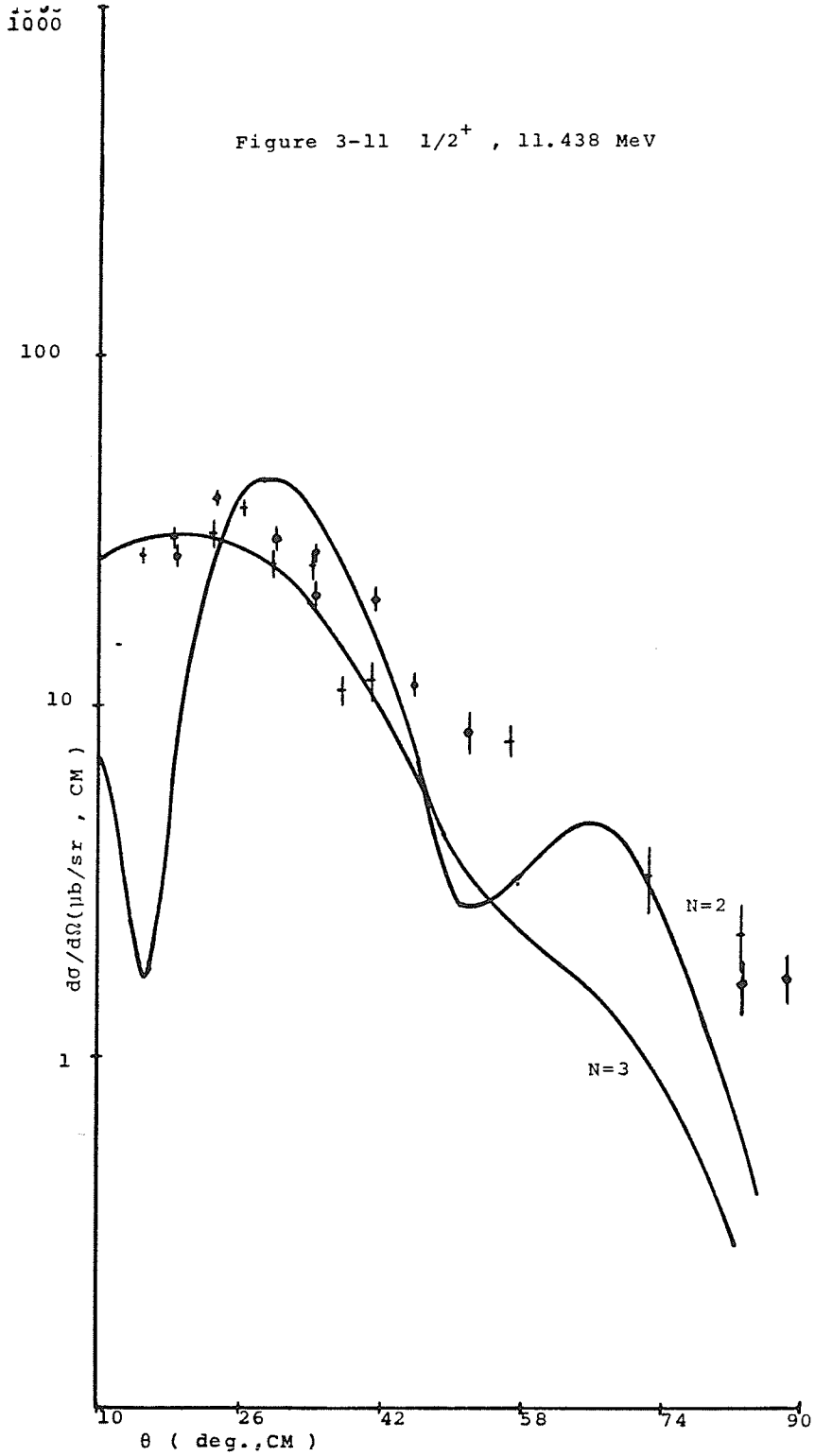

Figure 3-11 $1/2^+$, 11.438 MeV

J $=5/2^+$ 12.522 MeV and J=9/2 12.569 MeV States

This doublet is strongly excited in the $^{18}O(p,\alpha)^{15}N$ reaction but is relatively weak in the $^{12}C(\alpha,p)^{15}N$ reaction[28,34] . Shell model calculations[34] predict a 1p-2h $9/2^+$ state of ^{15}N near 12.55 MeV . Shown in figures 3-12 a and b , are cluster transfer calculations for the $5/2^+$, 12.522 MeV state . There is apparently a strong L-dependance in the 9/2 states , since the L=4 ($9/2^+$) and L=5 ($9/2^-$) states are very different . A strong L-dependance was not in general observed in the $^{12}C(\alpha,p)^{15}N$ reaction .

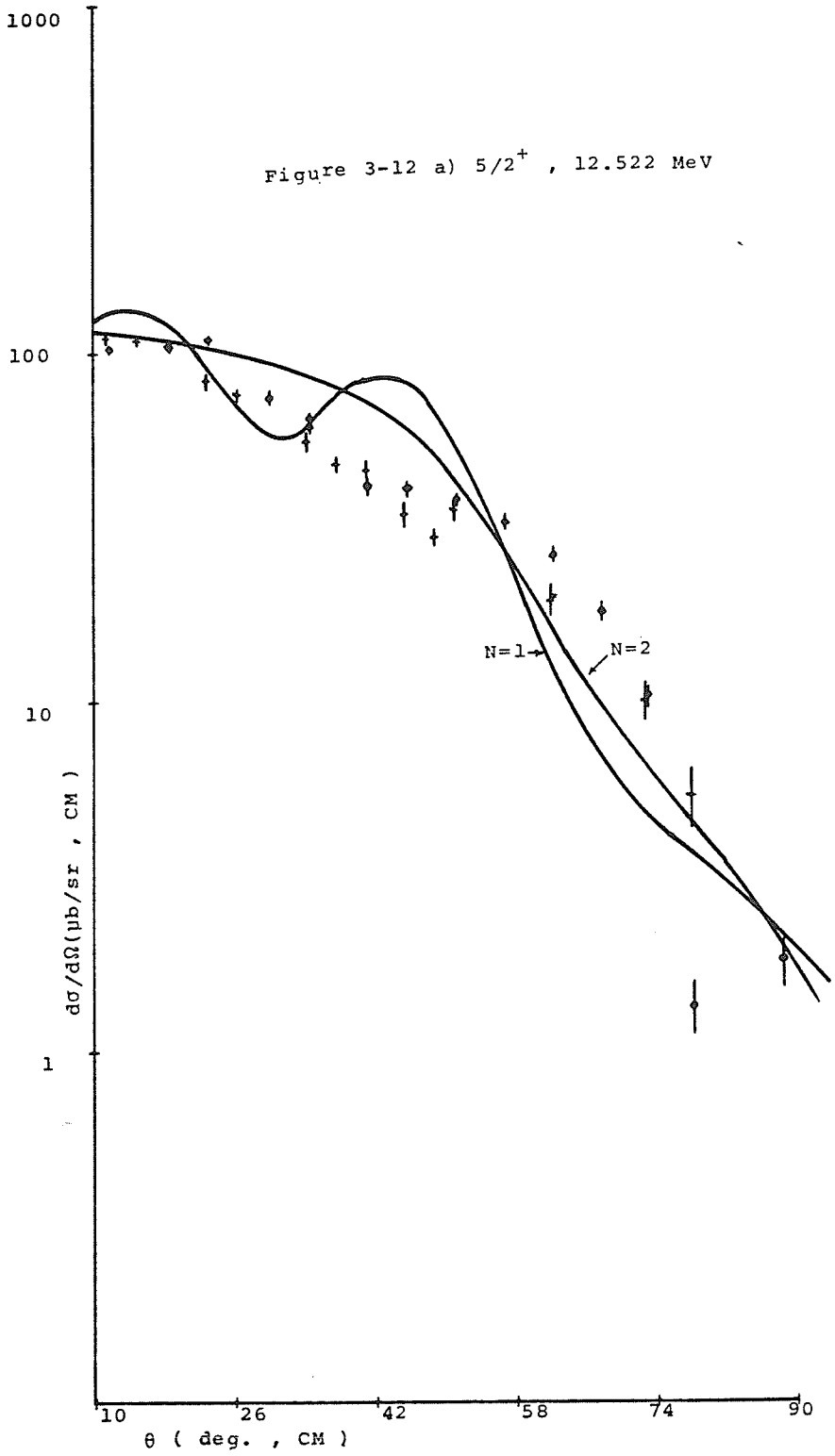

Figure 3-12 a) $5/2^+$, 12.522 MeV

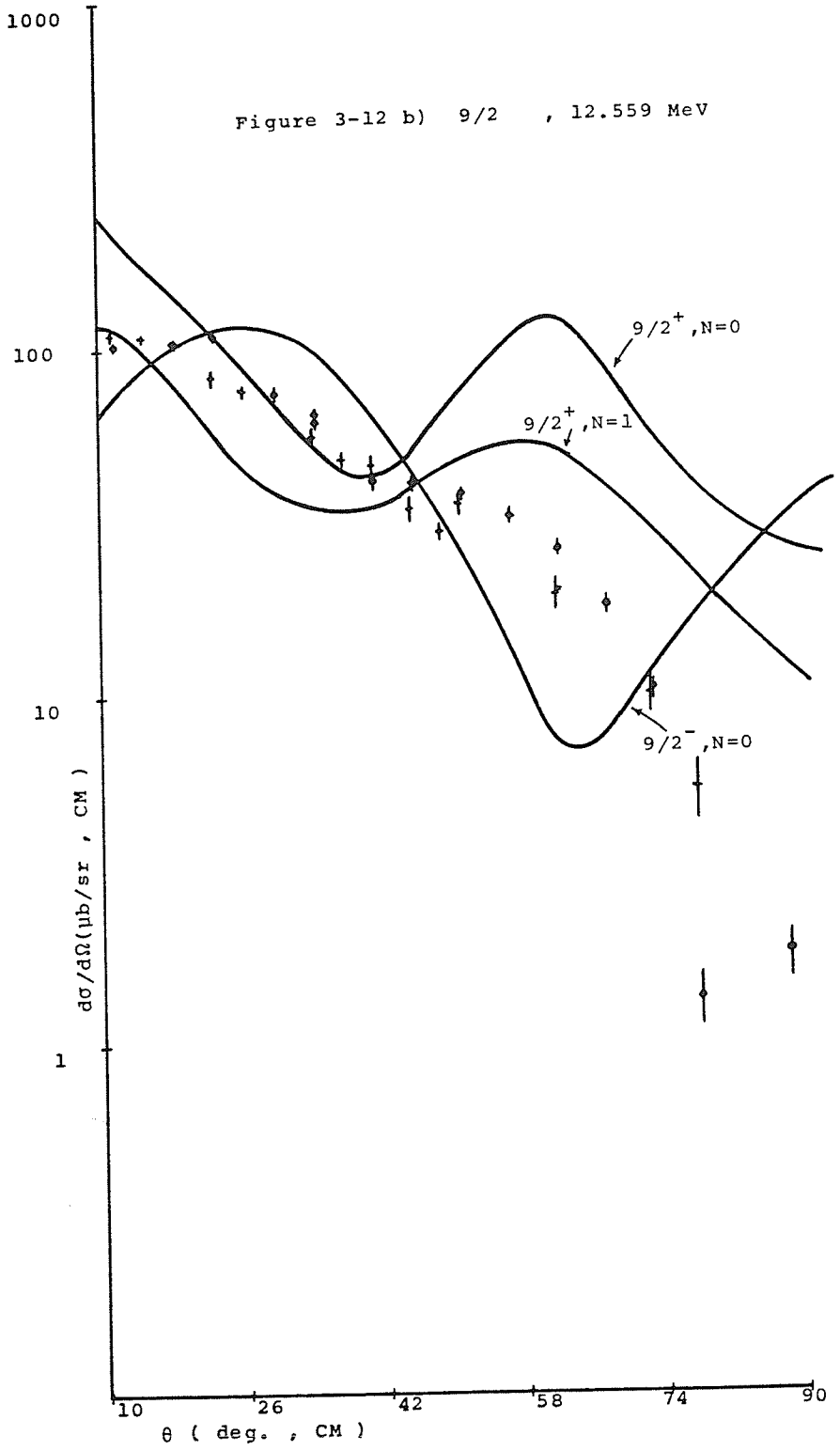

Figure 3-12 b) 9/2 , 12.559 MeV

14.09 MeV and $J^{\Pi} = 3/2^{+}$ 14.10 MeV States

No values of angular momenta or parity have been assigned to the 14.09 MeV state . This doublet was not observed in the $^{12}C(\alpha,p)^{15}N$ reaction , but was observed in the $^{12}C(^{7}Li,\alpha)^{15}N$ reaction [29] and is strongly excited in the $^{18}O(p,\alpha)^{15}N$ pickup reaction . Figure 3-13 shows a calculation for the $3/2^{+}$ state .

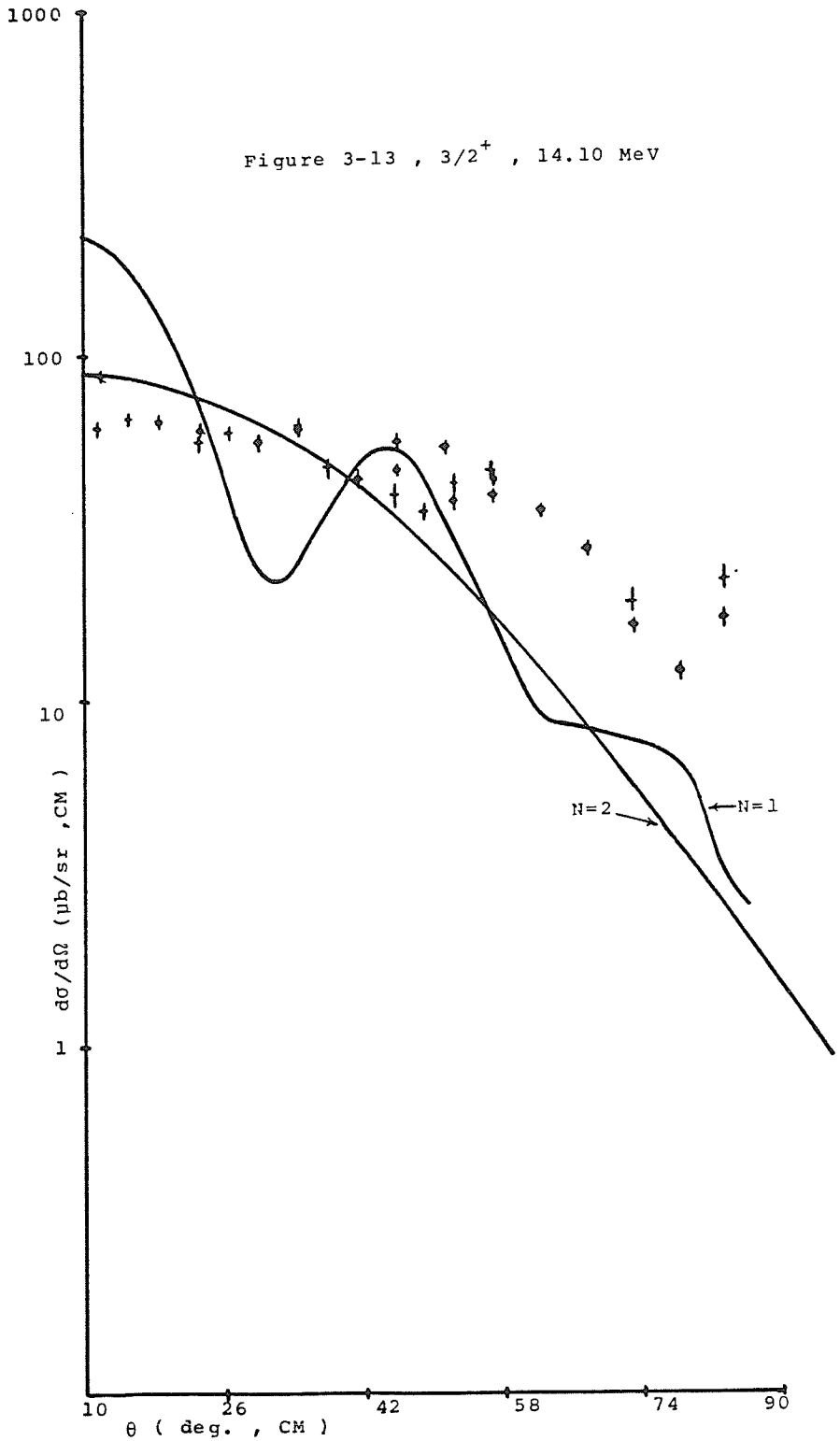

Figure 3-13 , $3/2^+$, 14.10 MeV

3-7 Conclusion

The simple model that a (p,α) reaction occurs as a transfer of a triton from the target nucleus to a proton appears to be of some value in the description of the $^{18}O(p,\alpha)^{15}N$ reaction at E_p=40.9 MeV . With the set of optical and bound state parameters chosen , there is excellent agreement in shpae with the $J^{\Pi}= 1/2^-$ ground state . Other data , when considered as a sum of two states yields an agreeable shape at forward angles , which breaks down at large angles.

Two of the most objectionable assumptions of the theory are that the elastic scattering potentials are the same for both the target and residual nuclei (see eqn. 3-4 and 3-5) , and that the transferred group exists as a single particle , represented by a triton , bound to a Woods- Saxon potential well . The first assumption may be valid for heavy nuclei , however in the present case, where the transferred triton represents 17% of the total mass of the target nucleus , this assumption becomes suspect . The second assumption ignores the relative motion of the transferred nucleons , this relative motion is dealt with in the semi-microscopic and microscopic theories of the form factor[39)] . The cross sections exhibited a pathological variation with respect to bound state values of radius and diffuseness . This is particularly disconcerting , since it would be desirable to find one set of parameters describing the reaction to all states of ^{15}N.

It is also assumed in the calculations that the nuclei may be represented by the spherical shell model . ^{18}O is considered to be deformed [40], which may have some effect on the calculation .

It is apparent that more degrees of complication must be introduced into the calculation before any concrete conclusions can be made concerning the nature of the reaction and the structure of the ^{15}N nucleus may be made.

Appendix

The appendix contains the tabulated cross sections for the two experiments which were performed . Tables whose filenames begin with "0X" were from the first experiment , those beginning with "01" are from the second experiment . The error quoted is based solely upon the error in the peak area (ie the square root of said area).

DIFFERENTIAL CROSS-SECTIONS FOR FILE 0X000
EXCITATION ENERGY 0.00000 MEV

VALUES IN MICROBARNS

THETA(LAB)	SIGMA(LAB)	THETA(CM)	SIGMA(CM)	ERROR(CM)
10.1	158.3	11.3	127.0	3.9
13.1	101.5	14.7	81.7	2.2
16.1	73.6	18.0	59.3	2.8
20.1	45.0	22.5	36.5	2.0
20.2	41.6	22.5	33.7	2.9
23.2	34.2	25.8	27.9	1.7
26.2	30.6	29.2	25.0	2.3
30.2	33.7	33.6	27.7	2.1
30.2	26.8	33.6	22.1	2.2
33.2	19.5	36.9	16.1	1.2
36.2	20.0	40.2	16.7	1.7
40.1	10.4	44.5	8.8	1.3
40.2	12.2	44.5	10.3	1.2
43.1	8.5	47.8	7.2	0.8
46.1	7.4	51.0	6.4	1.0
50.1	4.1	55.3	3.6	0.9
50.1	7.5	55.4	6.5	0.8
55.1	4.1	60.7	3.6	0.8
55.2	7.7	60.7	6.8	1.1
60.2	9.1	66.0	8.1	1.5
65.2	5.5	71.3	5.0	0.8
70.2	4.5	76.6	4.2	0.9
75.1	1.0	81.7	0.9	0.3
80.1	0.3	86.8	0.3	0.2

DIFFERENTIAL CROSS-SECTIONS FOR FILE 01000
EXCITATION ENERGY 0.00000 MEV

VALUES IN MICROBARNS

THETA(LAB)	SIGMA(LAB)	THETA(CM)	SIGMA(CM)	ERROR(CM)
10.4	172.1	11.7	138.1	3.6
13.4	130.6	15.0	105.0	4.3
16.4	79.6	18.4	64.2	2.7
20.4	46.2	22.8	37.5	2.4
20.4	51.9	22.8	42.0	1.7
23.4	38.1	26.1	31.0	2.8
26.4	30.2	29.5	24.7	1.9
30.4	29.1	33.8	24.0	1.8
30.4	35.3	33.9	29.1	1.6
33.4	22.3	37.1	18.5	2.0
36.4	15.9	40.4	13.2	1.2
40.4	13.9	44.8	11.7	1.5
40.4	11.9	44.8	10.1	0.8
43.4	10.0	48.1	8.5	1.5
45.4	6.1	50.3	5.2	0.5
46.4	5.1	51.3	4.4	0.8
50.4	6.9	55.6	6.0	0.7
50.4	6.7	55.7	5.8	0.6
55.4	9.3	61.0	8.2	0.7
60.4	10.2	66.3	9.2	0.7
65.4	7.4	71.6	6.8	0.5
70.4	4.2	76.8	3.9	0.4
75.4	2.2	82.0	2.1	0.3
80.4	0.7	87.1	0.6	0.2

DIFFERENTIAL CROSS-SECTIONS FOR FILE 0X527
EXCITATION ENERGY 5.27040 MEV

VALUES IN MICROBARNS

THETA(LAB)	SIGMA(LAB)	THETA(CM)	SIGMA(CM)	ERROR(CM)
10.1	169.6	11.4	134.2	4.0
13.1	87.4	14.8	69.3	2.0
16.1	85.0	18.1	67.6	2.9
20.1	69.7	22.6	55.7	2.4
20.2	67.2	22.7	53.8	3.6
23.2	59.4	26.0	47.8	2.2
26.2	59.2	29.4	47.8	3.1
30.2	46.1	33.8	37.5	2.4
30.2	45.8	33.8	37.3	2.9
33.2	38.5	37.1	31.5	1.7
36.2	35.7	40.4	29.4	2.3
40.1	27.4	44.8	22.9	2.1
40.2	26.6	44.8	22.2	1.7
43.1	19.5	48.1	16.4	1.1
45.1	13.1	50.3	11.1	1.3
46.1	13.8	51.4	11.7	1.3
50.1	11.9	55.7	10.2	1.6
50.1	11.2	55.7	9.6	1.0
55.2	11.0	61.1	9.6	1.3
60.2	10.6	66.4	9.5	1.6
65.2	15.1	71.7	13.7	1.4
70.2	11.5	77.0	10.6	1.4
75.1	10.6	82.2	10.0	1.0
80.1	7.0	87.3	6.7	1.0

DIFFERENTIAL CROSS-SECTIONS FOR FILE 01527
EXCITATION ENERGY 5.27040 MEV

VALUES IN MICROBARNS

THETA(LAB)	SIGMA(LAB)	THETA(CM)	SIGMA(CM)	ERROR(CM)
10.4	68.5	11.8	54.2	2.2
13.4	79.5	15.1	63.1	3.3
16.4	75.3	18.5	60.0	2.6
20.4	84.2	23.0	67.4	3.3
20.4	67.1	23.0	53.7	1.9
23.4	80.0	26.3	64.3	4.1
26.4	64.4	29.7	52.0	2.8
30.4	52.4	34.1	42.7	2.4
30.4	56.8	34.1	46.3	2.0
33.4	45.1	37.4	37.0	2.8
36.4	28.9	40.7	23.9	1.7
40.4	31.9	45.1	26.6	2.2
40.4	28.3	45.1	23.6	1.2
43.4	20.7	48.4	17.4	2.2
45.4	16.3	50.6	13.8	0.9
46.4	18.4	51.6	15.6	1.5
50.4	11.6	56.0	10.0	0.9
50.4	13.7	56.0	11.7	0.8
55.4	12.4	61.4	10.8	0.8
60.4	16.7	66.7	14.9	0.9
65.4	13.8	72.0	12.5	0.7
70.4	12.1	77.2	11.2	0.7
75.4	10.8	82.4	10.2	0.6
80.4	7.7	87.5	7.4	0.6

DIFFERENTIAL CROSS-SECTIONS FOR FILE 0X632
EXCITATION ENERGY 6.32385 MEV

VALUES IN MICROBARNS

THETA(LAB)	SIGMA(LAB)	THETA(CM)	SIGMA(CM)	ERROR(CM)
10.1	322.9	11.4	254.7	5.5
13.1	286.8	14.8	226.8	3.6
16.1	265.8	18.2	210.8	5.1
20.1	237.5	22.7	189.4	4.5
20.2	234.8	22.7	187.2	6.7
23.2	161.8	26.0	129.6	3.6
26.2	121.4	29.4	97.7	4.5
30.2	68.9	33.8	55.9	3.0
30.2	70.4	33.9	57.1	3.6
33.2	45.1	37.2	36.9	1.8
36.2	38.0	40.5	31.3	2.3
40.1	34.0	44.9	28.3	2.4
40.2	25.4	44.9	21.1	1.7
43.1	27.8	48.2	23.3	1.3
45.1	24.6	50.3	20.8	1.8
46.1	25.6	51.4	21.7	1.8
50.1	27.9	55.8	23.9	2.4
50.1	23.3	55.8	19.9	1.5
55.2	20.9	61.2	18.2	1.8
60.2	14.1	66.5	12.5	1.9
65.2	11.2	71.8	10.1	1.2
70.2	5.7	77.1	5.3	1.0
75.1	3.4	82.3	3.2	0.6
80.1	4.0	87.4	3.9	0.7

DIFFERENTIAL CROSS-SECTIONS FOR FILE 01632
EXCITATION ENERGY 6.32400 MEV

VALUES IN MICROBARNS

THETA(LAB)	SIGMA(LAB)	THETA(CM)	SIGMA(CM)	ERROR(CM)
10.4	298.8	11.8	235.7	4.7
13.4	323.7	15.2	256.0	6.6
16.4	290.5	18.5	230.5	5.0
20.4	248.7	23.0	198.4	5.6
20.4	248.9	23.0	198.6	3.7
23.4	172.8	26.3	138.5	6.0
26.4	124.6	29.7	100.5	3.9
30.4	80.5	34.1	65.4	2.9
30.4	91.1	34.1	74.0	2.6
33.4	53.2	37.5	43.5	3.0
36.4	35.9	40.8	29.6	1.8
40.4	34.2	45.1	28.5	2.3
40.4	29.2	45.2	24.3	1.3
43.4	26.5	48.4	22.3	2.5
45.4	28.7	50.7	24.2	1.1
46.4	26.3	51.7	22.3	1.8
50.4	27.6	56.1	23.6	1.4
50.4	29.2	56.1	25.1	1.2
55.4	22.8	61.5	19.9	1.0
60.4	20.3	66.8	18.0	1.0
65.4	11.5	72.1	10.5	0.6
70.4	8.8	77.3	8.1	0.6
75.4	5.9	82.5	5.6	0.5
80.4	3.3	87.6	3.2	0.4

DIFFERENTIAL CROSS-SECTIONS FOR FILE 0X757
EXCITATION ENERGY 7.56800 MEV

VALUES IN MICROBARNS

THETA(LAB)	SIGMA(LAB)	THETA(CM)	SIGMA(CM)	ERROR(CM)
10.1	26.1	11.5	20.5	1.6
13.1	33.0	14.8	26.0	1.2
23.2	39.3	26.1	31.4	1.8
26.2	26.0	29.5	20.9	2.1
33.2	15.7	37.3	12.8	1.1
36.2	16.4	40.6	13.4	1.5
43.1	20.9	48.3	17.5	1.2
45.1	22.4	50.4	18.9	1.7
46.1	24.9	51.5	21.0	1.8
50.1	28.7	55.9	24.6	2.4
55.2	18.5	61.3	16.1	1.7

DIFFERENTIAL CROSS-SECTIONS FOR FILE 01757
EXCITATION ENERGY 7.56800 MEV

VALUES IN MICROBARNS

THETA(LAB)	SIGMA(LAB)	THETA(CM)	SIGMA(CM)	ERROR(CM)
10.4	34.0	11.8	26.7	1.6
16.4	38.0	18.6	30.0	1.8
20.4	44.3	23.0	35.2	2.3
20.4	40.8	23.1	32.4	1.5
30.4	20.2	34.2	16.4	1.5
30.4	22.9	34.2	18.6	1.3
40.4	22.9	45.2	19.0	1.8
40.4	19.4	45.3	16.1	1.0
45.4	26.7	50.8	22.5	1.1
50.4	27.9	56.1	23.9	1.4
50.4	27.9	56.2	23.9	1.2
60.4	13.4	66.9	11.9	0.8
80.4	7.6	87.8	7.3	0.6

DIFFERENTIAL CROSS-SECTIONS FOR FILE 0X916
EXCITATION ENERGY 9.15500 MEV

VALUES IN MICROBARNS

THETA(LAB)	SIGMA(LAB)	THETA(CM)	SIGMA(CM)	ERROR(CM)
10.1	66.4	11.5	51.9	2.5
13.1	62.6	14.9	49.0	1.7
16.1	56.0	18.3	44.0	2.3
20.2	36.5	22.8	28.8	2.6
23.2	33.5	26.2	26.6	1.6
26.2	29.3	29.5	23.4	2.2
30.2	21.5	34.0	17.3	2.0
33.2	26.2	37.4	21.3	1.4
36.2	17.2	40.7	14.1	1.6
40.1	14.4	45.1	11.9	1.5
43.1	6.7	48.4	5.6	0.7
75.1	2.5	82.5	2.4	0.5
80.1	2.4	87.7	2.3	0.6

DIFFERENTIAL CROSS-SECTIONS FOR FILE 01916
EXCITATION ENERGY 9.15500 MEV

VALUES IN MICROBARNS

THETA(LAB)	SIGMA(LAB)	THETA(CM)	SIGMA(CM)	ERROR(CM)
10.4	91.2	11.8	71.3	2.6
16.4	58.4	18.6	45.9	2.2
20.4	40.5	23.1	32.1	2.2
20.4	51.2	23.1	40.5	1.7
26.4	32.6	29.8	26.1	2.0
30.4	30.7	34.3	24.7	1.8
30.4	31.8	34.3	25.6	1.5
36.4	22.7	40.9	18.6	1.5
40.4	23.8	45.3	19.6	1.9
40.4	20.5	45.4	17.0	1.1
45.4	12.0	50.9	10.1	0.7
50.4	5.6	56.3	4.8	0.6
50.4	6.7	56.3	5.7	0.6
55.4	7.3	61.7	6.3	0.6
60.4	8.7	67.1	7.7	0.7
65.4	6.9	72.4	6.3	0.5
70.4	7.5	77.6	6.9	0.5
75.4	5.9	82.8	5.5	0.5
80.4	1.6	87.9	1.6	0.3

DIFFERENTIAL CROSS-SECTIONS FOR FILE 0X983
EXCITATION ENERGY 9.82900 MEV

VALUES IN MICROBARNS

THETA(LAB)	SIGMA(LAB)	THETA(CM)	SIGMA(CM)	ERROR(CM)
10.1	45.3	11.5	35.3	2.1
13.1	46.6	14.9	36.4	1.4
16.1	43.8	18.3	34.3	2.1
20.2	32.2	22.8	25.4	2.5
23.2	21.5	26.2	17.1	1.3
26.2	19.7	29.6	15.7	1.8
30.2	14.9	34.0	12.0	1.6
33.2	13.4	37.4	10.9	1.0
45.1	10.7	50.6	9.0	1.2
75.1	2.3	82.6	2.2	0.5

DIFFERENTIAL CROSS-SECTIONS FOR FILE 01893
EXCITATION ENERGY 9.82900 MEV

VALUES IN MICROBARNS

THETA(LAB)	SIGMA(LAB)	THETA(CM)	SIGMA(CM)	ERROR(CM)
10.4	41.1	11.8	32.1	1.7
16.4	50.6	18.6	39.7	2.1
20.4	34.6	23.1	27.3	2.1
20.4	40.2	23.1	31.8	1.5
26.4	18.6	29.9	14.9	1.5
30.4	13.7	34.3	11.0	1.2
30.4	20.5	34.3	16.5	1.2
40.4	21.8	45.4	18.0	1.1
50.4	11.0	56.3	9.4	0.9
60.4	4.0	67.2	3.6	0.5
65.4	3.6	72.4	3.2	0.3
75.4	1.2	82.9	1.1	0.2
80.4	3.2	88.0	3.1	0.4

DIFFERENTIAL CROSS-SECTIONS FOR FILE 0X107
EXCITATION ENERGY 10.70000 MEV

VALUES IN MICROBARNS

THETA(LAB)	SIGMA(LAB)	THETA(CM)	SIGMA(CM)	ERROR(CM)
13.1	45.3	14.9	35.3	1.4
16.1	34.9	18.3	27.3	1.8
30.2	9.1	34.1	7.3	1.3
33.2	7.8	37.4	6.3	0.8
43.1	8.2	48.5	6.8	0.7
46.1	12.3	51.8	10.3	1.2
55.2	12.5	61.6	10.8	1.4

DIFFERENTIAL CROSS-SECTIONS FOR FILE 01107
EXCITATION ENERGY 10.70000 MEV

VALUES IN MICROBARNS

THETA(LAB)	SIGMA(LAB)	THETA(CM)	SIGMA(CM)	ERROR(CM)
10.4	51.6	11.9	40.1	1.9
16.4	47.7	18.7	37.3	2.0
26.4	13.5	29.9	10.7	1.3
30.4	17.2	34.4	13.8	1.1
40.4	13.7	45.5	11.3	1.4
40.4	12.9	45.5	10.6	0.8
50.4	17.6	56.4	14.9	1.1
55.4	12.2	61.9	10.5	0.7
70.4	1.5	77.8	1.4	0.2

DIFFERENTIAL CROSS-SECTIONS FOR FILE 0X112
EXCITATION ENERGY 11.23500 MEV

VALUES IN MICROBARNS

THETA(LAB)	SIGMA(LAB)	THETA(CM)	SIGMA(CM)	ERROR(CM)
13.1	10.4	14.9	8.1	0.7
16.1	22.2	18.3	17.3	1.5
20.2	22.3	22.9	17.5	2.0
23.2	27.6	26.3	21.8	1.5
26.2	34.1	29.6	27.1	3.3
30.2	21.5	34.1	17.2	2.0
33.2	17.3	37.5	14.0	1.1
36.2	11.3	40.8	9.1	1.3
46.1	5.5	51.8	4.6	0.8
65.2	8.5	72.3	7.6	1.0
75.2	8.9	82.8	8.4	0.9

DIFFERENTIAL CROSS-SECTIONS FOR FILE 01112
EXCITATION ENERGY 11.23500 MEV

VALUES IN MICROBARNS

THETA(LAB)	SIGMA(LAB)	THETA(CM)	SIGMA(CM)	ERROR(CM)
16.4	18.3	18.7	14.3	1.2
20.4	26.7	23.2	21.0	1.2
26.4	21.9	29.9	17.4	1.6
30.4	23.8	34.4	19.1	1.6
30.4	24.6	34.4	19.7	1.3
36.4	13.2	41.1	10.7	1.1
40.4	9.5	45.5	7.8	0.7
75.4	2.1	83.0	2.0	0.3

DIFFERENTIAL CROSS-SECTIONS FOR FILE 0X114
EXCITATION ENERGY 11.43800 MEV

VALUES IN MICROBARNS

THETA(LAB)	SIGMA(LAB)	THETA(CM)	SIGMA(CM)	ERROR(CM)
13.1	33.8	14.9	26.3	1.2
16.1	37.7	18.3	29.4	1.9
20.2	38.9	22.9	30.5	2.7
23.2	45.4	26.3	35.8	1.9
26.2	31.4	29.6	24.9	2.2
30.2	30.9	34.1	24.7	2.3
33.2	13.4	37.5	10.8	1.0
36.2	14.2	40.8	11.5	1.4
46.1	9.9	51.9	8.3	1.1
65.2	3.6	72.4	3.2	0.7
75.1	2.3	82.8	2.2	0.5

DIFFERENTIAL CROSS-SECTIONS FOR FILE 01114
EXCITATION ENERGY 11.43800 MEV

VALUES IN MICROBARNS

THETA(LAB)	SIGMA(LAB)	THETA(CM)	SIGMA(CM)	ERROR(CM)
16.4	33.6	18.7	26.2	1.7
20.4	48.9	23.2	38.4	1.6
26.4	37.1	30.0	29.4	2.1
30.4	25.5	34.4	20.4	1.6
30.4	33.6	34.4	26.8	1.5
36.4	24.4	41.1	19.8	1.5
40.4	13.7	45.5	11.3	0.9
50.4	9.2	56.5	7.8	0.8
75.4	1.7	83.1	1.6	0.2
80.4	1.7	88.2	1.7	0.3

DIFFERENTIAL CROSS-SECTIONS FOR FILE 0X125
EXCITATION ENERGY 12.53500 MEV

VALUES IN MICROBARNS

THETA(LAB)	SIGMA(LAB)	THETA(CM)	SIGMA(CM)	ERROR(CM)
10.1	140.1	11.6	108.1	3.6
13.1	137.4	15.0	106.3	2.5
20.2	104.0	22.9	81.2	4.4
23.2	94.5	26.3	74.2	2.7
30.2	68.2	34.2	54.3	2.5
33.2	58.7	37.6	47.1	2.0
36.2	55.8	40.9	45.2	2.8
40.1	41.1	45.3	33.6	2.6
43.1	35.1	48.7	29.0	1.5
45.1	41.8	50.9	34.8	2.3
55.2	22.1	61.8	19.1	1.9
65.2	11.0	72.5	9.9	1.2
70.2	5.7	77.8	5.3	1.0

DIFFERENTIAL CROSS-SECTIONS FOR FILE 01125
EXCITATION ENERGY 12.53500 MEV

VALUES IN MICROBARNS

THETA(LAB)	SIGMA(LAB)	THETA(CM)	SIGMA(CM)	ERROR(CM)
10.4	130.5	11.9	100.7	3.0
16.4	131.8	18.7	102.4	3.3
20.4	137.1	23.3	107.1	2.7
26.4	92.7	30.0	73.3	3.3
30.4	75.6	34.5	60.3	2.8
30.4	80.0	34.5	63.8	2.3
36.4	50.2	41.2	40.7	2.1
40.4	48.8	45.6	40.0	1.6
45.4	45.0	51.2	37.4	1.4
50.4	38.1	56.7	32.2	1.4
55.4	29.9	62.1	25.8	1.2
60.4	20.3	67.4	17.9	1.0
65.4	11.4	72.7	10.2	0.6
70.4	1.4	78.0	1.3	0.2
80.4	1.9	88.4	1.8	0.3

DIFFERENTIAL CROSS-SECTIONS FOR FILE 0X141
EXCITATION ENERGY 14.09600 MEV

VALUES IN MICROBARNS

THETA(LAB)	SIGMA(LAB)	THETA(CM)	SIGMA(CM)	ERROR(CM)
10.1	79.5	11.6	61.0	2.7
13.1	84.1	15.0	64.7	1.9
20.2	71.7	23.0	55.7	3.6
23.2	75.5	26.4	58.9	2.4
30.2	77.3	34.3	61.2	3.7
33.2	58.8	37.7	46.9	2.0
40.1	48.0	45.5	39.0	2.7
43.1	42.6	48.8	35.0	1.6
46.1	50.0	52.1	41.5	2.4
50.1	53.6	56.5	45.2	3.2
65.2	21.3	72.7	19.1	1.6
75.1	23.7	83.2	22.2	1.5

DIFFERENTIAL CROSS-SECTIONS FOR FILE 01141
EXCITATION ENERGY 14.09600 MEV

VALUES IN MICROBARNS

THETA(LAB)	SIGMA(LAB)	THETA(CM)	SIGMA(CM)	ERROR(CM)
10.4	112.0	11.9	85.9	2.8
16.4	81.9	18.8	63.2	2.6
20.4	75.9	23.3	59.0	3.0
20.4	76.3	23.3	59.3	2.0
26.4	69.9	30.1	54.9	2.8
30.4	76.6	34.6	60.7	2.8
30.4	75.4	34.6	59.8	2.8
36.4	53.9	41.3	43.4	2.2
40.4	67.6	45.8	55.1	3.1
40.4	56.2	45.8	45.8	1.7
45.4	64.1	51.3	53.1	1.7
46.4	44.5	52.4	37.0	2.3
50.4	45.3	56.8	38.2	1.8
50.4	51.2	56.8	43.2	1.6
55.4	40.1	62.2	34.5	1.4
60.4	30.5	67.6	26.7	1.3
65.4	18.1	72.9	16.2	0.7
70.4	12.9	78.2	11.9	0.7
75.4	18.1	83.4	17.0	0.8

References

1. P.H. Debenham, "E-Line User's Manual , Internal Report #75-12 , University of Manitoba Cyclotron Laboratory , 1975 , and P. H. Debenham and W.R. Falk , Nucl. Instrum. Meth. 175 , 281 (1980)

2. R.J. Kidney , "Proton Induced Charged Particle Reactions on Ne at 42.6 MeV " , Master's Thesis , University of Manitoba (1969) .

3. E. A. Silverstein , Nucl. Instrum. Meth. 4 , 53 (1959) .

4. J.B. Marion and F.C. Young , " Nuclear Reaction Analysis - Graphs and Tables " , North-Holland , (1968) .

5. U. Fano , Ann. Rev. of Nucl. Science 13 , 1 (1963)

6. N.M. Clarke , Nucl. Instrum. Meth. 96 , 497 (1971)

7

7. W. Falk et. al. , Nucl. Instrum. Meth. 137 , 261 (1971) .

8. Stragl- Energy Straggling Program

9. J.F. Janni , Technical Report No. AFWL-TR-65-150 , Clearinghouse , Springfield , Va. ,22151 ,(1966) .

10. Dr. R. Abegg (private communication) .

References (cont.)

11. H. Spath , "Spline Algorithms for Curves and Surfaces", Utilitas Mathematica , Winnipeg (1974)

12. A. Ralston and P. Rabinowitz , " A First Course in Numerical Analysis " , McGraw-Hill (1978)

13. P.D. Kunz , University of Colorado , Boulder , Colo. , 80302 .

14. G.R. Satchler , Nucl. Phys. 55 , 1 (1964)

15. N. Austern , "Direct Nuclear Reaction Theories", Wiley- Interscience (1970)

16. D.F. Jackson , "Nuclear Reactions" , Methuen and Co. Ltd. (1975) .

17. N.K. Glendenning , Ann. Rev. of Nuc. Science 13 , 191 (1963) .

18. J.M. Nelson and B.E.F. Macefield , " A General DWBA Computer Program for Particle Transfer Reactions " , Nuclear Physics Laboratory , Oxford.

19. N. Anantaraman , Phys. Rev. C10 , 945 (1980) .

20. M. Pignanelli et al. , Phys. Rev. C10 , 445 (1974)

21. E. Fabrici et al , Phys. Rev. C21 , 830 (1980)

22. a) B.G. Harvey et al , Phy. Rev. 146 , 712 (1966)
b) UCRL Report No. 16573 (unpublished)

References (cont.)

23. G. Wozniak et al , Phys. Rev. C14 , 815 (1976)

24. J.R. Rook , Nucl. Phys. 61 , 219 (1965)

25. M.A. Melanoff et al , Optical Model Search Code .

26. A. Messiah , "Quantum Mechanics " , John Wiley & Sons .

27. P. Debenham et al , J. Phys. G5 , 981 (1979)

28. W. Falk et. al. , Nucl. Phys. A252 , 452 (1975)

29. A.F. Zeller et al , Nucl. Phys. A344 , 307 (1980)

30. R.R. Sercely et al , Nucl. Phys. A324 , 53 (1979)

31. C.E. Steerman and F.C. Young , Nucl. Phys. A192, 353 (1972) .

32 G.W. Philips et al , Phys. Rev. C5 , 297 (1972)

33. J.J. Bevelacqua and S.V. Prewett , Can. J. Phys. = 57 , 1484 (1979) .

34. K. van-der Borg et al , Phys. Lett. 84b , 51 (1979)

35. S.K. Datta (private communication) , see Phys. Rev. C21 1687 (1980)

36. C.C. Maples , "Systematics of the Direct (p,α) Reaction" , PhD Thesis , Lawrence Berkely Laboratory , UCLA (1971)

37. H.T. Fortune et al , Phys. Lett. 87B , 29 (1979)

38. W. Kretschmer et al , Nucl. Phys. A333 , 13 (1980)

39. W. Falk , Phys. Rev. C8 , 1757 (1973) and W. Falk W. Falk , R. Abegg and S.K. Datta , Nucl. Phys. A334 , 445 (1980)

40. H.G. Benson and B.H. Flowers , Nucl. Phys. A126, 332 (1969) .